Aus der

Universitätsklinik für Zahn-, Mund- und Kieferheilkunde

Klinik und Poliklinik für Mund-, Kiefer- und Gesichtschirurgie

Establishment of a perfused system for 3D-cultured jaw periosteal cells and impact of the jaw periosteal cell secretome on dendritic cell maturation

Inaugural-Dissertation
zur Erlangung des Doktorgrades
der Zahnheilkunde

der Medizinischen Fakultät
der Eberhard Karls Universität
zu Tübingen

vorgelegt von

Cen, Wanjing

2023

Dekan: Professor Dr. B. Pichler

1. Berichterstatter: Professorin Dr. D. Alexander-Friedrich
2. Berichterstatter: Professorin Dr. S. Ehnert

Tag der Disputation: 16.10.2023

Table of Contents

1. Introduction

1.1 Bone tissue engineering

Bone is a crucial element of the skeletal system, supporting body shape and posture in vertebrates. In the clinic, large bone defects represent one of the most severe organ damages due to tumor resection, severe trauma, or congenital defects, which affect hundreds of millions of people worldwide every year, resulting in disfunction and socio-economic issues. Especially, maxillofacial bone defects seriously affect patient's pronunciation and chewing function, as well as self-confidence of their appearance. These reasons make the development of bone tissue engineering (BTE) imperative, which is a feasible approach for reconstructing large bone defects that exceed bone self-healing capacity.

Generally, BTE seeks to patient-own (autologous) stem cells and biocompatible scaffolds as well as biological factors that regulate osteoprogenitor cells proliferation, migration and differentiation to enhance and form functional bone structure. Figure 1.1 shows a representative workflow of BTE in oral and maxillofacial area. Jaw periosteal cells (JPCs) are isolated from the jaw periosteum and expanded in vitro. JPCs-seeded scaffolds are then cellularized and promoted to growth and maturation in bioreactors. JPCs-based bone constructs are analyzed for cell functions, properties and interaction with microenvironment, for example osteogenic differentiation, angiogenic and immunomodulatory capacities, and interaction with osteoclasts. Finally, JPCs-based bone constructs are applied for clinical implantation.

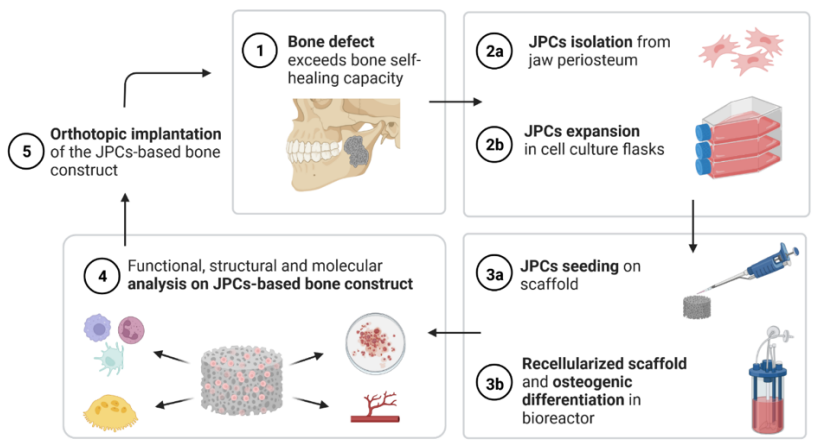

Figure 1.1 Schematic draft of a representative workflow for the development of JPC-based bone constructs for jaw bone tissue engineering. The daft is created by BioRender.

1.2 Periosteum derived stem cells

Periosteum is a highly vascularized membrane that covers the outer surface of most bones, consisting of an outer fibrous layer, and an inner cambium layer (Dwek, 2010) (Figure 1.2).

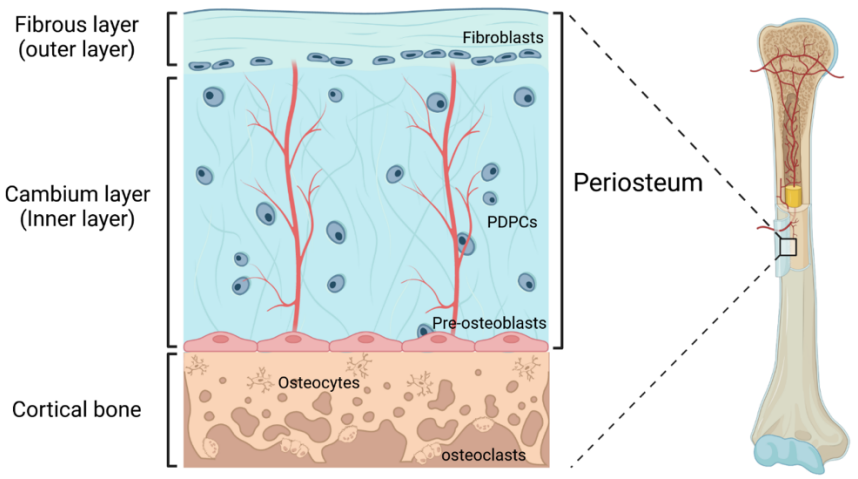

Figure 1.2 Schematic draft of the periosteum tissue. The daft is created by BioRender.

The outer fibrous layer is composed of collagenous matrix, elastic fibers, fibroblasts, micro vessels and neural network (Squier et al., 1990). The inner cambium layer contains mesenchymal progenitor cells and differentiated osteogenic progenitor cells (collectively referred to as periosteum derived progenitor cells, PDPCs), osteoblasts, micro vessels and sympathetic nerves (Squier et al., 1990, Allen et al., 2004). PDPCs play an important role in bone development and regeneration (Evans et al., 2013). Interestingly, the osteogenic differentiation potential of PDPCs differs with location. Studies have shown that cranial periosteum had less osteogenic potential than that of the tibia (Bilkay et al., 2008, Uddstromer, 1978). Regarding the 1,25-dihydroxyvitamin D_3 responsiveness, cranial periosteum appeared to be regulated differently from that of appendicular and axial bones (Hock et al., 1982). Compared to bone marrow derived cells, PDPCs divided more rapidly and mineralized in a more random

pattern in vitro responding to osteoinductive substances. When exposed to physiological levels of mechanical strain PDPCs increased proliferation and PGE2 production whereas osteoblasts of endosteal origin failed to respond (Jones et al., 1991). These studies indicated that PDPCs have partially unique properties compared to those of other osteogenic cells. Accordingly, PDPCs have been considered as a suitable alternative for BTE application due to their excellent characteristics including a high proliferation rate, easy isolation and expansion, as well as high osteogenic potential (Ferretti and Mattioli-Belmonte, 2014).

Thereby, jaw periosteal cells (JPCs) could be considered as a suitable stem cell source for BTE application in the oral and maxillofacial region. Schimming and Schmelzeisen first demonstrated in a clinical trial that mandibular periosteum-derived cells can form lamellar bone within 3 months after transplantation in human posterior maxilla (Schimming and Schmelzeisen, 2004). Regarding the basic researches on JPCs, numerous studies by Alexander's group have focused on application of JPCs for jaw BTE. Continuously, detection methods (Umrath et al., 2018, Alexander et al., 2009, Brauchle et al., 2017, Olbrich et al., 2012), culture conditions (Danalache et al., 2019, Wanner et al., 2017, Alexander et al., 2013), osteogenic potential of JPCs (Alexander et al., 2010) and related biomaterial aspects (Ardjomandi et al., 2012, Alexander et al., 2008) were optimized. After years of research, obtained results showed evidence for the suitability of JPCs for BTE applications.

1.3 Scaffold for osteogenic progenitor cells

Although autologous bone grafts are considered as the 'gold standard' for bone replacement/regeneration, they are facing inevitable limitations for example limited availability and donor site morbidity, which could be overcome by the application of synthetic scaffolds. Scaffolds play an important role in the tissue engineering triad concept (Figure 1.3) and should provide shape, promote cell anchorage and function, and finally tissue formation.

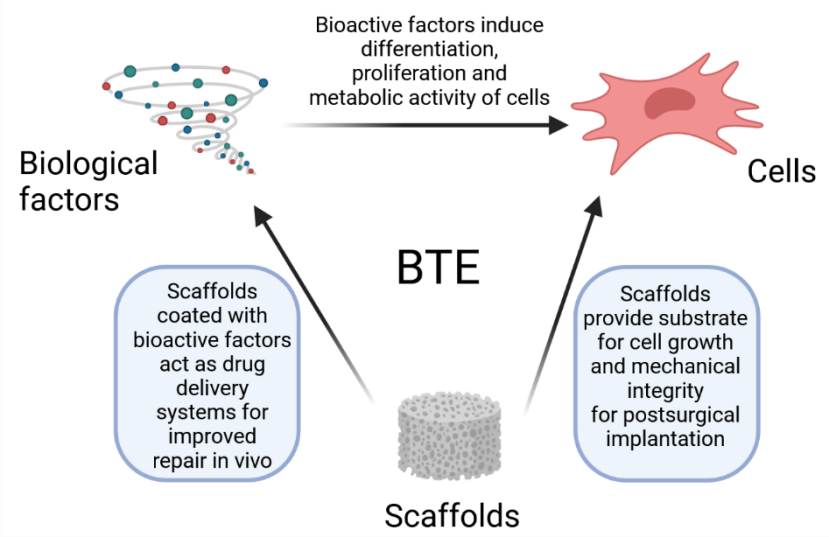

Figure 1.3 The role of scaffolds in BTE. Scaffolds are an important component of the tissue engineering triad. The daft is created by BioRender.

Ideal scaffolds applied in BTE must provide both an osteoconductive and osteoinductive environment. Osteoconduction refers to the capacity of constructs to integrate into the surrounding tissue. Osteoinduction refers to the supporting capacity of scaffolds to allow undifferentiated cells to differentiate into bone-forming cells or to the maintenance of the osteogenic phenotype of more mature cells. A high number of natural and synthetic scaffolds are available on the market but none has proven to replace thoroughly the autologous bone grafts as the 'gold standard' (Oryan et al., 2014). However, the application of biphasic calcium phosphate ceramics scaffolds is a big step in BTE due to their excellent performance in being bone bioactive (Oryan et al., 2014, Smith and Grande, 2015). Several commercial biphasic scaffolds, which are composed of β-tricalcium phosphate (β-TCP) and hydroxyapatite in a ratio of 85:15 or 80:20, were reported to produce similar fusion rates to autograft alone (Smucker et al., 2012, Miller et al., 2012, Kapur et al., 2010). Furthermore, hybrid scaffolds of PLGA/β-TCP skeleton with collagen I/apatite sponge composite coating, mimicking the specific bone extracellular matrix and being bone bioactive, are considered as promising candidates for BTE applications (Oryan et al., 2014).

1.4 Application of bioreactors in bone tissue engineering

Apart from the tissue engineering triad, novel approaches in BTE that including the application of a bioreactor are emerging. One of the key intentions behind the application of bioreactors for engineering thick tissues or cell-seeded constructs is to mimic the physiological environment and nutrient transport by blood flow in the human body. Some of the important applications of bioreactors in biomedical sciences and engineering area are listed in Figure 1.4.

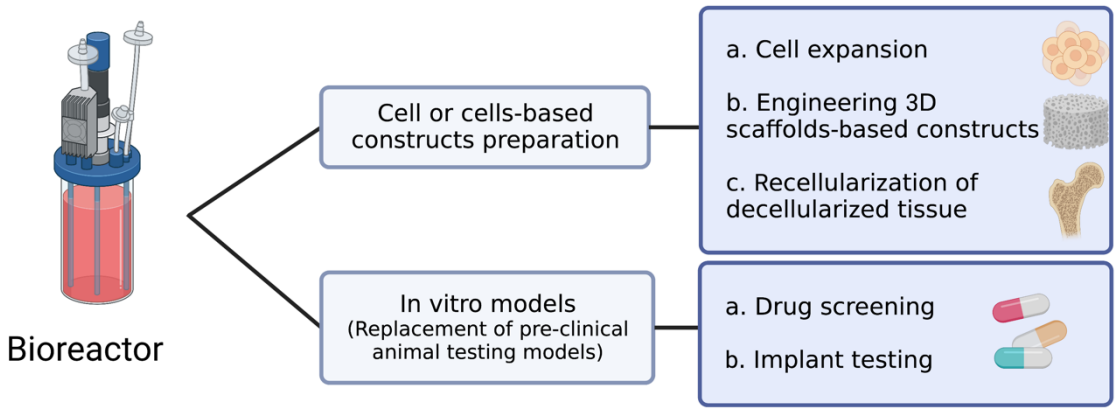

Figure 1.4. Applications of bioreactors in TE. The daft is created by BioRender.

Mimicking the physiological microenvironment of tissues with engineered cell-colonized constructs remains one of the biggest challenges in TE. Bioreactor systems are able to simulate in vitro an in vivo occurring environment conditions and help to analyze cell/molecular physiology, and to expand cells for medical purposes. The main reasons for their use in the field of TE are based on inducing physiological simulations, mimicking biological processes, by a monitored and controlled environment (Castro et al., 2020). It has been shown that the delivery of oxygen and nutrients within the in vitro-cultured 3D tissues is critically limited. Bioreactors are an alternative and efficient approach to increase diffusion of nutrients and leaching of waste products, while generating low levels of shear (Martin et al., 2004).

Perfusion bioreactors are mostly used in BTE (Grayson et al., 2008) and cartilage TE (Santoro et al., 2010) approaches, which utilize the flow to generate shear stress. Perfusion bioreactors are able to better mimic the in vivo environment, maintain the function of hypermetabolic cells, and increase the mass transport of

nutrients and oxygen through cell-seeded scaffolds by providing media flow to the cell culture (Martin et al., 2004). These devices have been reported to provide better results than stirred flask or rotating vessel bioreactors due to greater homogeneity of the mixed medium, allowing for better environmental and physical stimulation of larger structures (Gaspar et al., 2012). A novel tubular perfusion bioreactor has been reported to result in high levels of human mesenchymal stem cell viability, allowing the maximum size of an half-adult femur (Nguyen et al., 2016). In addition to improving growth conditions, perfusion bioreactors stimulate stem cell differentiation by enhancing osteogenic gene expression, thereby promoting tissue maturation within the bioreactor (Nguyen et al., 2016, Bancroft et al., 2002). However, the effect of perfusion may be highly dependent on the medium flow rate and the maturity stage of the perfused construct, as previously demonstrated in 3D-cultured chondrocytes (Davisson et al., 2002). Therefore, optimizing the application of perfusion bioreactors for 3D TE constructs must be carefully balanced between mass transfer of nutrients and waste into and out of cells, retention of newly synthesized extracellular matrix components in the construct and fluid-induced shear stress within the scaffold pores/surfaces (Martin et al., 2004). The perfusion rate of the medium has a significant effect on tissue characteristics (Grayson et al., 2008). It has been reported that low flow rates (0.075 to 0.2 mL/min) resulted in higher cell viability in human chondrocytes-seeded polyglycolic acid scaffolds (Shahin and Doran, 2011). But in the case of BTE, low flow rate didn't achieve proper distribution of nutrients, oxygen, and effective waste removal, while higher flow rate of 0.2 to 1 mL/min were optimal for a more positive effect on osteogenic differentiation, ECM deposition and distribution, obviously depends on the system used (Gaspar et al., 2012).

1.5 Immunomodulatory properties of mesenchymal stem/stromal cells

1.5.1 MSCs and immunocompetent cells

Mesenchymal stem cells (MSCs, also called mesenchymal stromal cells) actively influence the microenvironment of injured tissues, where they enhance tissue regeneration by cell attraction, by empowering the regenerative capacity of in situ

cells and through immunomodulatory mechanisms. MSCs are poorly recognized by HLA-incompatible hosts due to their poor immunogenicity, and able to differentiate into multiple mesenchymal and non-mesenchymal lineages, providing a promising tool for TE and immuno-mediated disease therapies (Uccelli et al., 2006). Multiple studies have demonstrated the immunoregulatory properties of MSCs. MSCs profoundly affect the immune response through their interactions with the cellular components of the innate and adaptive immune system through cell-to-cell contact and/or the secretion of soluble factors (Meisel et al., 2004, Aggarwal and Pittenger, 2005, Jiang et al., 2005).

As shown in Figure 1.5, many types of immune cells, including macrophages, neutrophils, T cells, B cells, plasma cells, dendritic cells (DCs) and natural killer (NK) cells, are present at sites of inflammation and can all be regulated by MSCs.

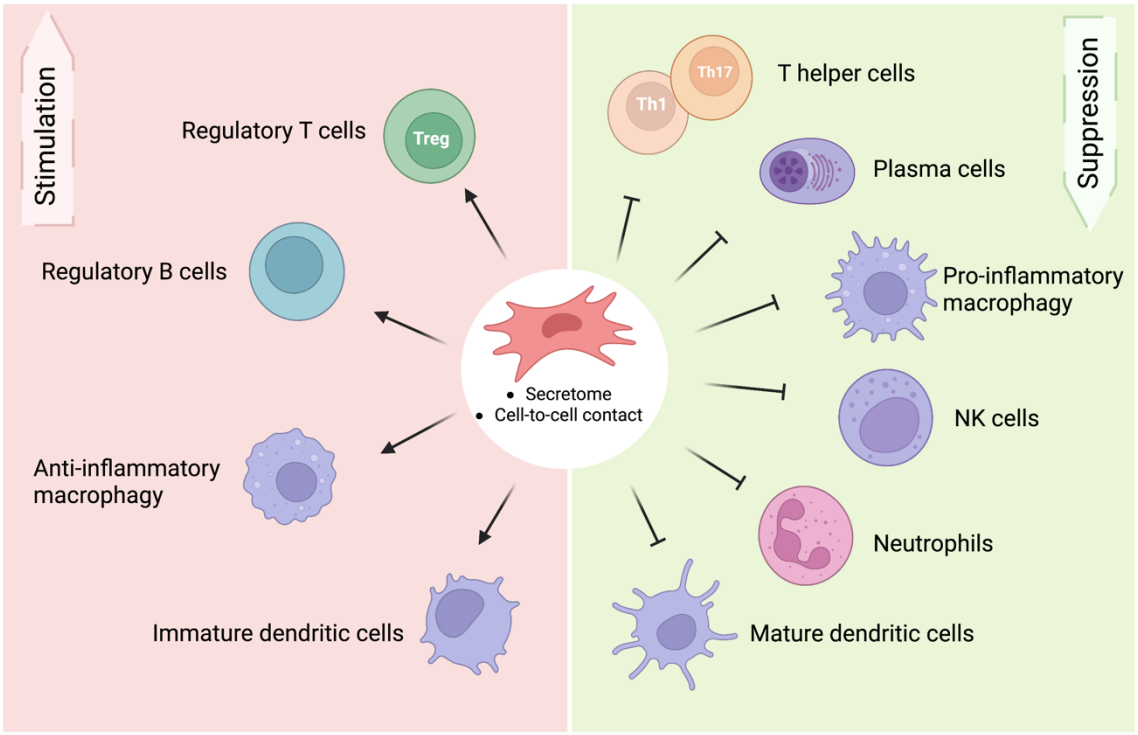

Figure 1.5. Stimulatory (left panel) and inhibitory (right panel) effects of MSCs on different immune cells. The daft is created by BioRender.

For example, MSCs can drive macrophages polarization from a pro-inflammatory to an anti-inflammatory phenotype by means of the secreted factors,

such as prostaglandin E_2 (PGE_2) (Vasandan et al., 2016), TNFα-stimulated gene 6 protein (Mittal et al., 2016), lactate (Selleri et al., 2016), kynurenic acid (Wang et al., 2018), and spermidine (Yang et al., 2016). MSCs affect the phenotype, proliferation, cytotoxic potential, and cytokine secretion of NK cells (Castro-Manrreza and Montesinos, 2015). Regarding their regulation on DCs, MSCs can affect the recruitment, maturation, and function of DCs (Jiang et al., 2005, Maccario et al., 2005, Zhang et al., 2004). Moreover, MSCs exert regulatory effects on proliferation, activation, differentiation and effector function of T cells and potentially B cells in an indirect manner by maintaining macrophages, monocytes and DCs in an immature or anti-inflammatory state, or in a direct manner through production of immunosuppressive molecules as summarized in Shi's review (Shi et al., 2018).

1.5.2 MSC secretome and immunoregulation

The MSC secretome contains multiple components, including chemokines, growth factors, cytokines, anti-inflammatory factors and exosomes. Recent data demonstrated that these soluble factors exert immunoregulatory effects on various immune cells. Cytokines produced by MSCs, including TGF-β, IL-10, CCL2, IL-6 and IL-7, are involved in immunoregulatory effects on various immune cells. TGF-β can reversibly diminish alloantigen-activated T lymphocyte proliferation (Groh et al., 2005) and induce regulatory T cells (English et al., 2009). IL-10 has been demonstrated to be important for the suppression of T cell proliferation (Taga and Tosato, 1992) and has been shown to be expressed by human MSCs (Ryan et al., 2007). Contradictorily, IL-10 was also been reported to be detected at only very low quantities in human MSCs either at mRNA or protein level (Hsu et al., 2013), or even not to be expressed by human MSCs (Najar et al., 2015). MSC-produced CCL2 played an important role in modulating Th17 cell function (Rafei et al., 2009). MSCs express IL-6 and IL-7, which are critical for T cell proliferation, differentiation and T cell survival (Tan et al., 2001, Rincon et al., 1997).

MSCs-produced chemokines such as CC-chemokine ligand 5 (CCL5), CXC-chemokine ligand 9 (CXCL9), CXCL10 and CXCL11 are chemoattractants for

immune cells (Shi et al., 2018). Importantly, pro-inflammatory cytokines are required to enhance immunosuppression by MSCs through the synergistic effects of chemokines and NO (Ren et al., 2008). MSCs express anti-inflammatory mediators with immunosuppressive function, including NO, IDO, PGE_2, TSG6, HO1 and galectins (Ma et al., 2014, Shi et al., 2018). MSC-produced growth factors, such as HGF and LIF, have been shown to inhibit effector T cell differentiation (Cao et al., 2011). Exosomes derived from MSCs, containing miR-15a, miR-15b and miR-16, have been shown to inhibit the CX3CL1 expression, a potent macrophage chemoattractant (Zou et al., 2014).

1.6 Aim of the present study

JPC-seeded constructs might be a suitable alternative for BTE applications in the oral and maxillofacial area. However, several issues need to be addressed before JPC-seeded constructs can be applied clinically. The culture conditions of JPC-seeded constructs need to be improved and optimized. Additionally, the immunomodulatory effects of JPC-secreted factors have still not been investigated to date. Therefore, this cumulative dissertation focused on the following two studies:

1. To establish an optimal perfusion condition in order to create cell-rich bone-like scaffolds by using a commercially available perfusion bioreactor for the cultivation of JPCs seeded on β-TCP scaffolds (corresponding to study I).

2. To investigate the effects of JPC secretomes collected from undifferentiated and osteogenically differentiated 2D-cultured cells on the maturation and function of $CD14^+$ monocyte-derived DCs (corresponding to study II).

2. Results and discussion

2.1 Study I: Impact of Fluid Dynamics on the Viability and Differentiation Capacity of 3D-Cultured Jaw Periosteal Cells

This part is a reprint of the following publication:

Wanjing Cen, Suya Wang, Felix Umrath, Siegmar Reinert and Dorothea Alexander. Impact of Fluid Dynamics on the Viability and Differentiation Capacity of 3D-Cultured Jaw Periosteal Cells. International journal of molecular sciences.2022; 23(9), 4682.

Abstract

Perfused bioreactor systems are considered to be a promising approach for the 3D culturing of stem cells by improving the quality of the tissue-engineered grafts in terms of better cell proliferation and deeper penetration of used scaffold materials. Our study aims to establish an optimal perfusion culture system for jaw periosteal cell (JPC)-seeded scaffolds. For this purpose, we used beta-tricalcium phosphate (β-TCP) scaffolds as a three-dimensional structure for cell growth and osteogenic differentiation. Experimental set-ups of tangential and sigmoidal fluid configurations with medium flow rates of 100 and 200 µL/min were applied within the perfusion system. Cell metabolic activities of 3D-cultured JPCs under dynamic conditions with flow rates of 100 and 200 µL/min were increased in the tendency after 1, and 3 days of culture, and were significantly increased after 5 days. Significantly higher cell densities were detected under the four perfused conditions compared to the static condition at day 5. However, cell metabolic and proliferation activity under dynamic conditions showed flow rate independency in our study. In this study, dynamic conditions increased the expression of osteogenic markers (ALPL, COL1A1, RUNX2, and OCN) compared to static conditions and the tangential configuration showed a stronger osteogenic effect than the sigmoidal flow configuration.

2.1.1 Introduction

Organ loss or failure due to tumor resection, severe trauma, or congenital defects,

is one of the most frequent, destructive, and cost-intensive problems, especially with regard to the regeneration of large bone defects. Due to the limitation of spontaneous bone self-healing, regeneration of large bone defects is beyond the normal healing potential (Sun et al., 2009, Huey et al., 2012). For these cases, the tissue engineering approach comprising the use of autologous stem cells and degradable biomaterials represents a suitable and very promising therapeutic option. For bone tissue engineering, 3D porous scaffold materials as supporting structures are usually combined with osteogenic progenitor cells (Cartmell et al., 2003, Leclerc et al., 2006, Alexander et al., 2008, Chen et al., 2015, Ardjomandi et al., 2016, Filipowska et al., 2016). Three-dimensional grafts used for transplantations, such as skin flaps, are usually thin due to the limited cell survival in the central area of thick grafts (Liu et al., 2015). Most mammalian cells are susceptible to culturing and stimulation conditions. The growth of 3D cultured cells in the static culture environment is limited by insufficient transport of oxygen and nutrients, and removal of waste products and metabolites within the scaffolds (Rouwkema et al., 2008). Additionally, in vitro static culture without appropriate mechanical stimulation does not simulate the natural microenvironment of bone tissue resulting in non-functional, poorly cell-colonized constructs (Rouwkema et al., 2008, Kanczler and Oreffo, 2008). To avoid these limitations, bioreactor systems were developed in order to provide dynamic culture conditions and to improve the quality of the tissue-engineered grafts (Wu et al., 2015, Nam et al., 2013, Zhang et al., 2009). In a study by Bruder et al., the implantation of a hydroxyapatite/β-TCP scaffold containing mesenchymal stem cells in a rat femoral gap model showed a positive impact on bone tissue growth around the periphery but lacked mineralization in the central region of the implant (Bruder et al., 1998). Considering these issues, the quality of tissue-engineered bone grafts has to be improved in terms of cell growth and differentiation within the whole construct. It has been reported that dynamic conditions within bioreactors resulted in a high level of human mesenchymal stem cell viability allowing a maximum size of a half adult femur (~200 cm3) (Nguyen et al., 2016). Besides improved growth conditions, dynamic culture conditions stimulated stem cell differentiation by enhancing osteogenic gene expression, and consequently

promoting tissue maturation within the bioreactor (Wu et al., 2015, Nguyen et al., 2016).

As developments progress, some of the bioreactors were put on the market and there are increasing reports of their clinical usage (Ravichandran et al., 2018). Different concepts of dynamic 3D bioreactors were developed in order to simulate the natural microenvironment within the bone tissue, for example, spinner flasks, rotating wall vessel constructs, perfusion bioreactors, and systems allowing mechanical or electromagnetic stimulation of cell/scaffold composites (Rauh et al., 2011).

Beta-tricalcium phosphate (β-TCP) is one of the most used synthetic bone substitute materials in bone tissue engineering due to its good biocompatibility, high osteoconductive and osteoinductive properties. β-TCP is not soluble in physiological conditions, but can be resorbed by osteoclasts, leading to material dissolution and final replacement by new bone formation (Eggli et al., 1988). Marc Bohner and co-authors has documented the widespread interest in this material, reflected in more than 200 articles published yearly (Bohner et al., 2020). In previous studies, we used this material for biofunctionalization strategies in order to improve cell functions of jaw periosteal cells (JPCs) (Ardjomandi et al., 2016, Dai et al., 2020, Weber et al., 2021, Ardjomandi et al., 2015). We have shown in numerous studies that JPCs represent a suitable stem cell source for the generation of bone tissue engineering (BTE) constructs which can be used without constraints for bone regeneration purposes in the oral and maxillofacial region (Alexander et al., 2008, Brauchle et al., 2017, Danalache et al., 2019).

In the present study, we aimed at establishing an optimal perfusion condition in order to create cell-rich bone-like scaffolds. For this purpose, we used a commercially available perfusion bioreactor for the cultivation of JPCs seeded on β-TCP scaffolds.

2.1.2 Results

2.1.2.1 Cell Proliferation within JPC-Seeded Scaffolds Cultured in the Perfusion System

Cell proliferation was analyzed indirectly by measuring the metabolic activity of JPC-seeded scaffolds under the indicated configuration, flow rate and position within the bioreactor (Figure 2.1.1A–C). As shown in Figure 2.1.1D, significantly higher metabolic activities were detected within perfused scaffolds in comparison to static conditions at day 5. Compared to day 1, significantly higher metabolic activities were obtained at day 5 under most of the conditions, except under the static condition and sigmoidal configuration with a flow rate of 100 µL/min. No significant differences were detected among dynamically cultured JPC-seeded scaffolds under different flow configurations, different flow rates or different positions within the bioreactor.

2.1.2.2 Visualization and Quantitative Analysis of Cell Distribution within β-TCP Scaffolds Cultured under Static and Perfusion Conditions by Crystal Violet Staining

To visualize proliferation, density, and distribution of JPCs on β-TCP scaffolds, JPC-seeded scaffolds cultured under different conditions were stained with crystal violet, which binds to proteins and nucleic acids of cells. On day 1 some small crystal violet spots were observed on the top of scaffolds under all conditions while crystal violet plaques were detected only at the bottom edges (side that touches the ground of the well plate) (Figure 2.1.2A). During further cultivation, small crystal violet spots became larger and merged on day 3 and day 5. Bigger and deeper violet plaques were observed at the bottom of scaffolds under all conditions on day 5 in comparison to day 1 and 3. Homogenous deep violet staining was visible on the top of the scaffolds under perfused condition on day 10, while lighter violet staining was detected on the top of the scaffolds under static conditions. To better compare cell densities on the JPC-seeded scaffolds cultured under different conditions, crystal violet staining was quantified. According to the absorbance detected at 550 nm, significantly higher densities of JPCs were detected under the four perfused conditions in comparison to the static condition on day 5 (Figure 2.1.2B). JPC densities on scaffolds under perfused conditions were shown to be higher in the tendency compared to those detected under static condition on day 10.

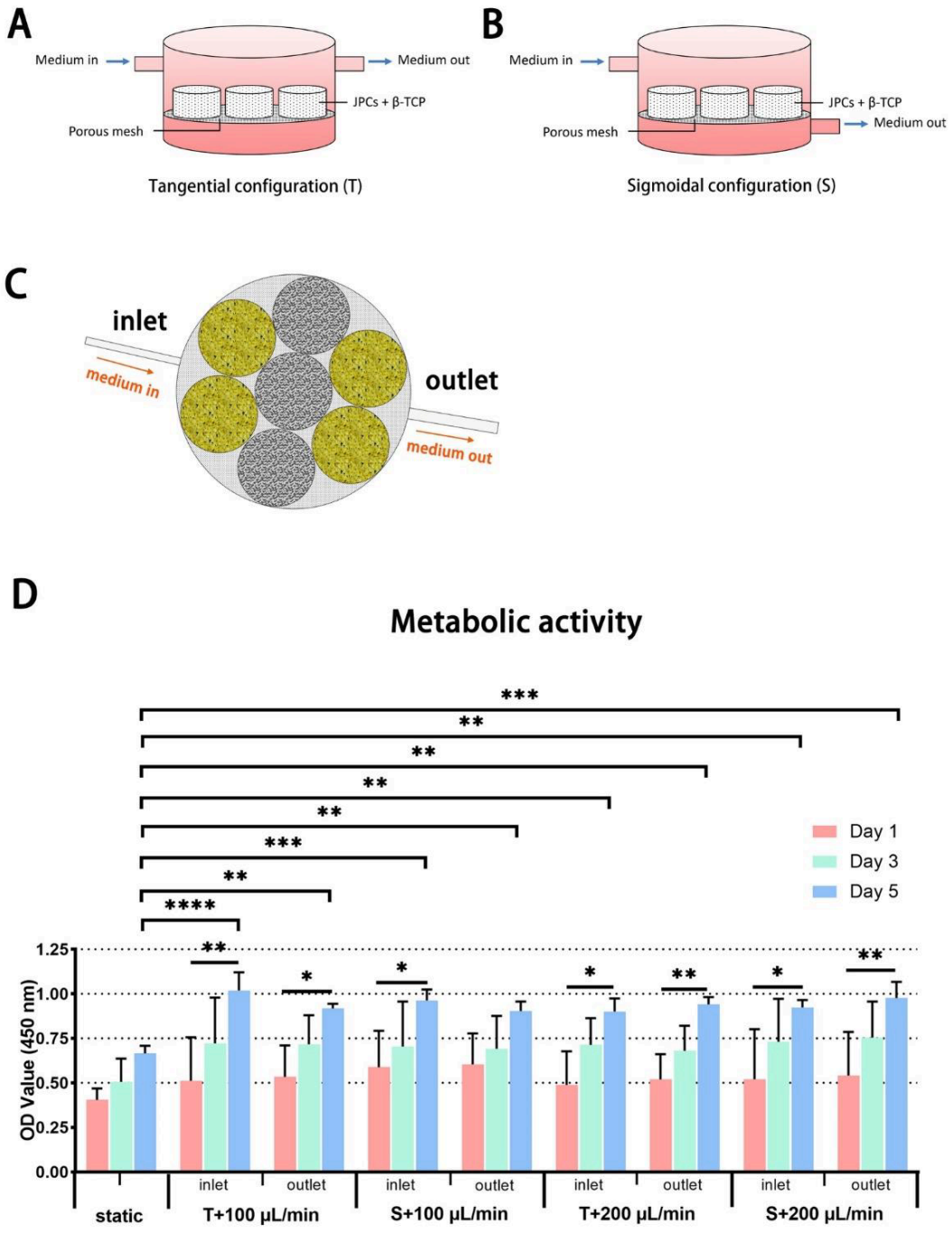

Figure 2.1.1 Schematic illustrations of (A) the tangential configuration and (B) the sigmoidal configuration. β-tricalcium phosphate (β-TCP) scaffolds were placed in the upper chamber of the bioreactor. (C) Position of scaffolds within the upper chamber of the bioreactor. (D) Metabolic activity of JPC-seeded scaffolds (yellow, positioned near the inlet and the outlet) under different culture conditions (static culture, tangential and sigmoidal configurations with flow rates of 100 and 200 µL/min) at day 1, 3 and 5 of in vitro cultivation. Optical density (OD) was measured at 450 nm and values are given as means ± standard deviation (SD). Results were compared using one-way ANOVA followed by Tukey's multiple comparisons tests, the asterisk character reflects different p-values (* $p < 0.05$, ** $p < 0.01$, *** $p < 0.001$, **** $p < 0.0001$ (n = 3 donors)).

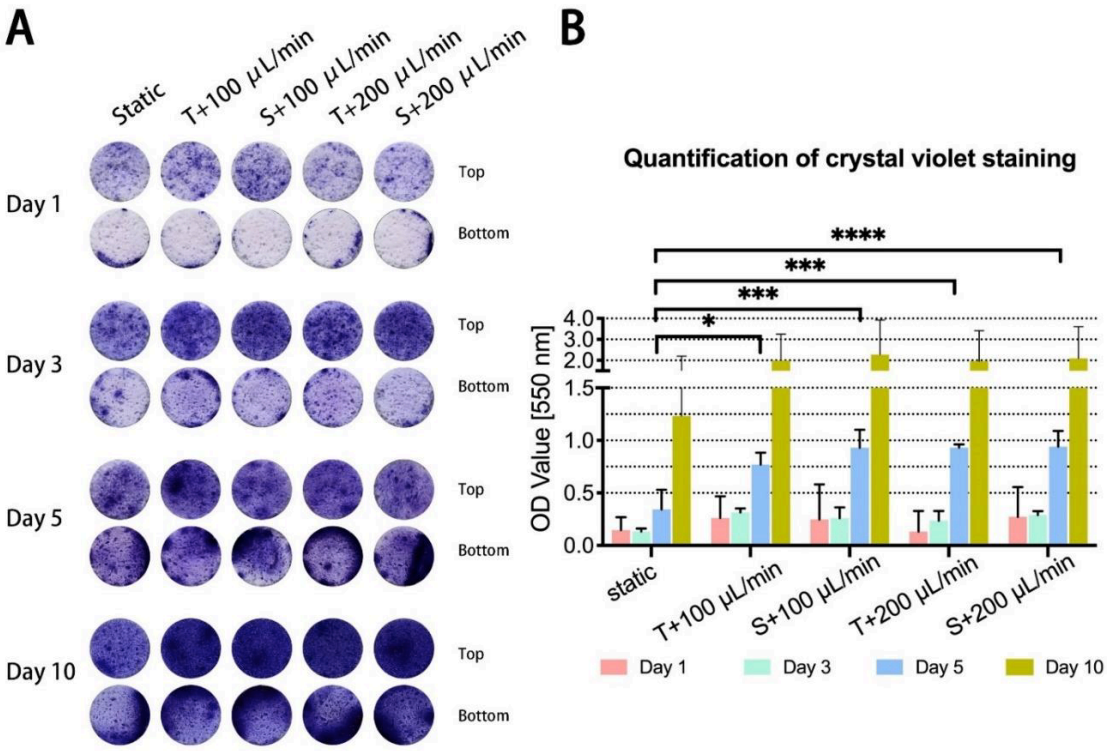

Figure 2.1.2 Crystal violet staining for the visualization and quantitative analysis of cell distribution within β-TCP scaffolds. (A) JPC-colonized scaffolds cultured under the indicated conditions (static culture, perfusion culture of tangential and sigmoidal configuration with flow rates of 100 and 200 µL/min) were stained with crystal violet dye at day 1, 3, 5 and 10 of in vitro cultivation. (B) Crystal violet staining was dissolved from stained scaffolds and optical density (OD) values were measured at a wavelength of 550 nm. The OD values are given as means ± SD and compared using one-way ANOVA followed by Tukey's multiple comparisons tests (* $p < 0.05$, *** $p < 0.001$, **** $p < 0.0001$ (n = 3 donors)).

2.1.2.3 Visualization of Cell Morphology on JPC-Seeded β-TCP Scaffolds and Quantification of Scaffold Porosity by Scanning Electron Microscopy

The morphology of the porous JPC-seeded β-TCP scaffolds was analyzed by scanning electron microscopy (SEM) after 1, 3 and 5 days of in vitro culture under the indicated conditions (Figure 2.1.3A–C). Differences in cell appearance were observed in different areas of the same scaffold surface, depending on the size of the pores into which the cells grew or which they spanned. In general, the JPCs appeared to preferentially grow inside small pores on the scaffold surface while the cells grew along the rim of the big pores as shown in images with 500-fold

magnification. The SEM images revealed that JPCs spread over the pores of β-TCP scaffolds, fully expanded with a flattened morphology.

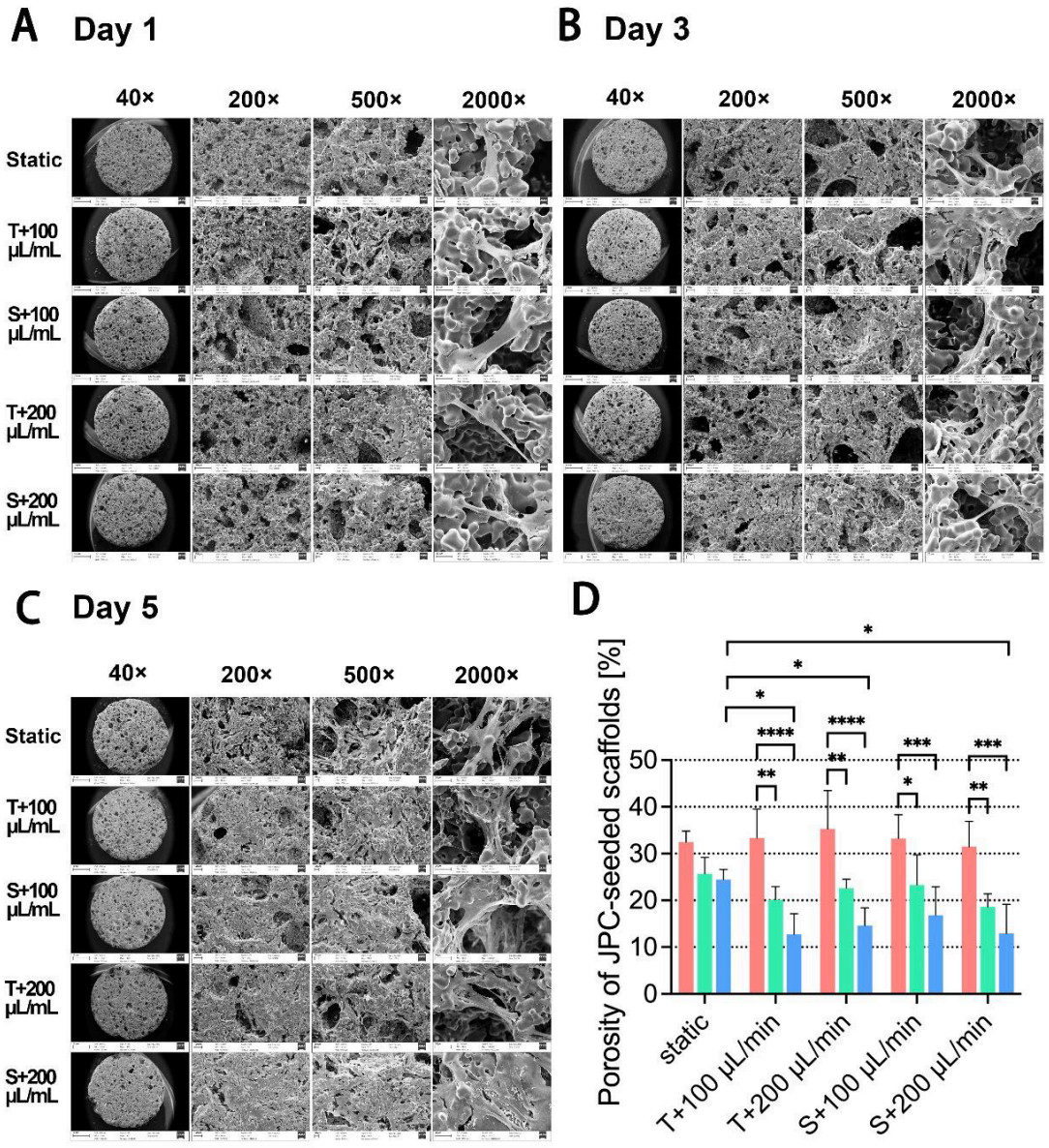

Figure 2.1.3 SEM micrographs of JPC-seeded scaffolds cultured for (A) 1, (B) 3 and (C) 5 days under the indicated conditions in different magnifications (40×, 200×, 500× and 2000×). Scale bars are 1 mm, 100 µm, 20 µm and 20 µm respectively. Representative images of three independent experiments (n = 3 donors with one experiment for each donor) are shown. (D) Pore areas in the 200× images were quantified with ImageJ software (red columns = day 1, green columns = day 3, blue columns = day 5). The porosity of JPCs-colonized scaffolds was calculated by the ratio of the total pore area to the whole area of the scaffolds. The ratios are given as means ± SD and compared using one-way ANOVA followed by Tukey's multiple comparisons tests (* $p < 0.05$, ** $p < 0.01$, *** $p < 0.001$, **** $p < 0.0001$ (n = 3 donors)).

On day 1, the porosity of β-TCP scaffolds appeared to be high under all examined conditions under 200× and 500× magnifications and cell attachment was rarely observed (Figure 2.1.3A). During consecutive cell cultivation, the pore size and number decreased due to cell attachment and proliferation. At day 5, JPCs cultured under perfused conditions showed more homogeneous and deeper distribution within the scaffolds in comparison to the JPCs cultured under the static condition. As shown in Figure 2.1.3D, porosity of JPC-seeded scaffolds cultivated under perfused conditions decreased significantly at day 3 and 5 compared to the porosity observed at day 1. Significant lower porosity on perfused scaffolds (T + 100 µL/min, T + 200 µL/min and S + 200 µL/min perfused conditions) in comparison to static conditions were detected at day 5.

2.1.2.4 Visualization of Cell Density and Distribution within Scaffolds by Fluorescent Staining and Microscopy

Since β-TCP scaffolds have a porous and brittle composition, we achieved the best experience with the polymethylmethacrylate (PMMA) embedding procedure. For further information about JPC distribution within the scaffolds under static or different perfusion conditions, sections of PMMA-embedded JPC-seeded scaffolds were stained by Sytox orange to visualize cell nuclei. The images of 1.25-fold magnification showed that JPCs were mainly located on the top (white arrows) and the bottom edge (rectangular boxes) of scaffolds after 5 days of culture. A higher fluorescence intensity was observed on the sections of the scaffolds under perfusion in comparison with scaffolds cultured under the static condition (Figure 2.1.4A). After 10 days of culture, cells appeared on both the surface and within the scaffolds under all conditions (Figure 2.1.4A). According to the quantification results of Sytox orange staining, means of red fluorescence under perfused conditions were higher than the ones obtained under static condition in the tendency at both day 5 and 10. Mean fluorescence under sigmoidal configuration with a flow rate of 100 µL/min was shown to be significantly higher compared to the detected mean fluorescence under static condition (Figure 2.1.4B).

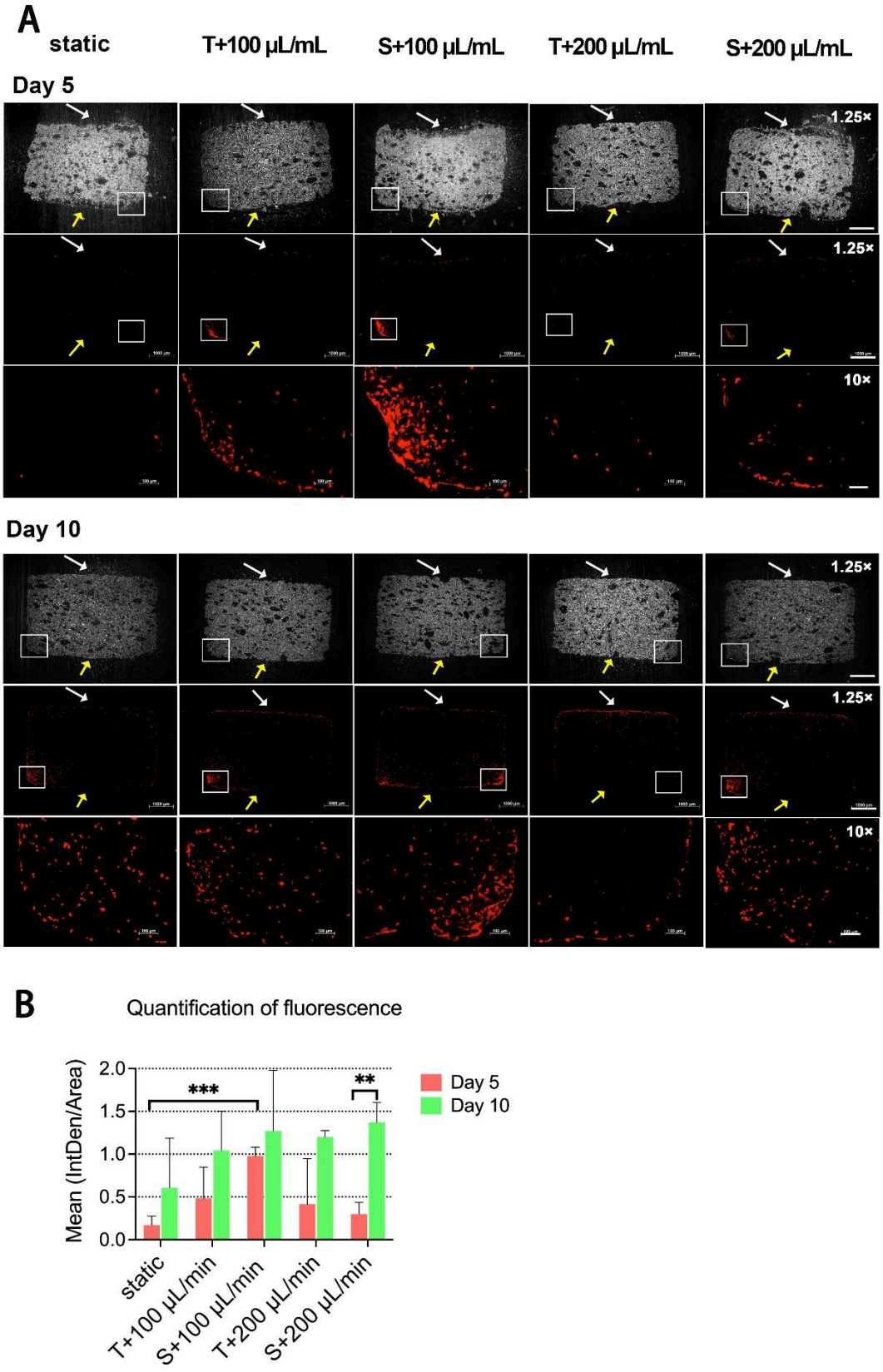

Figure 2.1.4 Visualization of cells in sections of PMMA-embedded scaffolds by Sytox orange nuclear staining. (A) Sytox orange staining was performed on sections of

Technovit 9100 embedded JPC-seeded scaffolds that were cultured under the indicated conditions for 5 or 10 days. Bright field images with 1.25× magnification are given. White and yellow arrows point to the top and the bottom of the scaffolds respectively. Images taken with a 10-fold objective represent the area of rectangular box in images taken with a 1.25-fold objective. Scale bars represents 1 mm (1.25× magnification) and 100 µm (10× magnification) respectively. (B) Integrated densities (IntDen) in sections with 1.25 magnification at day 5 and 10 were quantified by the ImageJ software. Mean fluorescence intensities are shown as a ratio of IntDen to the total area of sections. Mean fluorescence intensity values are given as means ± SD and compared using one-way ANOVA followed by Tukey's multiple comparisons tests (** $p < 0.01$, *** $p < 0.001$ (n = 3 donors)).

2.1.2.5 Gene Expression Analyses of Osteogenic Markers in 3D-Cultured JPCs Growing under Perfusion Conditions

JPC-seeded scaffolds were cultured dynamically or statically in osteogenic media and gene expression analysis was performed after 5, 10 and 15 days of 3D culture. mRNA expression levels of alkaline phosphatase (ALPL) and RUNX family transcription factor 2 (RUNX2) were significantly upregulated after 5 days of osteogenic induction under all performed conditions, but no significant differences between perfused conditions and static control (Figure 2.1.5A, B and Figure 2.1.6A, B) were observed. Gene expression levels of collagen 1α1 (COL1A1) were significantly higher under tangential configuration independently of the flow rates at day 5 (Figure 2.1.7A, B). In the case of osteocalcin (OCN), expression levels were increased significantly only under tangential configuration with 200 µL/min compared to obtained levels under static conditions in osteogenic media at day 5 (Figure 2.1.8A, B). At day 10, significantly higher ALPL and COL1A1 expression levels under tangential configuration with a flow rate of 100 µL/min were detected compared to levels under static condition in both control and osteogenic media. Further, significantly higher expression levels of OCN were observed under tangential configuration compared to levels detected under static and osteogenic condition. At day 15, significantly higher ALPL expression was detected under tangential configurations in osteogenic medium. Higher expression of RUNX2 was observed under sigmoidal configuration with a flow rate of 200 µL/min in control media, while increased expression of COL1A1 was detected under sigmoidal configuration with a 200 µL/min flow rate after 15 days of osteogenic differentiation (Figure 2.1.5, Figure 2.1.6, Figure 2.1.7 and Figure 2.1.8).

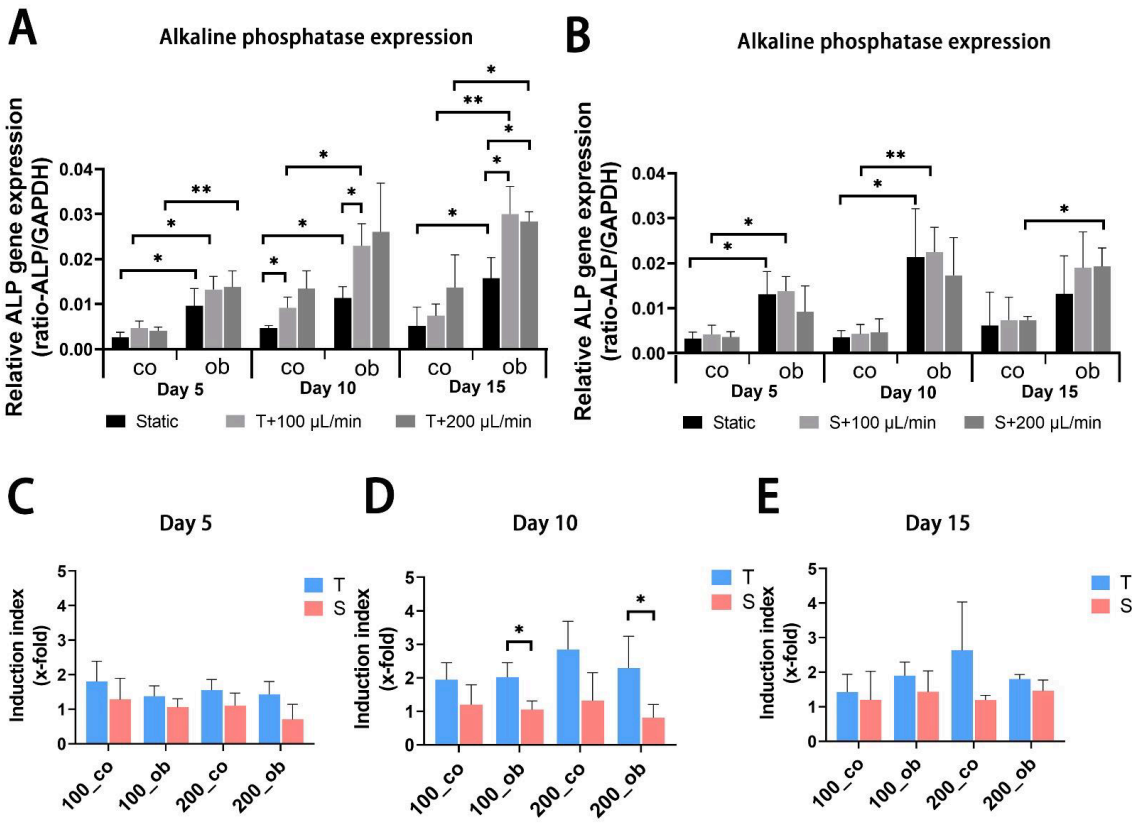

Figure 2.1.5 Gene expression levels of alkaline phosphatase (ALPL) in JPC-seeded β-TCP scaffolds after 5 days, 10 days and 15 days of osteogenic differentiation under static or perfusion conditions. mRNA expression levels under (A) tangential and (B) sigmoidal configuration were quantified and normalized to the housekeeping gene GAPDH. To calculate induction indices, gene expression levels were normalized to untreated (co) JPCs or osteogenically induced (ob) under static conditions. Induction indices of tangential (T) and sigmoidal (S) configuration after (C) 5 days, (D) 10 days and (E) 15 days of culture were calculated. The gene expression and induction values are given as means ± SD. Gene expression levels under different culture conditions (dynamic conditions and static condition) are compared using one-way ANOVA followed by Tukey's multiple comparisons tests. To compare levels of osteogenic to control condition and induction values between T and S configuration condition, two-tailed Student's t-test was used (* $p < 0.05$, ** $p < 0.01$, (n = 3 donors)).

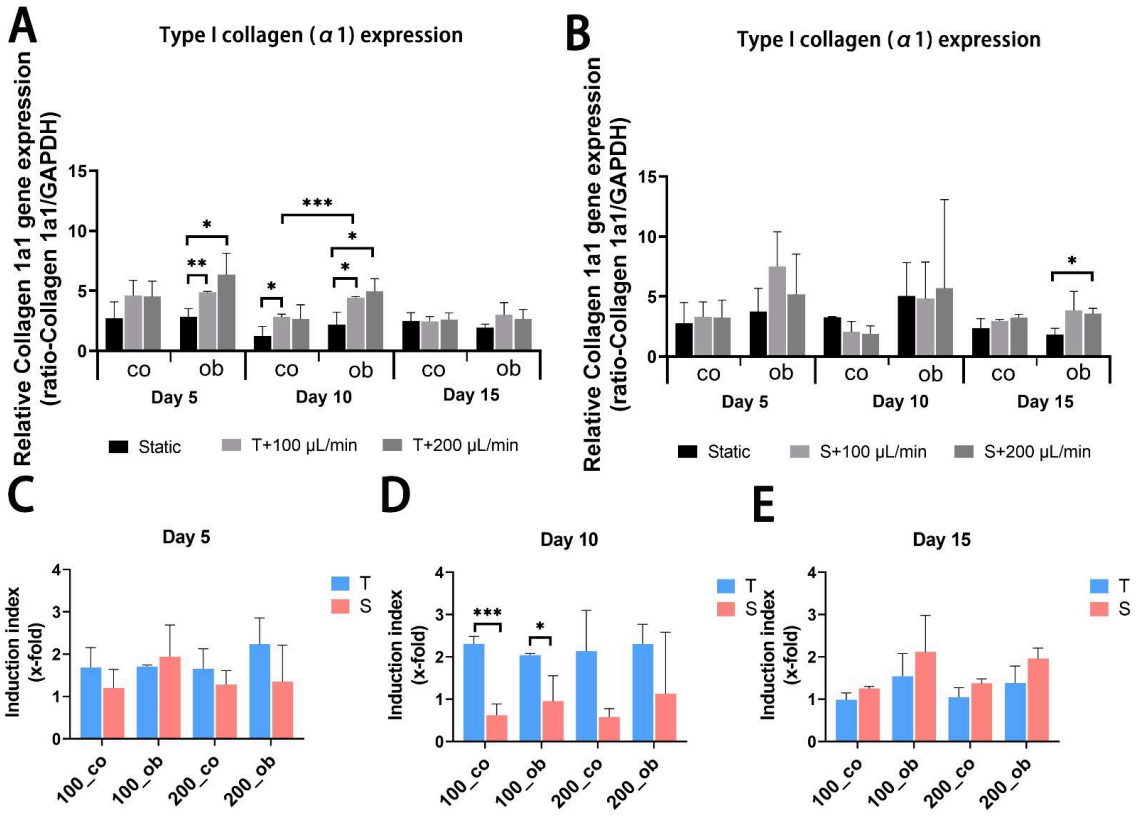

Figure 2.1.6 Gene expression levels of collagen 1α1 (COL1A1) in JPC-seeded β-TCP scaffolds after 5, 10 and 15 days of osteogenic differentiation under static or perfusion conditions. mRNA expression levels under (A) tangential and (B) sigmoidal configuration were quantified and normalized to the housekeeping gene GAPDH. To calculate induction indices, gene expression levels were normalized to untreated (co) or osteogenically induced (ob) JPCs under static condition. Induction indices of tangential (T) and sigmoidal (S) configuration after (C) 5 days, (D) 10 days and (E) 15 days of culture were calculated. The gene expression and induction values are given as means ± SD. Gene expression levels under different culture conditions (dynamic and static conditions) were compared using one-way ANOVA followed by Tukey's multiple comparisons tests. For comparing levels of osteogenic condition to control and induction values between T and S, two-tailed Student's t-test was used (* $p < 0.05$, ** $p < 0.01$, *** $p < 0.001$ (n = 3 donors)).

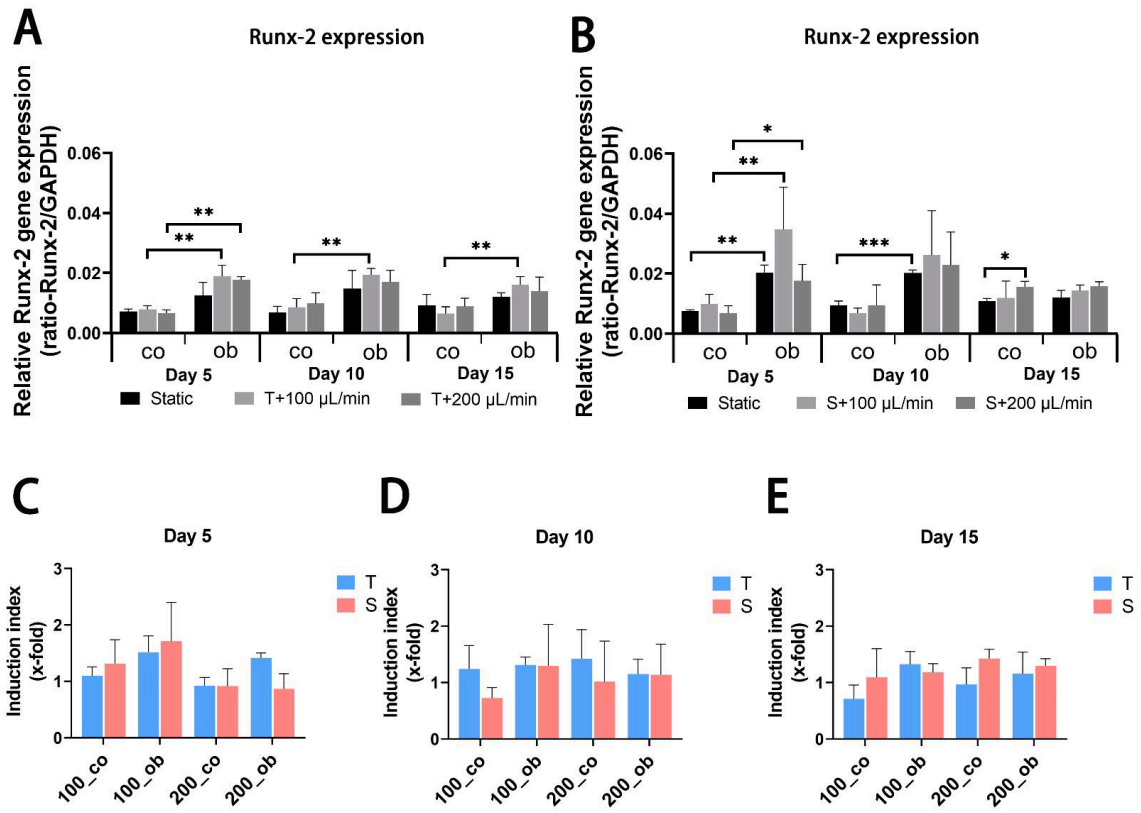

Figure 2.1.7 Gene expression levels of runt-related transcription factor 2 (RUNX2) in JPC-seeded β-TCP scaffolds after 5, 10 and 15 days of osteogenic differentiation under static or perfusion conditions. mRNA expression levels under (A) tangential and (B) sigmoidal configuration were quantified and normalized to the housekeeping gene GAPDH. To calculate induction indices, gene expression levels were normalized to untreated (co) or osteogenically induced (ob) JPCs under static condition. Induction indices of tangential (T) and sigmoidal (S) configuration after (C) 5 days, (D) 10 days and (E) 15 days of culture were calculated. The gene expression and induction values are given as means ± SD. Gene expression levels under different culture conditions (dynamic and static condition) are compared using one-way ANOVA followed by Tukey's multiple comparisons tests. For comparing levels of osteogenic condition to control and induction values between T and S, two-tailed Student's t-test is using (* $p < 0.05$, ** $p < 0.01$, *** $p < 0.001$ (n = 3 donors)).

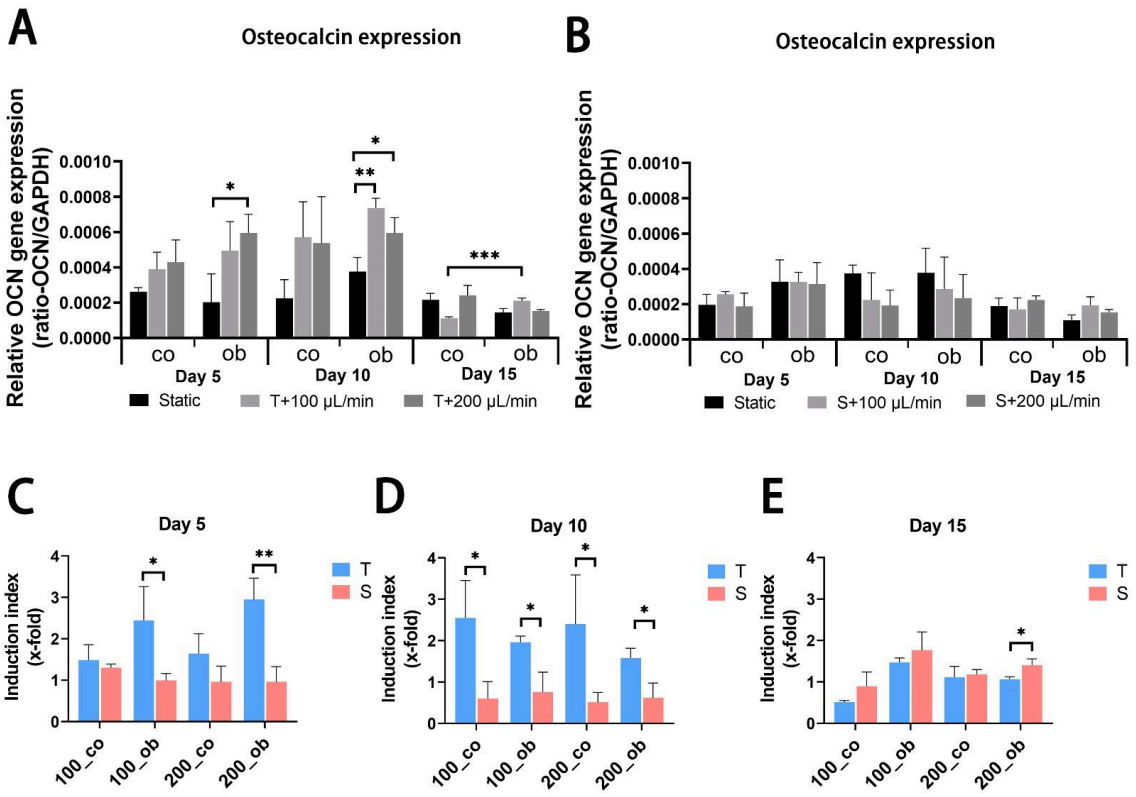

Figure 2.1.8 Relative gene expression levels of osteocalcin (OCN) in JPCs cultured within β-TCP scaffolds after 5, 10 and 15 days of osteogenic differentiation under the indicated conditions. mRNA expression levels under (A) tangential and (B) sigmoidal configuration were quantified and normalized to the housekeeping gene GAPDH. To calculate induction indices, gene expression levels were normalized to untreated (co) or osteogenically induced (ob) JPCs under static condition. Induction indices of tangential (T) and sigmoidal (S) configuration after (C) 5 days, (D) 10 days and (E) 15 days of culture were calculated. The gene expression and induction values are given as means ± SD. Gene expression levels under different culture conditions (dynamic conditions and static condition) were compared using one-way ANOVA followed by Tukey's multiple comparisons tests. For comparing levels of osteogenic condition to control and induction values between T and S, two-tailed Student's t-test is using (* $p < 0.05$, ** $p < 0.01$, *** $p < 0.001$ (n = 3 donors)).

2.1.3 Discussion

Since cell fate and function are susceptible to the cells' microenvironment, control over the microenvironment is essential in order to regulate cellular activities and behavior (Barthes et al., 2014). Many studies have shown that fluidic bioreactors are useful to control the microenvironment and have a high impact on promoting cell proliferation and differentiation. Perfusion bioreactor systems have shown promise for the 3D cultivation of stem cells for bone regeneration (Gandhi et al.,

2019). Beta-tricalcium phosphate, the scaffold material we used in this study, is a resorbable material that is widely used in clinics as a synthetic bone substitute (Ishikawa et al., 2018). It can be biofunctionalized in order to improve functions of the colonizing cells, as we reported in a previous study (Ardjomandi et al., 2016). The aim of the present study was to establish optimal perfused conditions for the cultivation of JPC-seeded beta-TCP scaffolds, and to compare cell behaviors/functions under different perfusion conditions in comparison to the static culture condition. Flow rates during perfusion have to be optimized, since cells can be damaged at high flow rates, or may not have sufficient nutrients and oxygen supply at low flow rates. In our study, cell metabolic activities were increased in the tendency under dynamic conditions with flow rates of 100 and 200 µL/min after day 1, and 3 of perfusion culture, and reached significantly higher values at day 5 compared to the static culture (Figure 2.1.1C). This result was confirmed by the crystal violet staining which showed similar results (Figure 2.1.2B) as detected by the colometric assay. The flow rates we used in this study were supposed to be in the range of values reported to promote osteogenic cell proliferation (Cartmell et al., 2003, Leclerc et al., 2006). Cartmell et al. (Cartmell et al., 2003) reported that a flow rate of 1.0 mL/min led to significant cell death and lowering of flow rate resulted in increased numbers of viable MC3T3-E1 cells. Best results were achieved with a flow rate of 100 µL /min compared to 200 µL /min and to the static controls (Cartmell et al., 2003). However, in our study, very similar cell metabolic activities were obtained under dynamic conditions independently of the used flow rate. An important difference to these studies might be the fact, that perfusion chambers used here were much bigger than the scaffolds, which allowed the medium flow to go around the scaffolds. As a result, we made the observation that cells did not grow into the scaffolds and did not homogeneously cover the scaffolds, as shown by the crystal violet and Sytox orange staining. The flow of our perfusion system exerted shear stress in a unidirectional laminar manner to the scaffold surface under both configuration types (Figure 2.1.1A, B). A previous study demonstrated that bone cells respond to fluid-generated shear stress by an increase in intracellular calcium, providing evidence that fluidic flow alone can stimulate bone cells (Williams et al., 1994). In

our study, we expected that the shear stress exerted by the fluidic flow onto the scaffolds in the same chamber depended on the distance between the scaffolds and the medium inlet. But as shown in Figure 2.1.1C, flow configuration made no difference in cell viability of 3D-cultured JPCs, implying that shear stress forces within the chamber were uniformly distributed or too little to direct cell proliferation. Since the amount of medium in the perfusion system was 200 times more than in the cell culture plate for static culture, enhanced cell proliferation on perfused scaffolds can be explained by better supply of nutrients and better transportation of metabolic waste. Cell distribution on the surface of scaffolds was initially determined by the seeding procedure/density in the 96-well plate outside the perfusion system, showing cell-rich distribution on the top and bottom edge of the scaffolds (Figure 2.1.2A and Figure 2.1.4A). Crystal violet staining and SEM images revealed higher cell densities on scaffolds cultured under dynamic conditions compared to the static controls during the analyzed culture time period. McCoy and co-authors summarized in his review article that cells attached flatly to the rim of the scaffold pores were more prone to active impact of perfusion compared to cells that bridged pores thereupon underwent cytoskeleton deformations due to resistance to flow (McCoy and O'Brien, 2010). We observed JPCs with a flat morphology attached to the side or the inside of the beta-TCP scaffold pores, in the perfusion experiments at day 1 by SEM. At day 5, cells were prone to bridge some of the scaffold pores because of increasing confluence under perfusion conditions resulting in significantly decreased porosity on the perfused scaffolds (Figure 2.1.3D). On one hand, achieving higher cell densities is desired. However, reduced scaffold porosity minimizes the nutrient transport and the stimulating effect on the cells growing within the scaffold by flow perfusion. Further experiments are needed to determine the cell viabilities within the scaffolds for long-term culture. Overall, the data suggested that the perfusion system promoted JPCs proliferation in beta-TCP scaffolds under tangential and sigmoidal configuration with flow rates of 100 and 200 µL/min, with no evidence pointing to different effects in different types of configurations or flow rates.

Within the osteons, bone cells are exposed to interstitial fluid flow through the bone canaliculi, where they respond to changes in fluid flow shear stress

controlling bone formation (Wittkowske et al., 2016). Additionally, progenitor cells can be affected in their differentiation by changes in hydrostatic pressure and shear stress within the bone marrow (Gurkan and Akkus, 2008). The perfusion system can also be used to mimic mechanical stimulation to the cells growing within the constructs to promote osteogenic differentiation and extracellular matrix production. In our study, the comparison of static and dynamic cultivation in terms of osteogenic gene expression (ALPL, COL1A1, RUNX2, and OCN) revealed that dynamic conditions obviously increased the expression of the analyzed osteogenic markers and the tangential flow configuration had stronger osteoinductive effect than the sigmoidal configuration. As an early marker of osteogenic differentiation (Hoemann et al., 2009, Farley et al., 1983), alkaline phosphatase is reported to be upregulated by fluidic shear stress both on mRNA and protein expression level in MC3T3-E1 cells (Cartmell et al., 2003, Leclerc et al., 2006), and human osteoblasts (Chen et al., 2015) as well as in human MSCs (Filipowska et al., 2016, Mygind et al., 2007). Cartmell and co-authors reported from increased ALPL gene expression levels at 200 µL/min compared to conditions under lower flow rates. In our perfusion system mRNA levels of ALPL significantly increased compared to static conditions, and higher ALPL levels were induced under tangential compared to sigmoidal configuration in the tendency and at significant level under osteogenic condition at day 10. However, no significant change was achieved at different flow rates (100 and/or 200 µL/min). Compared to results obtained under sigmoidal configuration (Figure 2.1.6D, E) the tangential configuration setting seemed to be also more effective in the upregulation of COL1A1 gene expression (Figure 2.1.6D, E). RUNX2 represents an essential transcription factor involved in osteoblastic differentiation and skeletal morphogenesis (Zeng et al., 2017, Jung et al., 2018). Induction of RUNX2 was detected in osteogenic samples compared to the untreated ones, but perfused configurations had no significant effect on it. Osteocalcin (OCN) expression was significantly upregulated in the tangential configuration setting at day 5 and 10 of perfusion culture (Figure 2.1.8A, C, D).

Taken together, in terms of metabolic activity/proliferation and distribution within the β-TCP scaffolds, we detected significant differences compared to static

conditions, but we did not detect any correlation to fluidic dynamics or to the scaffold position within the used bioreactor. The tangential flow configuration seemed to activate osteogenic gene expressions by JPCs at a higher extent than the sigmoidal configuration set-up.

2.1.4 Materials and Methods

2.1.4.1 Isolation and Expansion of Jaw Periosteal Cells (JPCs)

The jaw periosteal tissue of three donors was obtained during routine surgery after informed written consent (approval number 6182017BO2 from the local ethics committee). The tissue (≤1 cm^2) was cut into small pieces and washed with Dulbecco's phosphate buffered saline (DPBS, Lonza, Basel, Switzerland). Then the fragments were enzymatically digested by 1500 U/mL collagenase (Sigma-Aldrich, Darmstadt, Germany) in DMEM/F12 medium for 2 h at 37 °C. After digestion, the cells were centrifuged, and cultured with DMEM/F12, containing the GlutaMAX supplement (Thermo Fisher Scientific, Waltham, MA, USA), 10% fetal bovine serum (Sigma-Aldrich, Darmstadt, Germany), 1% penicillin/streptomycin (Lonza, Basel, Switzerland), and 1% amphotericin B (Biochron GmbH, Berlin, Germany) at 37 °C in a humidified incubator. After 2 weeks of culture, JPCs were harvested for further expansion. The JPCs derived from 3 donors (two donors were 74 and one donor was 80 years old) of passage 5 were used in the experiment and culture medium was changed every other day.

2.1.4.2 Cell Seeding of β-TCP Scaffolds

The β-TCP scaffolds (Curasan AG, Kleinostheim, Germany) were soaked in culture medium for 1 h in low binding polypropylene 96-well plates before cell seeding. The JPCs were detached from the culture flasks with TrypLE Express (Thermo Fisher Scientific, Waltham, MA, USA) after reaching 80% confluency and resuspended in culture medium at a concentration of 1×10^6 cells/mL. The medium was aspirated from the scaffolds and 50 µL of cell suspension (5×10^4 cells) per scaffold was added. After 2 h of incubation, additional 150 µL of culture medium was added to the cell-seeded scaffolds, resulting in 200 µL final volume. For osteogenic differentiation, JPC-seeded scaffolds were cultured with

osteogenic (OB) medium containing DMEM/F12, 10% FBS, 1% penicillin/streptomycin, 1% amphotericin B, 100 µM ascorbic acid 2-phosphate, 10 mM β-glycerophosphate and 4 µM dexamethasone (Sigma-Aldrich, Darmstadt, Germany) for the indicated time periods.

2.1.4.3 Cultivation and Configuration of the Perfusion Bioreactor

The double flow bioreactor (LB2, IVTech S.r.l., Ospedaletto, Italy), contains two chambers, with two flow inputs and outputs respectively (Figure 2.1.1A, B). The JPC-seeded scaffolds were placed in the upper chamber of the bioreactor on a porous nylon mesh (Merck, Darmstadt, Germany) with a pore size of 100 µm. Different set-ups of tangential and sigmoidal configurations (Figure 2.1.1A, B) with flow rates of 100 and 200 µL/min were applied (T100, T200, S100, and S200). JPC-seeded scaffolds cultured in a 24-well plate under control (CO) or osteogenic (OB) medium were used as controls for static conditions.

2.1.4.4 Cell Metabolic Activity Assay

The JPC-seeded scaffolds were cultured within the bioreactor under the indicated flow rate and flow configuration. After 1, 3 and 5 days of culture, JPC-seeded scaffolds were placed in a 96-well plate and incubated with 20 µL substrate (EZ4U, Biozol, Eching, Germany) and 200 µL culture medium for 2.5 h at 37 °C in a humidified incubator. 150 µL mixture of substrate and culture medium was pipetted into a fresh well, and the absorbance at 450 nm was measured using a microplate reader (Biotek, Bad Friedrichshall, Germany).

2.1.4.5 Crystal Violet Staining and Quantification

JPC-seeded scaffolds cultured under different conditions were fixed with 4% formaldehyde (Otto Fischar GmbH, Saarbrücken, Germany) for 20 min and then washed with PBS twice. 0.1% crystal violet dye (Sigma, St. Louis, MO, USA) was used to stain the fixed scaffolds for 20 min at room temperature. The scaffolds were washed with distilled water overnight on a shaker and dried at room temperature. The dye which was bound by the scaffolds was dissolved in 200 µL methanol for 30 min on a shaker. 150 µL of eluant was pipetted to a fresh well,

and absorbance was measured at a wavelength of 550 nm with a microplate reader (Biotek, Bad Friedrichshall, Germany).

2.1.4.6 Scanning Electron Microscope (SEM) Analysis of JPC-Seeded Scaffolds

The JPC-seeded scaffolds were fixed with 4% glutaraldehyde (Applichem, Darmstadt, Germany) in 0.1 M sodium cacodylate (Merck, Darmstadt, Germany) buffer for 30 min and washed twice with PBS. All scaffolds were dehydrated with an ascending ethanol series (50%, 70%, 80%, 90% and 100%), liquids were completely removed by the critical point drying method and sputtered with a thin gold/palladium layer. The surface of the gold/palladium coated scaffolds was visualized with a scanning electron microscope (Carl Zeiss, Oberkochen, Germany). Scaffold porosities were measured in the 200× images using the quantification tools of the ImageJ software 1.53.

2.1.4.7 Embedding and Microtome Sectioning of Embedded JPC-Seeded Scaffolds

JPC-seeded scaffolds were fixed with 4% formaldehyde for 30 min, washed twice with PBS, and distilled water, respectively. Then, samples were dehydrated and degreased with an ascending ethanol series (70%, 80%, 96% and 100%) for 15 min, and xylene for 15 min, respectively. Afterwards, all samples were pre-infiltrated with acetone twice for 1h and incubated with solution A of Technovit 9100 (Kulzer, Wehrheim, Germany) overnight at −20 °C. The following day, scaffolds were embedded with nine parts of solution A and one part of solution B in a 5 mL syringe and incubated again at −20 °C overnight. Finally, the syringes containing the scaffolds were incubated at 37 °C in a water bath for 1 h. Embedded scaffolds were cut to 15 µm sections with a microtome before fluorescent cell labeling.

2.1.4.8 Fluorescent Cell Labeling with Sytox Orange

Microtome sections were stained with 1:1000 Sytox orange dye (Thermo Fisher Scientific, Waltham, MA, USA) in PBS for 15 min and washed with PBS. All slices were mounted with Fluoromount-G (Thermo Fisher Scientific, CA, USA) before visualization by a fluorescent microscope (Carl Zeiss, Oberkochen, Germany).

2.1.4.9 Gene Expression Analyses by Quantitative PCR

The JPC-seeded scaffolds were placed in Lysing Matrix D microtubes with ceramic beads (MP Biomedicals, Irvine, CA, USA) and lysis buffer (Macherey-Nagel, Dueren, Germany), and shredded by a FastPrep-24 device (MP Biomedicals, Irvine, CA, USA). RNA isolation from the obtained lysates of JPC-seeded scaffolds was carried out using the NucleoSpin RNA Mini kit (Macherey-Nagel, Dueren, Germany) following the manufacturer's instructions. After RNA quantification using the Nanodrop spectral photometer (Thermo Fisher Scientific, Waltham, USA), 200 ng of RNA was synthesized to cDNA using the SuperScript VILO kit (Thermo Fisher, Darmstadt, Germany) following the manufacturer's instructions. mRNA transcription levels were quantified by a real-time LightCycler system (Roche Diagnostics, Mannheim, Germany). DNA Master SYBR Green 1 (Roche, Mannheim, Germany) and the primer kits (Search LC, Heidelberg, Germany) for the target genes (ALPL, COL1A1, RUNX2, OCN, GAPDH) were used for the PCR reactions. 35 cycles of amplification were carried out for each mRNA. The ratio of target gene copy numbers to those of the housekeeping gene (GAPDH) were calculated.

2.1.4.10 Statistical Analysis

Statistical analysis was conducted for three independent experiments using the GraphPad Prism 8.1.0 software (GraphPad, San Diego, CA, USA), and all the results were presented as means ± SD. All data were tested for normality using the Shapiro-Wilk test. Statistical analysis was performed for comparing results of different culture conditions (dynamic conditions and static condition) using one-way ANOVA followed by Tukey's multiple comparisons tests, for comparing results of osteogenic condition to control using two-tailed Student's t-test. p values ≤ 0.05 were considered significant.

2.1.5 Conclusions

In this study, we tested a perfusion system for the simultaneous cultivation of several JPC-seeded beta-TCP scaffolds, which promotes cell proliferation and enhances osteogenic differentiation. Perfusion conditions stimulated cell growth

on β-TCP scaffolds independently of the flow configuration and applied flow rates. The tangential configuration of the bioreactor seemed to up-regulate JPC gene expressions at a higher extent than the sigmoidal set-up and seems to be more suitable for the used beta-TCP constructs.

2.1 Study II: Secretomes derived from osteogenically differentiated jaw periosteal cells inhibit phenotypic and functional maturation of $CD14^+$ monocyte-derived dendritic cells

This part is a reprint of the following publication:

Wanjing Cen, Felix Umrath, António José Salgado, Siegmar Reinert and Dorothea Alexander. Osteogenically differentiated jaw periosteal cell secretome inhibits phenotypic and functional maturation of $CD14^+$ monocyte-derived dendritic cells. Frontiers in Immunology. 2023; 13:1024509.

Abstract

The jaw periosteal tissue is generally recognized as a suitable source for the isolation of mesenchymal stem cells (MSCs). In previous studies we showed evidence that two- and three-dimensionally cultured jaw periosteum-derived MSCs (JPCs) are able to induce a more immature phenotype of dendritic cells (DCs). To further expand our knowledge of JPCs' immunoregulative function, we investigated the effects of JPC secretomes derived from undifferentiated (CO) or osteogenically differentiated cells (treated with or without dexamethasone: OB+/-D) on $CD14^+$ monocyte-derived DCs (MoDCs). We detected a remarkably reduced formation of MoDC homotypic clusters under the influence of secretomes from osteogenically induced JPCs. Further, significantly decreased numbers of $CD83^+$ cells, up-regulated CD209 and down-regulated CD80, CD86 and CD197 expression levels were detected on the surface of MoDCs. Whereas secretomes from JPCs osteogenically stimulated with dexamethasone significantly enhanced FITC-dextran uptake capacity of MoDCs, the increase by secretomes of JPCs treated without dexamethasone did not reach significance. The analysis of mixed lymphocyte reactions revealed that OB+/-D secretomes were able to significantly reduce the numbers of proliferating $CD14^-$ peripheral blood mononuclear cells (PBMCs) and of proliferating $CD4^+$ T cells. The OB-D secretome significantly promoted the expansion of regulatory $CD25^+$ T cells. Regarding gene expression of MoDCs, remarkably up-regulated mRNA expression of CD209, HLA-DRA, CSF3, IL10 and IL8 was detected when DCs

were cultured in the presence of OB+/-D secretomes. At the same time, secretomes seemed to have an impact in the down-regulation of IFNγ and IL12B gene expression. At protein level, OB+/-D secretomes significantly up-regulated IL-10 and IDO (indoleamine-pyrrole 2,3-dioxygenase) levels whereas IL-12/IL-23p40 levels were down-regulated in supernatants of MoDCs when cultured under the presence of OB+/-D secretomes. Taken together, while secretomes from untreated JPCs had only little effects on the process of maturation of MoDCs, secretomes derived from osteogenically induced JPCs were able to inhibit the phenotypic and functional maturation of MoDCs.

Keywords: mesenchymal stem cells; jaw periosteal cells; osteogenic differentiation; secretomes; $CD14^+$ monocytes; dendritic cell maturation; dextran-uptake; mixed lymphocyte reactions.

2.2.1 Introduction

Mesenchymal stem cells (MSC) are guardians of adult tissue maintenance and generally considered to be weakly immunogenic cells which implement their immunomodulatory functions by producing a plethora of growth factors, cytokines and chemokines (Uccelli et al., 2006, Kim et al., 2005). Bone marrow MSCs suppress different T, B, NK and dendritic cell (DC) functions involved in their maturation, activation and antigen presentation process (Uccelli et al., 2006).

Jaw periosteum-derived cells (JPCs) with their advantages of simple tissue harvesting and cell isolation, represent a highly suitable mesenchymal stem cell source for regeneration purposes in the jaw bone area. In different studies we were able to prove the osteogenic potential of these cells (Alexander et al., 2008, Brauchle et al., 2017, Danalache et al., 2019). The primary function of the immune system is to protect the host from foreign pathogens, but its dysregulation can lead to failure of transplanted organs or in the case of tissue engineering (TE) of implanted TE constructs. Reducing the immune response to implanted cell-seeded constructs may be achieved by choosing a cell source that can prevent activation of the immune system via suppressing the function of antigen-presenting cells (APC). In previous studies, we started with examinations

in terms of the immunogenicity of JPCs and could demonstrate that 2D/3D cultured JPCs suppress monocytic DC maturation in a transwell coculture system (Dai et al., 2018, Dai et al., 2020) and that they are also empowered to regulate THP-1-derived macrophage polarization in a direct and a horizontal coculture in system (He et al., 2021a, He et al., 2021b).

DCs are rare, heterogeneous bone marrow (BM)-derived professional APCs (Steinman and Cohn, 1973), which arise from hematopoietic stem cells through specialized progenitor subsets (Watowich and Liu, 2010). They can be broadly categorized as hematopoietic progenitor cell-derived DCs and monocyte-derived DCs. Monocytes are precursors of macrophages, and can also serve as DC precursors (Shortman and Naik, 2007). Monocyte-derived DCs have been the model for studies of DC development and function (Sallusto and Lanzavecchia, 1994). DCs build an important link between the innate and adaptive immune system and are crucial in determining the balance between immunity and tolerance (Matta et al., 2010, Morelli and Thomson, 2007, Maldonado and von Andrian, 2010). In the steady state, the majority of DCs are in an immature state within tissues where they constantly present self-antigens to T cells but lack adequate co-stimulatory ability, deliver inhibitory and produce tolerance-promoting cytokines, such as IL-10 (Morelli and Thomson, 2007) and maintain self-tolerance (Steinman et al., 2003a, Steinman et al., 2003b, Steinman and Nussenzweig, 2002). Further, immature DCs promote T cell deletion and/or expansion of regulatory T cells (Dhodapkar and Steinman, 2002, Dhodapkar et al., 2001), inducing peripheral tolerance. When activated, immature DCs recognize danger signals and undergo further maturation (Kaisho and Akira, 2001). Mature DCs lose their antigen-capturing and obtain an antigen-presenting combined with the T cell co-stimulatory ability, thereby migrate in the following step to the lymph nodes, and stimulate T cells (Pierre et al., 1997).

Toward the development of cell-free therapeutic strategies for regenerative medicine, the usage of MSC-sourced secretome receives more and more awareness. Compared to the difficulties associated with the transplantation of living and proliferating cell populations in terms of embolism, transmission of

infectious diseases or immune incompatibility, secretomes are safer and dosage and potency/storage can be evaluated in a similar manner to that of pharmaceuticals (Vizoso et al., 2017). The aim of the present study was to investigate whether JPC-secreted factors are efficient enough to inhibit DC activation/maturation. Since for bone tissue engineering purposes osteogenically differentiated MSCs are commonly used, we compared the effects emanating from both undifferentiated and osteogenically induced JPCs. Dexamethasone is typically supplemented to the osteogenic differentiation medium of MSCs. However, our previous study has shown that dexamethasone is not indispensable for the osteogenic differentiation of JPCs when the medium was supplemented with human platelet lysate (hPL) instead of fetal calf serum (FCS) (Wanner et al., 2017). Therefore, we analyzed the effects of JPC secretomes from untreated and osteogenically induced cells with and without dexamethasone on the morphology, phenotype and function of MoDCs.

2.2.2 Materials and Methods

2.2.2.1 Isolation and culture of jaw periosteal cells (JPCs)

JPCs obtained from three donors were included in this study after the approval (number 618/2017BO2) from the local ethics committee. Jaw periosteal tissue was extracted during routine surgery after obtaining written informed consent and JPCs were isolated as mentioned previously (Umrath et al., 2019). JPCs were cultured in DMEM/F-12+GlutaMAX medium (Gibco, Waltham, MA, USA) supplemented with 10 % human platelet lysate (hPL, PL BioScience GmbH, Aachen, Germany), 1 % penicillin-streptomycin (Pen-Strep, Lonza, Basel, Switzerland) and 1 % amphotericin B (Biochrom, Berlin, Germany). In previous works, we published minimal criteria fulfillment and tri-lineage differentiation potential of JPCs (Wanner et al., 2017, Umrath et al., 2019, Umrath et al., 2020).

2.2.2.2 Osteogenic differentiation of JPCs

The cell culture flasks and plates were coated with 0.1 % gelatin from bovine skin (Sigma-Aldrich, St. Louis, MO, USA) prior to osteogenic differentiation in order to allow better JPC adherence and avoid detachment from the culture flasks during

long-term incubation. For osteogenic differentiation, JPCs were cultured in osteogenic medium (DMEM/F-12+GlutaMAX medium, 10 % hPL, 1 % Pen-Strep, 1 % amphotericin B, 100 µM L ascorbic acid 2-phosphate (Sigma-Aldrich, St. Louis, MO, USA), 10 mM β glycerophosphate (AppliChem, Darmstadt, Germany) supplemented with or without 4 µM dexamethasone (Sigma-Aldrich, St. Louis, MO, USA) for 10 days for secretome collection or for 15 days for the analysis of the JPC osteogenic potential.

2.2.2.3 JPC secretome collection and enrichment

For secretome collection, 0.1 % gelatin was used to coat the 175- cm^2 cell culture flasks and incubate at 37°C for at least 30 min. JPCs of passage 5 were seeded onto the coated cell culture flasks at a cell density of 1 million cells per flask. After overnight incubation, medium was changed to osteogenic medium with (OB+D) or without dexamethasone (OB-D). Cells cultured in normal medium (CO) were used as control. After 10-day of cultivation, cells were washed with PBS (Lonza, Basel, Switzerland) three times and 37 mL DMEM/F12 medium containing 1 % Pen-Strep and 1 % amphotericin B were added to the JPCs for accurately 24 h. Secretome was collected from the flasks and centrifuged at 600 g to remove cell debris. 34 mL of supernatant were collected and shock frozen in liquid nitrogen instantly and stored at -80 °C. After thawing, the secretome was concentrated 100-fold by centrifugation using Vivaspin 20 (Sartorius, Goettingen, Germany) as recommended by the manufacturer. Collected and enriched secretomes (S_CO, S_OB+D, S_OB-D) from three JPCs donors were pooled before use for further experiments. The concentration of JPC secretomes was determined using the Qubit protein assay kit (Invitrogen, Waltham, MA, USA) and the Qubit 3.0 fluorometer (Thermo Fisher Scientific, Waltham, USA) following the manufacturer's instructions. 100-fold basal DMEM/F12 medium was used as a blank. In Table 2.1 the measured concentrations of the 100-fold concentrated JPC secretomes (S_CO, S_OB+D, S_OB-D) are given.

Table 2.1. Protein concentration of 100-fold concentrated JPC secretomes

		S_CO	S_OB+D	S_OB-D
Concentration (mg/mL)	1st thawing	0.93 ± 0.03	0.92 ± 0.02	1.04 ± 0.07
	2nd thawing	0.92 ± 0.09 #	0.97 ± 0.05 #	1.16 ± 0.11 #

The aliquots of concentrated secretomes derived from JPCs treated with control medium (S_CO), osteogenic medium with or without dexamethasone (S_OB+D/S_OB-D) stored at -80 °C were thawed before first use (1st thawing) and stored at -20 °C till second use for medium change (2nd thawing). The protein concentration of secretomes was determined using the Qubit protein assay kit and the Qubit 3.0 Fluorometer. 100-fold concentrated DMEM/F12 medium was used as a blank. The data of three independent experiments are shown as means ± SD and compared using paired t test (n=3, # represented no significant difference compared to 1st thawing).

2.2.2.4 Alizarin red staining and OsteoImage mineralization assay of JPCs

After 15 days of osteogenic stimulation, JPCs were fixed with fixation buffer (Biolegend, California, USA) and stained with 40 mM Alizarin red solution (pH 4.2, Sigma-Aldrich) for 20 min. Unbound dye was removed by washing with deionized water and images were taken using an inverted microscope (Leica, Wetzlar, Germany). The stained plates were quantified using alizarin red S staining quantification assay kit (ScienCell, California, USA) following the manufacturer's instructions and photometrical quantification of the alizarin staining was performed at a wavelength of 405 nm using a microplate reader (Biotek, Bad Friedrichshall, Germany). JPCs were further stained for hydroxyapatite detection using the OsteoImage mineralization assay kit (Lonza, Basel, Switzerland) following the manufacturer's instructions. Images were taken using an Axio Observer Z1 fluorescence microscope (Zeiss, Oberkochen, Germany).

2.2.2.5 Separation of $CD14^+$ cells from human peripheral blood mononuclear cells (PBMCs)

PBMCs were isolated from fresh blood collected using S-monovettes with 1.6 mg EDTA/mL (SARSTEDT AG & Co. KG, Nümbrecht, Germany) using the gradient centrifugation with Ficoll-Paque PLUS (Cytiva, Uppsala, Sweden). After extraction of the PBMC fraction and washing three times with PBS, PBMCs were used for further separation of the $CD14^+$ population using the CD14 MicroBeads

kit (Miltenyi Biotec, Bergisch Gladbach, Germany) following the manufacturer's instructions. The obtained $CD14^+$ cells were used for DC differentiation experiments and the fraction of the $CD14^-$ cells was cryopreserved in freezing medium consisted of 45 % RPMI 1640 medium (Gibco, Waltham, MA, USA), 45 % fetal calf serum (FCS, Gibco, Waltham, MA, USA), and 10 % DMSO (Sigma-Aldrich, Darmstadt, Germany), and used for further mixed lymphocyte reactions experiments.

2.2.2.6 Development of $CD14^+$ monocyte-derived dendritic cells (MoDCs)

$CD14^+$ monocytes were seeded at a density of 10^6 monocytes/mL in 24-well plates and cultured for 6 days in RPMI 1640 medium containing 10 % FCS, 1 % pen-strep and 1 % amphotericin B, supplemented with the DC cytokine cocktail (40 ng/mL IL-4 and 100 ng/mL GM-CSF (Sigma-Aldrich, Darmstadt, Germany) for the first 5 days; 40 ng/mL IL-4, 100 ng/mL GM-CSF, 10 ng/mL TNF- α, 10 ng/mL IL-1β, 10 ng/mL IL-6 (Tebu Bio, Offenbach, Germany), and 1 µg/mL PGE2 (Bio Trend, Köln, Germany) for the last 24 h). Four different DC populations were generated, three of them were treated with 5-fold or 10-fold concentrated JPC secretomes (from untreated JPCs (S_CO), and from osteogenically induced JPCs with (S_OB+D) or without (S_OB-D) dexamethasone stimulation for 10 days). The fourth DC population served as a control sample without additional secretome supplementation (control).

2.2.2.7 Flow cytometry analysis of cell surface marker expression on MoDCs

$CD14^+$ monocytes and the four differentiated DC populations were collected and analyzed for surface marker expression by flow cytometry. 2×10^5 cells per sample were blocked with 20 µL 10 % Gamunex (human immune globulin solution, Talecris Biotherapeutics, Germany) in FACS buffer (PBS, 0.1 % BSA, and 0.1 % sodium azide) for 15 min on ice. Cells were incubated on ice with PE-labeled mouse anti-human CD83 (BD Pharmingen, New Jersey, USA, clone: HB15e, isotype: IgG1κ), CD80 (clone: 2D10, isotype: IgG1κ), CD86 (clone: BU63, isotype: IgG1κ), and CD1a (clone: HI149, isotype: IgG1κ), and APC-labeled mouse anti-human CD209 (clone: 9A9E8, isotype: IgG2aκ), HLA-DR (clone:

L243, isotype: IgG2aκ), CD14 (clone: M5E2, isotype: IgG2aκ) and CD197 (clone: G043H7, isotype: IgG2aκ) antibodies (BioLegend, San Diego, USA) for 15 min in dark. For the isotype controls, PE-labeled IgG1 and APC-labeled IgG2a antibodies (Biolegend, San Diego, CA, USA) were used. After washing with FACS buffer twice, cell pellets were resuspended in 200 µL FACS buffer and analyzed using the Guava easyCyte 6HT-2L device (Merck Millipore, Billerica, MA, USA). The analyzed cells were gated according to their size and granularity (Supplementary Figure 1A, B). All percentages, mean fluorescent intensities and statistical analysis were performed inside the gate, thus excluding cell debris. For data evaluation, the guavaSoft 2.2.3 (InCyte 2.2.2, Luminex Corporation, Chicago, IL, USA) software was used.

2.2.2.8 Analysis of the phagocytic activity of generated DC populations

To measure the phagocytotic activity of the four generated DC populations, cells were resuspended in 100 ml RPMI 1640 medium containing 10 % FCS and incubated with 1 mg/mL FITC-dextran (wt 40000; Sigma-Aldrich, St. Louis, MO, USA) at 37 °C and on ice (negative control) for 60 min. After incubation, cells were washed twice with cold PBS and fixed with fixation buffer (BioLegend, San Diego, USA). The uptake of FITC-dextran by DCs was determined by flow cytometry. The analyzed cells were gated according to their size and granularity (Supplementary Figure 1C). All percentages, mean fluorescent intensities and statistical analysis were performed inside the given gate, thus excluding cell debris. At least 5000 cells per sample were analyzed. For confocal microscopy image acquisition, cells were stained for nuclei using DAPI (Life Technologies, Lima, USA) and spun onto a Shandon Cytospin 4 slide (Thermo Fisher Scientific, Waltham, USA). The slides were examined with a confocal laser scanning microscope system (Leica NS-CT; Leica Lasertechnik, Heidelberg, Germany) fitted with lasers emitting light at 488 and 405 nm.

2.2.2.9 Analysis of T cell stimulatory capacity of generated DC populations

To analyze T cell stimulatory ability of MoDCs generated under the presence of different JPC secretomes, $CD14^-$ PBMCs were thawed 1 day before coculturing

with DCs. Before use, thawed cells were stained with 1 µg/mL propidium iodide (PI, Invitrogen, Waltham, MA, USA) for cell viability by flow cytometry on the same day (day 0) and the day after thawing (day 1), as shown in Table 2.2.

Table 2.2. Percentages of viable $CD14^-$ PBMCs after thawing

	Day 0	Day 1
Viable cell percentage (%)	95.64 ± 1.17	92.12 ± 0.97

Frozen $CD14^-$ PBMCs were thawed one day before use. Cell viability was measured after propidium iodide staining by flow cytometry on day 0 and the second day (day 1) after thawing. The data of three independent experiments are shown as mean ± SD.

On day 1, $CD14^-$ PBMCs were used for further separation of the $CD4^+$ T cells using the $CD4^+$ T cell isolation kit (Miltenyi Biotec, Bergisch Gladbach, Germany) following the manufacturer's instructions. The $CD4^+$ cell fraction was stained with mouse anti-human CD4-PE (clone: M-T466, isotype: IgG1κ, Miltenyi Biotec, Bergisch Gladbach, Germany) and analyzed using flow cytometry. $CD14^-$ PBMCs and $CD4^+$ T cells were firstly labeled with the CFSE cell proliferation kit (Invitrogen, Waltham, MA, USA) following manufacturer recommendations respectively. 2×10^5 CFSE-labeled cells were cocultured (ratio of 1:1) with DCs previously generated under the four different conditions (in the absence of JPC secretome or under the addition of the 3 JPC secretomes) in RPMI 1640 medium containing 10 % FCS in U-bottom 96-well plates for 72 h. $CD14^-$ PBMCs were analyzed by flow cytometry. $CD4^+$ T cells were stained with mouse anti-human CD25-APC (clone: 3G10, isotype: IgG1κ, Miltenyi Biotec, Bergisch Gladbach, Germany) and at least 5000 cells per sample were analyzed by flow cytometry. The monocultured CFSE-labeled cells were used as unstimulated control. The analyzed cells were gated according to their size and granularity (Supplementary Figure 1D-G). The mean fluorescent intensities and statistical analysis were performed inside the gate, excluding cell debris. For data evaluation, the guavaSoft 2.2.3 software and FlowJ 10 (BD, New Jersey, USA) were used.

2.2.2.10 Quantitative gene expression analysis of generated DC populations

The total mRNA of DCs generated under the four different conditions was extracted using the NucleoSpin RNA kit (Macherey-Nagel, Dueren, Germany) as manufacturer recommended. After determining the concentrations of RNA using the Nanodrop One device (Thermo Fisher Scientific, Waltham, USA), 500 µg of RNA was used for cDNA synthesis using the LunaScript RT SuperMix Kit (New England Biolabs, Ipswich, MA, USA). The mRNA expression levels were quantified by the QuantStudio 3.0 device (Thermo Fisher Scientific, Waltham, USA). The LUNA universal probe qPCR master mix (New England Biolabs, Ipswich, MA, USA) and primers of indicated genes (GAPDH (Hs.PT.39a.22214836), CD209 (Hs.PT.58.15573799.g), HLA-DRA (Hs.PT.58.15096946), CCL3 (Hs.PT.58.27485430.g), CSF3 (Hs.PT.58.27044427.g), IL10 (Hs.PT.58.2807216), IL8 (Hs.PT.58.39926886.g), IL4 (Hs.PT.58.46539563.g), TNF (Hs.PT.58.45380900), IFNG (Hs.PT.58.3781960), IL12A (Hs.PT.58.1687020), IL12B (Hs.PT.58.2925830), IL12RB1 (Hs.PT.58.14547172) and IL12RB2 (Hs.PT.58.40444640)) were purchased from Integrated DNA Technologies (Coralville, Iowa, USA) and used for the PCR reactions. PCR amplification of each of the indicated genes was carried out for 40 circles (95 °C 60 sec, 95°C 1 sec, and 60 °C 20 sec). The relative gene expression levels were calculated using the $^{\Delta\Delta}$Ct method and the data presented as $2^{-\Delta\Delta Ct}$.

2.2.2.11 Analysis of immunomodulatory factors in supernatants of generated DC populations and JPC secretomes

IL-10, IDO (Indoleamine-pyrrole 2,3-dioxygenase) and IL-12/IL-23p40 secretion levels in supernatants of generated DC populations and 5-fold concentrated JPC secretomes were quantified using the human IL-10 (assay range: 0.39-25.0 pg/mL), human IDO (assay range: 0.819-200 ng/mL), and human IL-12/IL-23p40 (assay range: 0.0313-2 ng/mL) ELISA kits (Invitrogen, Waltham, MA, USA) according to the manufacturer's instructions. All measurements were performed in triplicates and determined at 450 nm with a microplate reader (Biotek, Bad Friedrichshall, Germany).

2.2.2.12 Statistical analysis

Statistical analysis was conducted for three independent experiments using the GraphPad Prism 8.1.0 software (GraphPad, San Diego, CA, USA). Data were tested for normality using the Shapiro-Wilk test. All results were presented as means ± SD. Results of JPC secretome concentration were compared using paired t test. Results of FACS measurements of cell surface markers on $CD14^+$ monocytes and MoDCs (Control group), and ELISAs were compared using the multiple t test, other results were compared using one-way ANOVA followed by Tukey's multiple comparisons tests. P values < 0.05 were considered significant.

2.2.3 Results

2.2.3.1 Analysis of osteogenic potential of JPCs

The three used JPC donors mineralized in both media (with/without dexamethasone, OB+/-D) containing 10 % hPL after 15 days of osteogenic induction. JPCs cultured in the OB-D medium revealed less calcium deposits as stained by alizarin red (Figure 2.2.1A). The differences between the mineralization in osteogenically stimulated JPCs (OB+/-D) and control wells (CO) were significant. However, differences between OB+D and OB-D conditions were not statistically significant, due to high donor variations (Figure 2.2.1B). Consistent with the results of the alizarin red staining, hydroxyapatite particles of smaller size were detected under OB-D condition by the fluorescent OsteoImage staining (Figure 2.2.1C).

2.2.3.2 Effect of JPC secretome on cell surface marker expression of MoDCs

To analyze the phenotypic features of DC precursors and MoDC, surface markers were detected by flow cytometry. In pre-experiments, we compared the influence of 5- and 10-fold concentrated secretomes on DC maturation (as shown in the supplementary figure 2). Since no significant differences were observed between both groups, we decided to continue the experiments with 5-fold concentrated JPC secretomes. As illustrated in Figure 2.2.2A and Table 2.3, separated $CD14^+$ population weekly expressed CD83, CD80, CD1a, CD209 and CD197, but they show strong CD86, CD14 and HLA-DR surface expression.

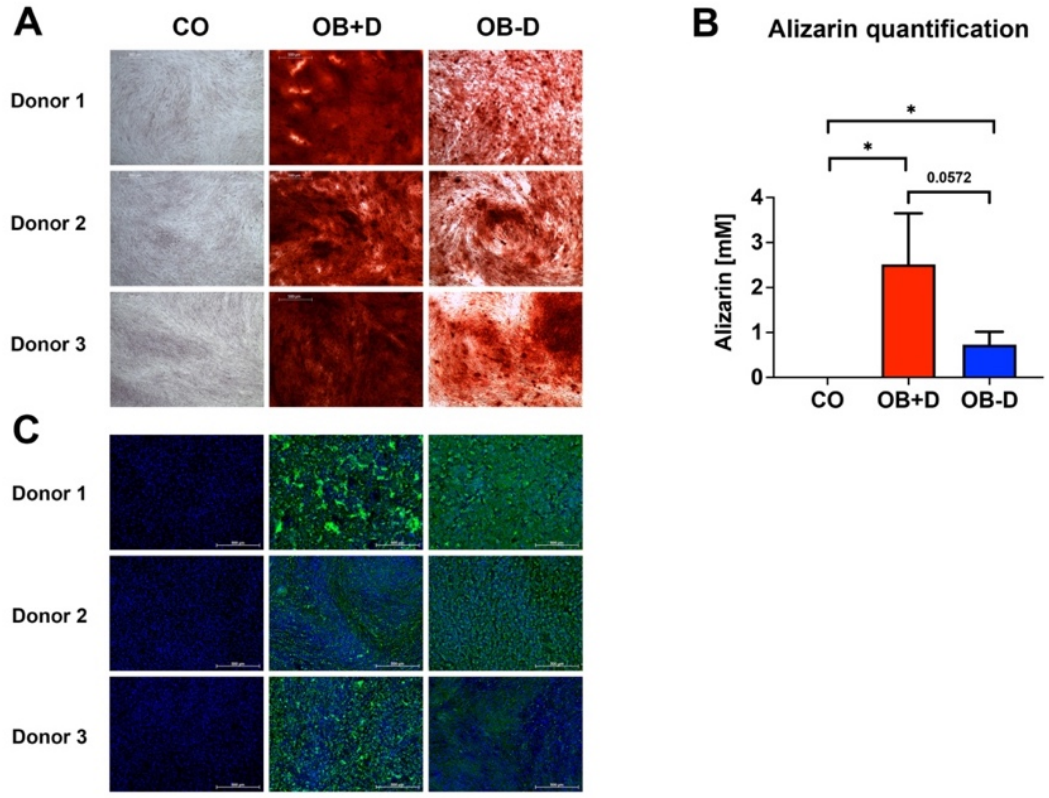

Figure 2.2.1 Mineralization capacity of JPCs from used donors. JPCs (3 donors) were cultured with control medium (CO), osteogenic medium with (OB+D) and without dexamethasone (OB-D) for 15 days. (A) Calcium deposits were stained with alizarin red. (B) Quantification of alizarin staining. Data of three independent experiments are given as means ± SD and compared with each other using student's t test (n=3, *p<0.05). (C) Hydroxyapatite particles were stained using the fluorescent OsteoImage assay (green) and cell nuclei were stained with Hoechst (blue). Scale bars represent 500 µm.

Highly purified $CD14^+$ monocytes (vitality of 97.4% ± 0.6%) were stimulated by DC induction cytokine cocktails. After 6 days, the number of $CD14^+$ cells decreased to 1.7% ± 1.4%. The percentages of CD83, CD80, CD1a, CD209 and CD197 positive cells were 96.8% ± 2.8%, 98.7% ± 0.7%, 38.8% ± 40.7%, 96.8% ± 1.4% and 95.4% ± 1.4% respectively. Higher expressions of CD86 and HLA-DR were detected on the induced cells compared to their precursors (Table 2.3). Therefore, MoDCs maturation in this study was shown to be efficient. The addition of 5-fold and 10-fold concentrated JPCs secretomes to DCs during the maturation process had no effect on the viability of MoDCs (as shown in Table 2.4).

Table 2.3. Efficiency of $CD14^+$ monocyte-derived DC maturation

Surface markers	Percentages of positive cells (%)		MFI	
	Day 0	Day 6	Day 0	Day 6
CD83	0.7 ± 0.6	96.8 ± 2.8 *	3.6 ± 16.8	36.9 ± 10.2
CD80	0.7 ± 0.7	98.7 ± 0.7 *	19.1 ± 5.2	78.4 ± 5.7 *
CD86	90.9 ± 2.8	98.9 ± 0.6	27.8 ± 4.6	527.2 ± 58.9 *
CD1a	6.6 ± 1.3	38.8 ± 40.7 *	55.3 ± 31.9	122.7 ± 183.5
CD209	2.7 ± 0.9	96.8 ± 1.4 *	39.6 ± 22.9	129.3 ± 30.8
CD197	1.8 ± 2.5	95.4 ± 1.4 *	35.4 ± 7.9	360.9 ± 95.8 *
CD14	97.4 ± 0.6	1.7 ± 1.4 *	69.5 ± 19.2	22.3 ± 11.4
HLA-DR	90.9 ± 0.9	99.6 ± 0.4	17.0 ± 6.5	80.9 ± 12.3 *

After separation of $CD14^+$ cells from PBMCs, the population was analyzed for cell surface markers using FACS (day 0). Cells were further cultured in DC cytokine cocktail for 6 days and analyzed for cell surface markers on day 6. Data of three independent experiments are given as means ± SD and compared using student's t tests (n=3, *$p<0.05$ compared to day 0).

Table 2.4. Percentages of viable DCs generated in the presence of JPC secretomes.

			Addition of JPC secretomes		
	Control	Concentration	S_CO	S_OB+D	S_OB-D
Percentage of viable cells (%)	94.47± 1.23	5-fold	96.76 ± 0.54	94.02 ± 1.54	93.51 ± 2.30
		10-fold	96.78 ± 1.01	93.26 ± 0.67	90.34 ± 3.20

The viability of DCs generated without (control) or in the presence of JPC secretomes (S_CO/S_OB+D/S_OB-D) was determined after propidium iodide staining by flow cytometry. The data of four independent experiments are shown as mean ± SD (n=4).

Significantly decreased number of cells expressing CD83 and significantly increased number of cells expressing CD14 were detected in the S_OB+/-D DC groups compared to surface expression on DCs cultured without secretomes or under S_CO (from untreated JPCs) conditions (Figure 2.2.2B). MoDCs from the S_OB+/-D cell groups expressed significantly lower levels of CD80, CD86 and CD197, and significantly higher levels of CD209 in comparison to those detected under control conditions (without secretome) and S_CO conditions (Figure 2.2.2C, D). MoDCs generated under S_CO condition showed no significant effects on cell surface marker expression. We observed only little differences in induced effects on DC cell surface marker expression when treated with 5-fold and 10-fold secretomes (Supplementary Figure 2). Therefore, 5-fold concentrated secretomes were used for further experiments. The effect of 5-fold secretomes on CD1a and HLA-DR expression was further analyzed. S_OB+D decreased $CD1a^+$ cells compared to number of others but not significantly, due to high donor variations (Figure 2.2.2E). There's no significant difference in HLA-DR expression on cells generated under different conditions (Figure 2.2.2E).

2.2.3.3 Effect of JPC secretome on homotypic cluster formation of MoDCs

As shown in Figure 2.2.3A, large homotypic cell clusters were formed after culturing in DC differentiation cocktail (control) and under the influence of the cocktail additionally supplemented with the JPC secretome of undifferentiated JPCs (S_CO) for 6 days. Only a small number of aggregated cells were observed under the influence of the secretome from osteogenically differentiated JPCs, treated with or without dexamethasone (S_OB+D/S_OB-D). The quantification of the cell cluster size resulted in significantly decreased formation of large DC clusters under the influence of S_OB+D and S_OB-D secretomes. The smallest DC cluster size was detected in the S_OB+D group. However, differences to the S_OB-D did not reach significance and were just as little as between of the Control and S_CO groups (Figure 2.2.3B). In terms of cell shape, MoDCs showed a characteristic morphology in the Control and S_CO groups with numerous dendrites and a round and "tree-like" shape. Some adherent cells in non-round shape were observed in the S_OB+/-D groups (black arrows).

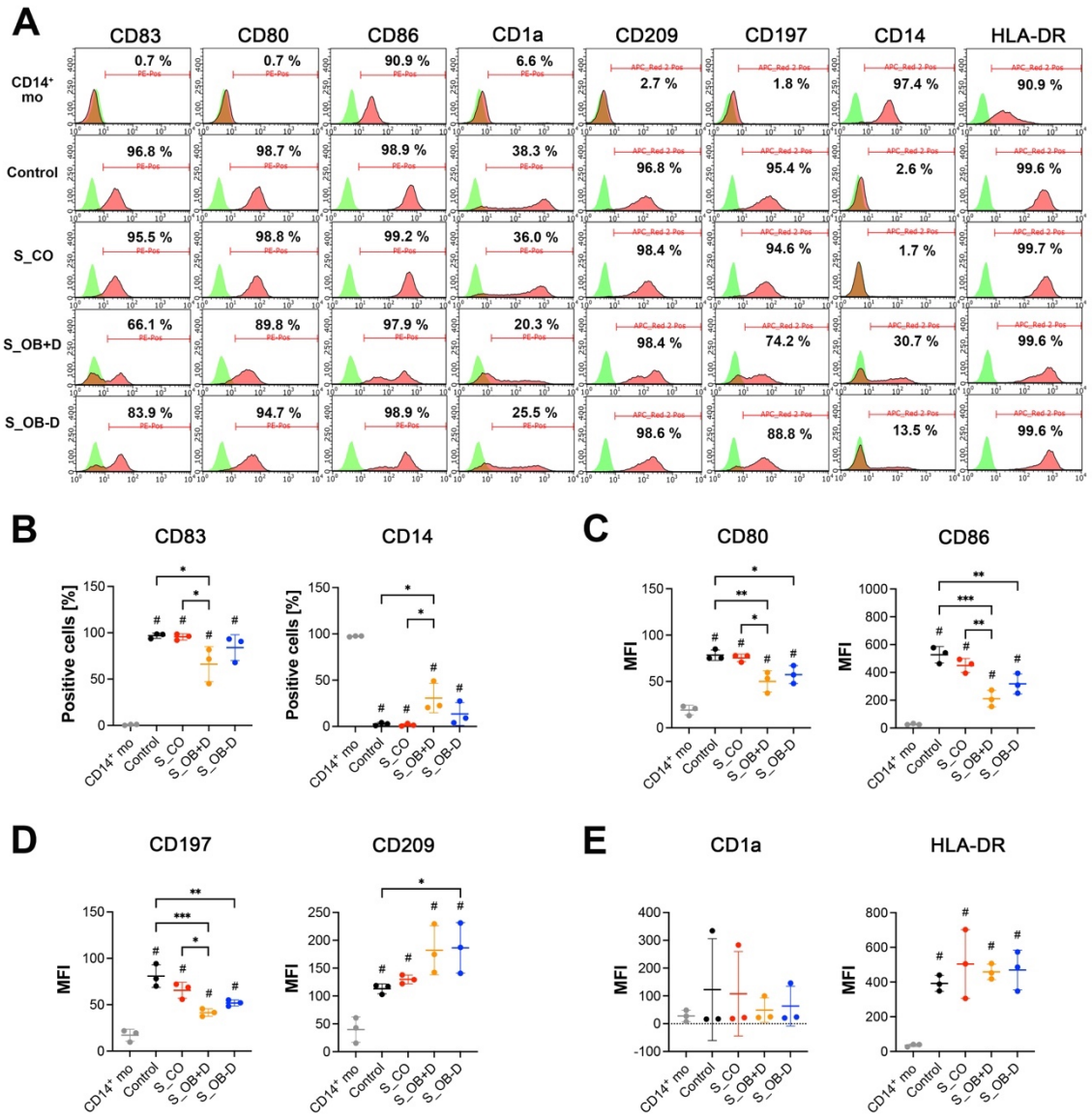

Figure 2.2.2 Cell surface marker expression of CD14⁺ monocytes and DCs generated by various treatments. (A) Flow cytometry analysis (FACS) of cell surface markers on CD14⁺ monocytes (CD14⁺ mo) and DCs generated without (control) or in the presence of JPC secretomes derived from untreated (S_CO), and osteogenically induced cells with or without dexamethasone (S_OB+D/S_OB-D. Representative results from three independent experiments are given. Mean frequencies calculated from three independent experiments are given in each histogram. (B) Percentages of CD83 and CD14 positive cells. (C-E) Median fluorescence intensities (MFI) of CD80, CD86, CD197, CD209, CD1a and HLA-DR expression. Data of three independent experiments are given as means ± SD and compared using one-way ANOVA followed by Tukey's multiple comparisons tests (n=3, *p<0.05, **p<0.01, ***p<0.001; # p< 0.5 compared to CD14⁺ mo).

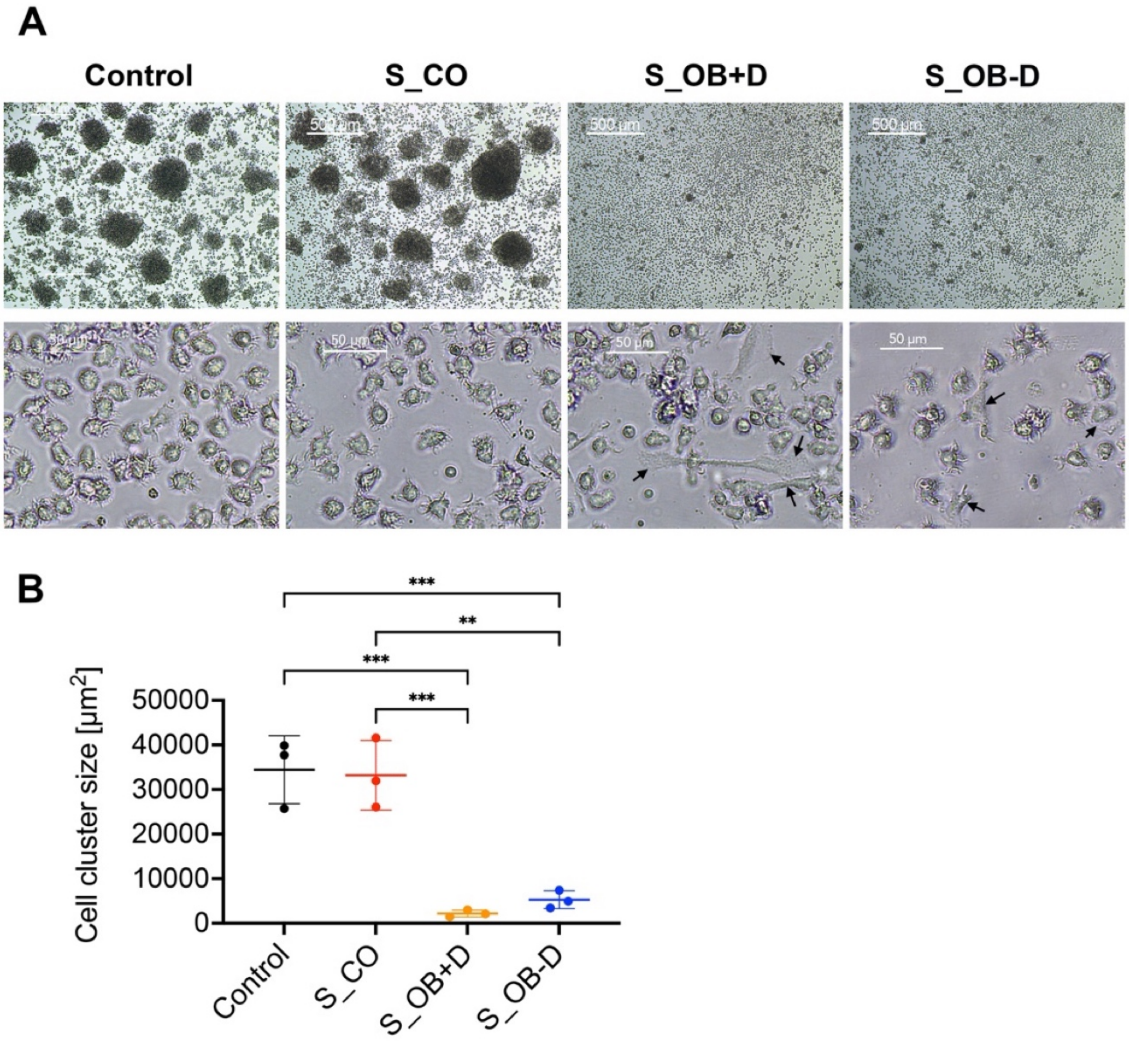

Figure 2.2.3 Effects of JPC secretomes on the homotypic cluster formation and the morphology of MoDCs. $CD14^+$ monocytes were cultured with DC cocktails for 6 days (control). 5-fold concentrated secretomes of JPCs treated with control medium (S_CO), osteogenic medium with or without dexamethasone (S_OB+D/S_OB-D) were added to the DC induction cocktail respectively. (A) Representative microscopic images of three independent experiments (scale bars represent 500 and 50 µm respectively). Black arrows are pointing at adherent cells in non-round shape. (B) Quantification of cell cluster size using ImageJ. Results of three independent experiments are given as means ± SD and compared using one-way ANOVA followed by Tukey's multiple comparisons tests (n=3, **p<0.01, ***p<0.001).

2.2.3.4 Effect of JPC secretome on dextran uptake activity of MoDCs

MoDCs generated without the addition of secretomes or in the presence of different JPC secretomes were compared in terms of their phagocytic activity by testing their ability for FITC-dextran uptake. S_OB+/-D developed MoDCs both showed phagocytic ability (Figure 2.2.4A). The percentage of dextran-positive

cells was significantly increased in the S_OB+D compared to the Control and S_CO DC groups, whereas a clearly increased trend of dextran-positive cells was also detected in the S_OB-D DC group without reaching significance (Figure 2.2.4B, C). Figure 2.2.4D show representative microscopic images of green fluorescence FITC-dextran uptake mainly in DCs generated under the influence of secretomes from osteogenically induced JPCs.

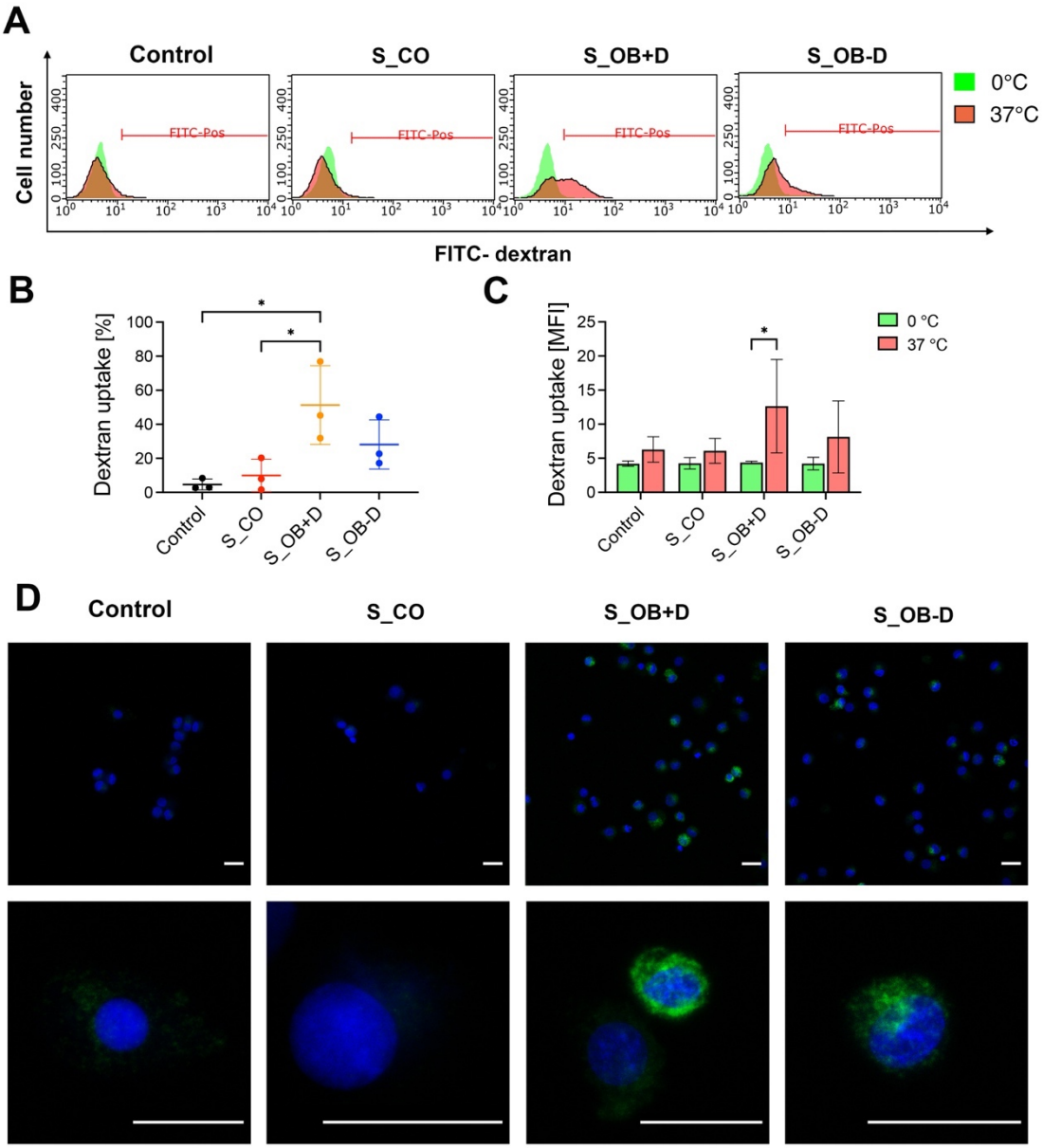

Figure 2.2.4 Effects of JPC secretomes on the dextran uptake ability of maturated MoDCs. DCs generated by indicated treatments (without secretomes or after the addition of 5-fold concentrated JPC secretomes) were incubated with 1 mg/mL FITC-dextran either on ice (0 °C) or within an incubator (37 °C) for 1 hour and analyzed by flow

cytometry and fluorescence microscopy. (A) Representative FACS graphs of three independent experiments. (B) Percentage of dextran-positive DCs. (C) Mean fluorescence intensity (MFI) of dextran uptake by DCs on ice and at 37°C. Results of three independent experiments are given as means ± SD and compared using one-way ANOVA followed by Tukey's multiple comparisons tests (n=3, *p<0.05). (D) Microscopic fluorescence images of FITC-dextran uptake (green) by DCs. Cell nuclei were stained by DAPI (blue). Scale bars represent 20 µm.

2.2.3.5 Effect of JPC secretome on T cell stimulation ability of MoDCs

To compare the stimulatory ability of differently generated MoDCs on lymphocytes, they were cocultured with autologous CFSE-labeled $CD14^-$ PBMCs for 3 days. After this incubation period, cells mainly gathered in the center of the well bottom under all cultivation conditions. However, cell distribution within the wells where $CD14^-$ PBMCs were cocultured with DCs from S_OB+/-D conditions described a higher spreading beyond the well center, as shown in Figure 2.2.5A. The sizes and densities of formed cell clusters in the well center were shown to be significantly smaller/lower when $CD14^-$ PBMCs were cocultured with MoDCs from the S_OB+/-D groups compared to those from the control and S_CO groups (Figure 2.2.5B, C), indicating fewer proliferating cells in these groups. This result was also confirmed by flow cytometry: significantly lower numbers of proliferating $CD14^-$ PBMCs were detected in the coculture with S_OB+D DCs (Figure 2.2.5D-F), whereas the number of $CD14^-$ PBMCs proliferating cells in S_OB-D coculture condition was also remarkably decreased, but without reaching significance (Figure 2.2.5E, F). Further, purified $CD4^+$ T cells from $CD14^-$ PBMCs (Figure 2.2.5G) were cocultured with differently generated MoDCs for 3 days. In contrast to the results of $CD14^-$ PBMCs, significantly higher percentage of proliferating $CD4^+$ T cells were detected in the S_OB+/-D groups (Figure 2.2.5H). However, both the proportion of the whole $CD4^+$ T cell population and that of proliferating $CD4^+$ T cells significantly decreased in the S_OB+/-D groups (Figure 2.2.5I). The increased percentage of proliferating $CD4^+$ T cells and observed decreased concentration of all $CD4^+$ T cells in the S_OB+/-D groups indicated that $CD4^+$ T cell numbers of parent generation were decreased probably due to cell apoptosis. After CD25 labeling of the $CD4^+$ cell population, we detected the highest ratio of regulatory $CD4^+/CD25^+$ T cells in the cocultures with MoDCs from the S_OB-D secretome group (Figure 2.2.5J, K).

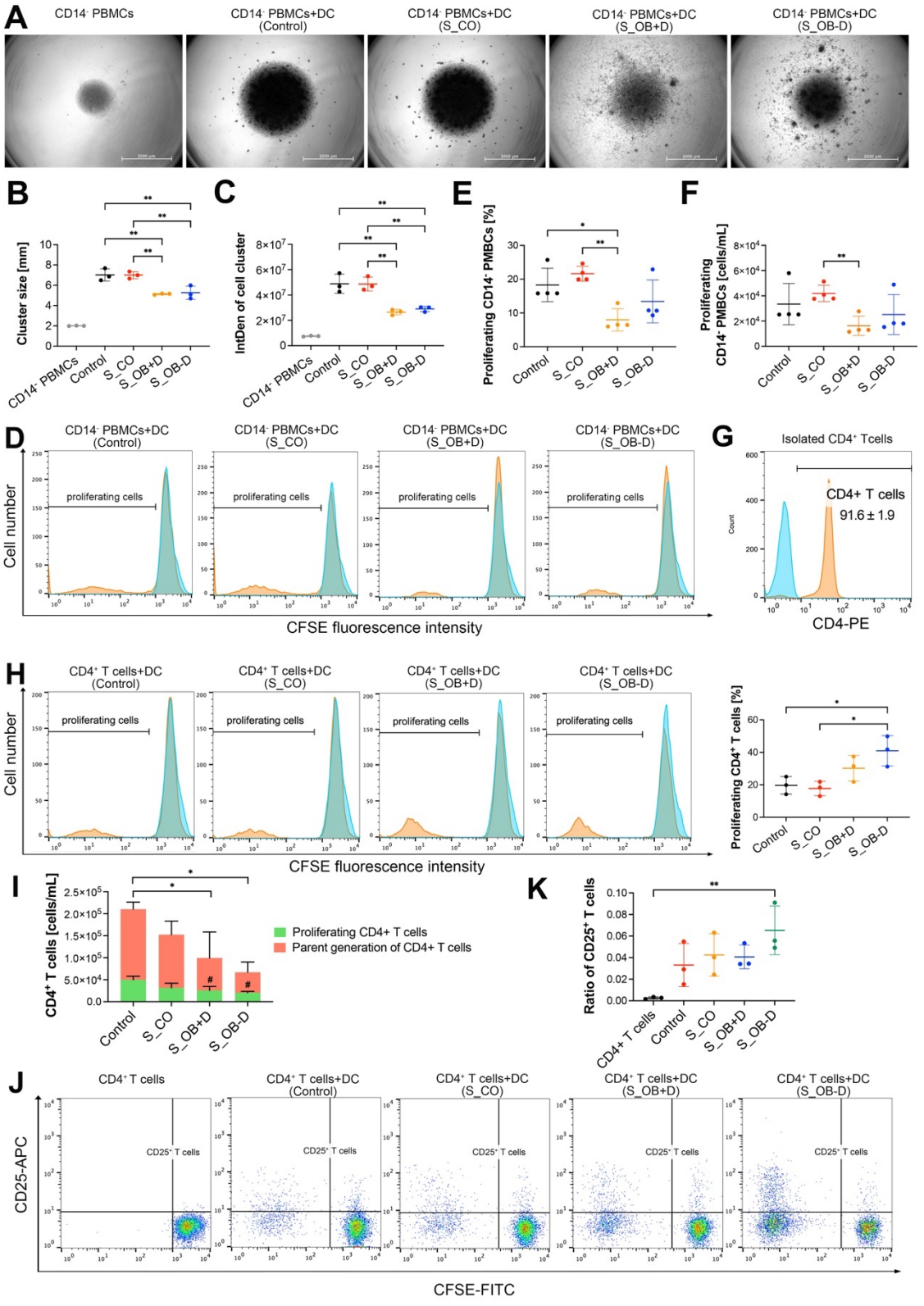

Figure 2.2.5 Effects of JPC secretomes on lymphocytes stimulatory ability of maturated MoDCs. CFSE-labeled CD14$^-$ PBMCs (A-F) and CD4$^+$ T cells (G-K) were cocultured (ratio 1:1) with MoDCs generated under different conditions (without secretomes (control) or in the presence of 5-fold concentrated JPC secretomes) for 3 days. Cell cluster size

and density of the cocultured $CD14^-$ PBMCs was observed by microscopy and quantified by ImageJ. (A) Representative microscopic images of three independent experiments (scale bars represent 2000 µm). Quantification of cell cluster size (B) and integrated density (C) by ImageJ. Data of three independent experiments are given as means ± SD and compared using one-way ANOVA followed by Tukey's multiple comparison tests (n=3, *p<0.05, **p<0.01). (D) Representative histograms of three independent experiments of $CD14^-$ PBMCs. Blue peaks represent monocultured CFSE-labeled $CD14^-$ cells (unstimulated parent generation). Percentage (E) and concentration (F) of proliferating $CD14^-$ PBMCs. Results of four independent experiments are given as means ± SD and compared using one-way ANOVA followed by Tukey's multiple comparisons tests (n=4, *p<0.05, **p<0.01). (G) Purity of $CD4^+$ T cells after isolation using the $CD4^+$ T cell isolation kit (%). (H) Representative histograms of $CD4^+$ T cell stimulatory experiments and percentage of proliferating $CD4^+$ T cells. Blue peaks represent monocultured CFSE-labeled $CD4^+$ T cells (unstimulated parent generation). (I) Concentration of $CD4^+$ T cells after coculturing with differently generated MoDCs. Concentration of all $CD4^+$ T cells and proliferating cells are given as means ± SD respectively and compared using one-way ANOVA followed by Tukey's multiple comparison tests ($^{\#}$ means p<0.05 compared to the control group). (J) Representative dot blots for CD25 expression of monocultured $CD4^+$ T cells or cocultures with differently generated DCs. (K) Ratio of $CD25^+$ T cells within the whole $CD4^+$ T cell population was calculated ($CD25^+$ T cells/$CD25^-$ T cells). (G-K) Data of three independent experiments are given as means ± SD and compared using one-way ANOVA followed by Tukey's multiple comparison tests (n=3, *p<0.05, **p<0.01).

2.2.3.6 Effect of JPC secretome on gene expressions of MoDCs

The mRNA levels of MoDCs generated under the different conditions were quantified by real-time PCR. As shown in Figure 2.2.6, mRNA levels of CD209, HLA-DRA, CSF3 (G-CSF), IL10 and IL8 were significantly up-regulated in the S_OB+/-D DC cell groups compared to those detected in the control group without secretomes (control). CCL3 (MIP-1α) gene expression levels were significantly higher in the S_OB+D but not in the S_OB-D DC group compared to those detected in the control and S_CO cell groups. No significant differences of IL4 and TNF- α levels were detected. MoDCs differentiated under S_OB+/-D conditions expressed extremely low or undetectable IFN- γ levels. Generated MoDCs expressed under all conditions extremely low levels of IL12A (IL-12p35), but they expressed IL12B (IL-12p40). IL12B mRNA levels were significantly reduced in MoDCs which were supplemented with the JPC secretome from untreated and osteogenically induced cells (S_CO, S_OB+/-D). Levels of IL-12 receptor (IL-12Rβ1/IL-12Rβ2) were detected to be significantly reduced only in MoDCs from the S_OB+D cell group in comparison to those detected in the S_CO

group. IL-12Rβ2 gene expression showed in the tendency also a clear downregulation, without reaching significance.

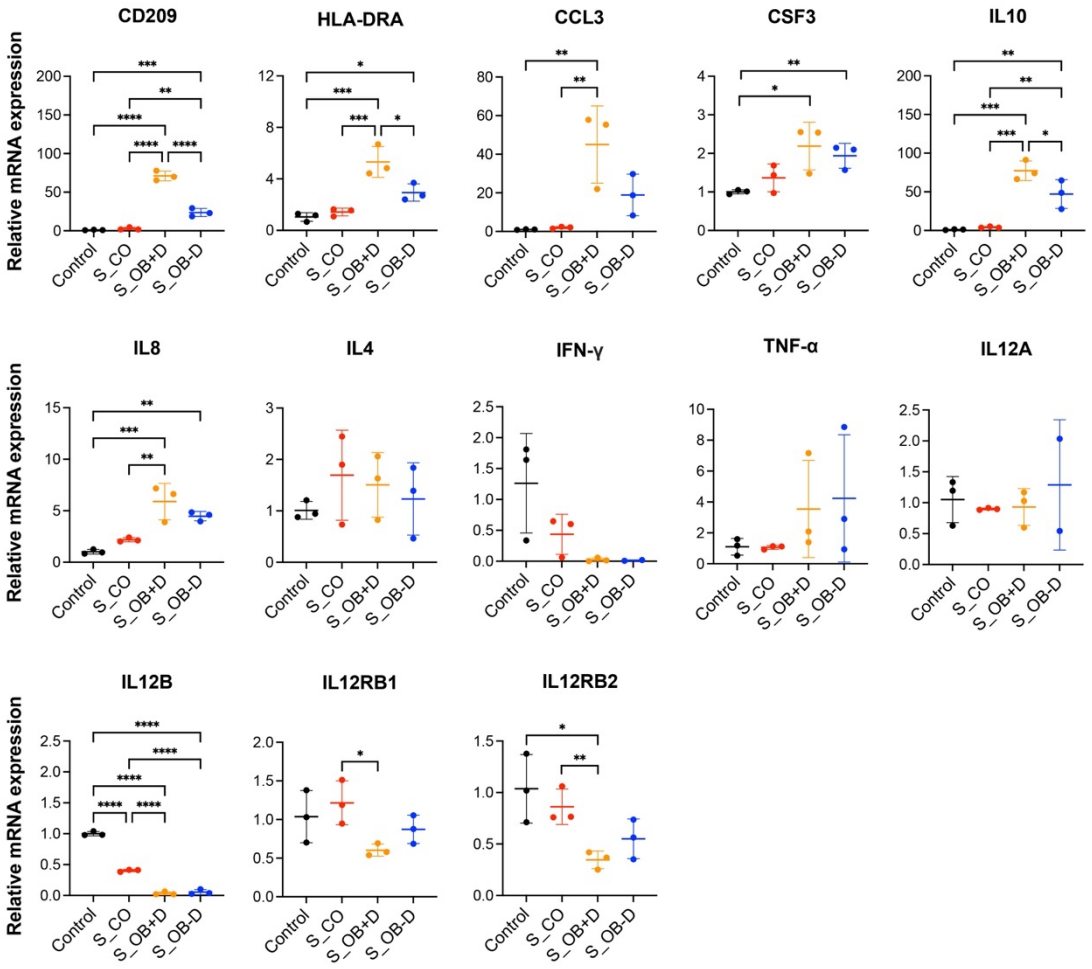

Figure 2.2.6 Effects of JPC secretomes on gene expression levels of maturated MoDCs. The relative gene expression levels of DCs generated by indicated treatments (control or after supplementation with 5-fold concentrated JPC secretomes) were presented as $2^{-\Delta\Delta Ct}$. Mean ± SD values of three independent experiments were calculated and compared using one-way ANOVA and Tuckey's multiple comparison tests (n=3, * p< 0.05, ** p< 0.01, *** p< 0.001, **** p< 0.0001).

2.2.3.7 Effect of JPC secretome on secretory of DCs

To detect key factors of immunosuppression and/or inflammation released by MoDCs generated without or in the presence of secretomes, supernatants of MoDCs and JPC secretomes were analyzed by specific ELISAs. IL-10, IDO or IL-12/IL-23p40 were undetectable in JPC secretomes. As shown in Figure 7, MoDCs generated under S_OB+/-D conditions significantly up-regulated IL-10

protein expression (Figure 2.2.7A) and suppressed their IL-12/IL-23p40 release (Figure 2.2.7C), consistent with the results obtained by quantitative gene expression analysis. Additionally, significantly increased levels of indoleamine 2,3-dioxygenase 1 (IDO) were detected under S_OB+/-D in comparison to control culture conditions, levels under the S_OB-D condition were shown to be significantly higher than IDO levels under the S_OB+D condition (Figure 2.2.7B).

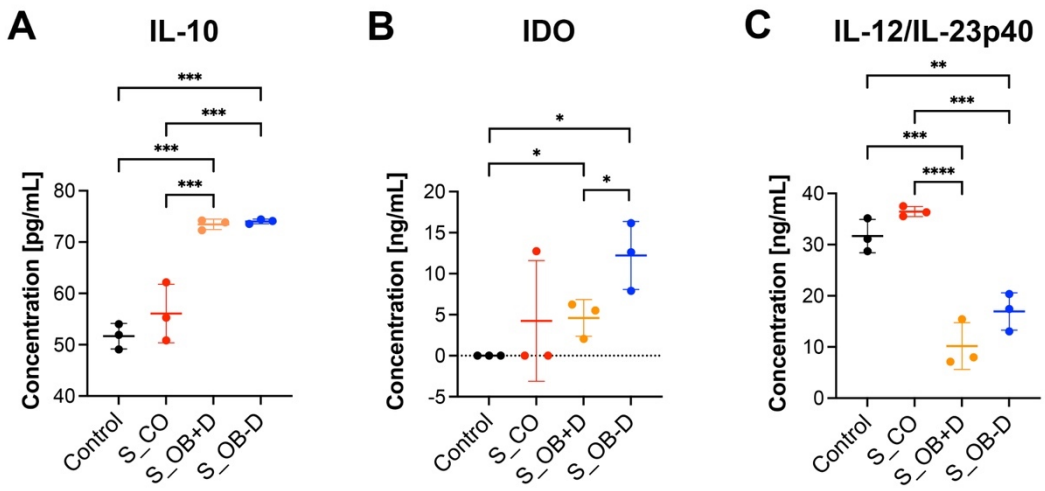

Figure 2.2.7 Effects of JPC secretomes on protein release by maturated MoDCs. (A-C) IL-10, IDO and IL-12/IL-23p40 levels in supernatants from DCs generated under the indicated treatments (control – without secretome or after the addition of 5-fold concentrated JPC secretomes). Quantification was performed using specific ELISAs. Mean ± SD values of three independent experiments were calculated and compared using multiple t tests (n= 3, * p< 0.05, ** p< 0.01, *** p< 0.001, **** p< 0.0001).

2.2.4 Discussion

Originating from experiments focusing on the immunomodulatory function of bone marrow MSCs, considerable knowledge regarding MSC-mediated inhibition of DC maturation and activation has been gained (Beyth et al., 2005, Jiang et al., 2005, Zhang et al., 2004, Ramasamy et al., 2007). For jaw bone regeneration, we are working with MSCs derived from the jaw periosteum tissue. In previous studies we were able to confirm that two- and three-dimensionally cultured JPCs effectively suppressed monocyte-derived DC maturation in a transwell coculture system (Dai et al., 2018, Dai et al., 2020). As stem-cell free therapies are easier to transfer from bench site into the clinical routine, we investigated the effects of secretomes from undifferentiated and osteogenically differentiated JPCs on the

maturation and function of MoDCs. For DC generation, a protocol different from the original one used for our previous studies was chosen starting from the isolation of $CD14^+$ monocytes. Using this highly purified $CD14^+$ cell fraction (97.4% ± 0.6%), generated MoDCs aggregated and formed large homotypic clusters while MoDCs supplemented with secretomes from osteogenically induced JPCs (S_OB+/-D) were reduced in their capability of cluster formation (Figure 2.2.3A). Termeer and colleagues showed evidence that DCs are able to form cell clusters, and reveal characteristics of mature DCs after isolation from formed clusters with high expression of MHC class II, CD80 and CD86 (Termeer et al., 2001). Kubo and co-authors report on DC cluster formation after LPS stimulation, which could be inhibited by tofacitinib, a JAK (Janus kinase) inhibitor resulting in reduced CD80/CD86 surface expression on DCs (Kubo et al., 2014). Homotypic clustering of DCs seems to be closely correlated with the maturation state of DCs and might facilitate intercellular signal transduction or even an exchange of antigenic material between APCs (Delemarre et al., 2001, Lehner et al., 2003). In addition to the reduced capacity of cluster formation, JPC secretomes from osteogenically induced cells significantly down-regulated the expression of B7-costimulatory molecules (CD80/CD86), C-C chemokine receptor (CD197) on maturating MoDCs (Figure 2.2.2C, D and Supplementary Figure 2C-2E) and decreased the number of CD83 expressing MoDCs (Figure 2.2. 2B and Supplementary Figure 2A). CD83 represents an activation marker for antigen presenting cells (Li et al., 2019). The same secretomes were able to increase the number of $CD14^+$ cells (Figure 2.2.2B and Supplementary Figure 2B). This marker is specific for immature monocytes (Ziegler-Heitbrock and Ulevitch, 1993). Secretomes from osteogenically induced JPCs in the absence of dexamethasone showed similar but in tendency lower effects than those from dexamethasone-treated JPCs (Figure 2B-2D and Supplementary Figure 2.2.2A-E). These results indicated that osteogenically differentiated JPC secretomes inhibit phenotypic maturation of MoDCs.

Surprisingly, HLA-DR surface expression was not affected by JPC secretomes although mRNA levels were significantly up-regulated (Figure 2.2.2E and Figure 2.2.6). These opposite results can be explained by the theory that immature DCs

constitutively present self-peptides bound to MHC II molecules, but these complexes are degrading quickly and therefore a more transient expression on the cell surface is observed compared to that on mature DCs (Wilson et al., 2004). Therefore, up-regulation of HLA-DRA mRNA but not up-regulated expression of HLA-DR on the surface of MoDCs supplemented with OB +/- dexamethasone secretomes suggested that these MoDCs were less mature than MoDCs of the control and S_CO groups. Further, there is the possibility that only a DC subset responds to the JPC secretome treatment. This issue should be analyzed in future studies.

CD209 is a cell surface C-type lectin expressed on DCs involved in cell-cell interactions through its capacity to bind ICAM-3 and ICAM-2 (Geijtenbeek et al., 2000a, Geijtenbeek et al., 2000b). CD209 surface expression is usually upregulated in particular on immature DCs (Tassaneetrithep et al., 2003, Bullwinkel et al., 2011). In our study, CD209 surface expression was strongly induced after the DC maturation. We detected a significant increase in CD209 surface expression (Figure 2.2.2D and Supplementary Figure 2F) and mRNA expression (Figure 2.2.6) under the influence of secretomes from osteogenically induced JPCs. Since CD209 is known to be an antigen-uptake receptor for pathogens (Cambi et al., 2003, Colmenares et al., 2002, Ngaosuwankul et al., 2008, Tassaneetrithep et al., 2003), we analyzed the phagocytic ability of MoDCs generated under the different conditions. The same secretome (from dexamethasone-treated JPCs) which led to significantly upregulated CD209 gene expression, simultaneously induced the highest dextran-uptake in MoDCs (Figure 2.2.4B).

Mature DCs lose their antigen-capturing capacity, but they obtain a T cell stimulatory function (Pierre et al., 1997). The coculture experiments performed in our study gave evidence for significant lower cluster formation, density and proliferating $CD14^-$ PBMCs in the presence of JPC secretomes from osteogenically treated JPCs, whereas the highest effect came from secretomes of dexamethasone-treated JPCs (Figure 2.2.5D-F). When $CD4^+$ T cells were applied in the coculture experiment, MoDCs generated with secretomes from

osteogenically treated JPCs significantly reduced the number of proliferating $CD4^+$ T cells and the number of the parental $CD4^+$ T cells (Figure 2.2.5I). CD80/CD86 co-stimulatory involvement for optimal T cell activation was firstly described by Azuma and co-authors (Azuma et al., 1992, Azuma et al., 1993). Blockage of CD80 and CD86 on MoDCs led to a decreased capacity in activation of naive $CD4^+$ T cells (Dilioglou et al., 2003). This could be at least partially the underlying mechanism by which JPC secretomes are able to elicit the observed reduced $CD4^+$ T cell stimulatory function.

In addition, interactions between DCs and helper T (Th) cells during antigen presentation determine the Th cell differentiation fate (Hilligan and Ronchese, 2020). Apart from direct cell-to-cell interactions by costimulatory molecules, mature DCs also exert T cell stimulatory functions by the secretion of pro-/anti-inflammatory cytokines. IL-12p40 is a component of IL-12p70 and IL-23 and a cytokine activating T cells (Cooper and Khader, 2007). Previous studies have reported that IFN-γ (Lighvani et al., 2001) and IL-12 (Macatonia et al., 1995, Zhu et al., 2012) drive the pro-inflammatory Th1 transcriptional program. DC-derived IL-12p40 is required for the activation and maintenance of IFN-γ-producing Th1 cells (Stobie et al., 2000, Macatonia et al., 1995). In our study, DC cocktail supplementation with secretomes from osteogenically induced JPCs led to significant down-regulated IL12B mRNA levels (Figure 2.2.6) and a significant down-regulation of IL-12p40 release by MoDCs (Figure 2.2.7C). IFN-γ mRNA levels were almost completely abolished in the presence of the secretome from osteogenically induced JPCs. These results indicate that JPC secretomes are potentially able to suppress Th1 cell polarization function of MoDCs by an effective down-regulation of the pro-inflammatory cytokines IFN-γ and IL-12p40.

IDO is an enzyme capable to degrade the essential amino acid tryptophan, participating in regulation of T cell immunity by the tryptophan metabolic pathway (Yang et al., 2021). Numerous studies report on the promotion of T cell tolerance and suppression of T cell responses by IDO expressing cells (Mellor and Munn, 2004). In our study, the secretome derived from osteogenically induced JPCs was able to significantly up-regulate IDO expression in MoDCs, and the

secretome from osteogenically induced JPCs in the absence of dexamethasone seemed to be the most powerful supplement in inducing IDO up-regulation (Figure 2.2.7B). Apart from this, the addition of the same secretomes significantly induced the up-regulation of mRNA and protein levels of the anti-inflammatory cytokine IL-10 (Figure 2.2.6 and Figure 2.2.7A). IL-10 is known to inhibit T cell proliferation and to initiate the development of regulatory T cells limiting the development of Th1 or Th2 effector cells (Taga and Tosato, 1992, Couper et al., 2008). The coculture experiments performed in this study revealed that DCs generated with secretomes from osteogenically induced JPCs significantly suppressed proliferation of $CD4^+$ T cells and potentially induce $CD4^+$ T cell apoptosis (Figure 2.2.5I). MoDCs generated with secretome from osteogenically induced JPCs in the absence of dexamethasone significantly increased the number of regulatory $CD25^+$ T cells within the $CD4^+$ T cell population (Figure 2.2.5K). These evidences revealed that MoDCs generated in the presence of secretomes from osteogenically induced JPCs without dexamethasone seemed to act as tolerogenic DCs and induced expansion of regulatory T cells. This finding indicates that JPC secretomes, especially those of osteogenically stimulated cells without dexamethasone could be able to suppress immune responses and induce tolerance after implantations of cell-free engineered constructs.

It has been reported that MIP-1α (macrophage inflammatory protein-1 or CCL3) is not active on mature but immature DCs, mediating their migration into peripheral sites (Yanagihara et al., 1998). In our experiments, we detected a significant upregulation of MIP-1α gene expression in DCs supplemented with JPC secretomes, in particular with those from dexamethasone-treated JPCs. Further MoDC gene expression of other chemokines such as G-CSF (CSF3) and IL-8 were shown to be significantly up-regulated, indicating that JPC secretomes were not only able to up-regulate expression or release of anti-inflammatory cytokines (IL-10) and to downregulate the secretion of pro-inflammatory cytokines (IL-12, IFN-γ, MIP-1α), but also to enhance the production of chemokines.

Strategies were developed for the use of DCs as “positive vaccines” for anti-tumor therapeutic approaches whereby monocytes are isolated from the peripheral blood of the patient, loaded with tumor antigens, and subsequently matured. The activated DCs are then re-infused into the patient where they migrate to the lymph nodes to interact with naïve T cells in order to induce the activation of effector T cells (Vasaturo et al., 2013). Another therapeutic option is to apply tolerogenic DCs as “negative vaccines” in order to induce tolerance against transplanted tissues (Svajger and Rozman, 2014). In our study, we could demonstrate that osteogenic JPC secretomes activate the generation of tolerogenic DCs. This finding indicates that TE constructs colonized with JPCs will probably not induce an inflammatory immune reaction. On the other site, it is conceivable that tolerogenic DCs can be applied together with TE grafts in order to ensure the prevention of immune reactions and to facilitate a favorable integration of the implants into the surrounding tissue.

Taken together, in the present study we examined for the first time the effects emanating from different JPC secretomes on DC maturation of $CD14^+$ monocytes. JPC secretomes seemed to be sufficient to efficiently inhibit MoDC maturation and this ability is linked to their osteogenic differentiation state. Interestingly, JPC secretomes from untreated cells had little to no effect on maturation of MoDCs, and secretomes derived from dexamethasone-treated cells showed stronger effects compared to those from cells osteogenically stimulated in the absence of dexamethasone. Since it is well-known that dexamethasone elicits immunosuppressive effects, it is important to note that the obtained results are not mediated by dexamethasone contained in the culture medium/secretomes. Before secretome collection, dexamethasone dissolved in the culture medium was removed and JPCs were incubated with the basal medium only for the last 24 hours (as mentioned in the section 2.2 of materials and methods).

2.2.5 Conclusion

JPC secretomes from osteogenically induced cells are able to inhibit phenotypic maturation of MoDCs by destabilizing cluster formation and down-regulation of co-stimulatory surface markers. Generated MoDCs show enhanced antigen

uptake ability and suppressed CD4⁺ T cell stimulatory function displaying a more immature phenotype. MoDCs generated in the presence of JPC secretomes from osteogenically induced cells without dexamethasone were able to promote regulatory CD25⁺ T cell expansion. The underlaying mechanism probably involves the up-regulation of IL-10 and IDO, the down-regulation of the co-stimulatory molecules CD80/86 and the down-regulation of the pro-inflammatory IL-12p40 (Figure 2.2.8). These findings indicate that TE constructs colonized with JPCs will probably not induce an inflammatory immune reaction after implantation. In order to ensure the prevention of immune reactions and to facilitate a favorable integration of the implants into the surrounding bone tissue, it is conceivable that tolerogenic DCs generated in the presence of osteogenic JPC secretomes will be applied together with TE grafts. The present study contributes to a better understanding of JPCs' paracrine activity in order to optimize bone regenerative strategies using this cell type.

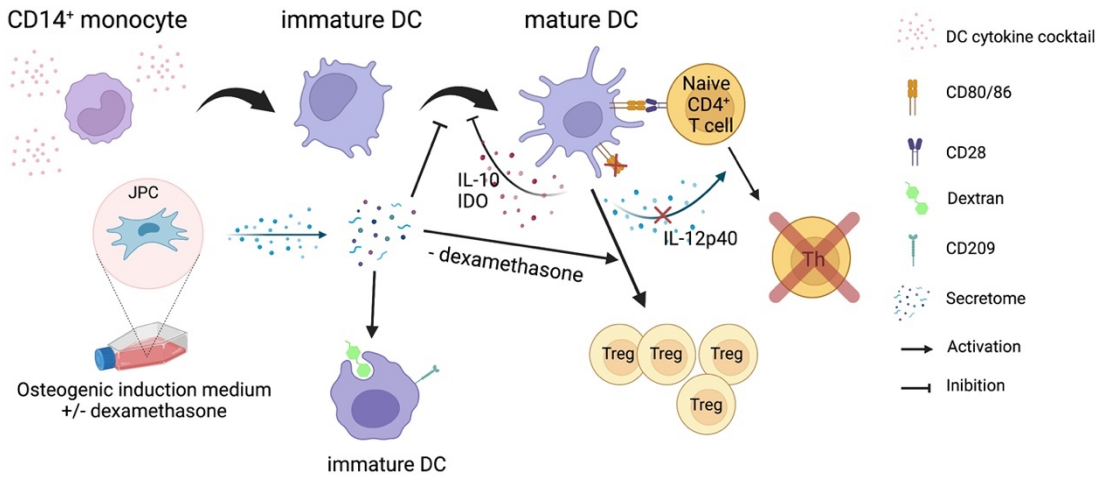

Figure 2.2.8 Summary of the results obtained in the present study. Illustration of the effects of JPC secretomes derived from osteogenically differentiated cells on MoDC maturation and function. Secretomes from osteogenically induced JPCs inhibit the maturation of CD14⁺ monocyte-derived DCs and their CD4⁺ T cell stimulation function, but promote phagocytic function of immature DCs. Secretome from osteogenically induced JPCs in the absence of dexamethasone induced expansion of regulatory T cells. The illustration was created with BioRender.

2.2.6 Supplementary Material

Supplementary Table 1. Information in terms of age and gender of included PBMCs donors. PBMCs for the generation of monocyte-derived dendritic cells differentiation were obtained from healthy donors.

	Age	Gender
Donor 1	26	male
Donor 2	32	female
Donor 3	31	male
Donor 4	29	female

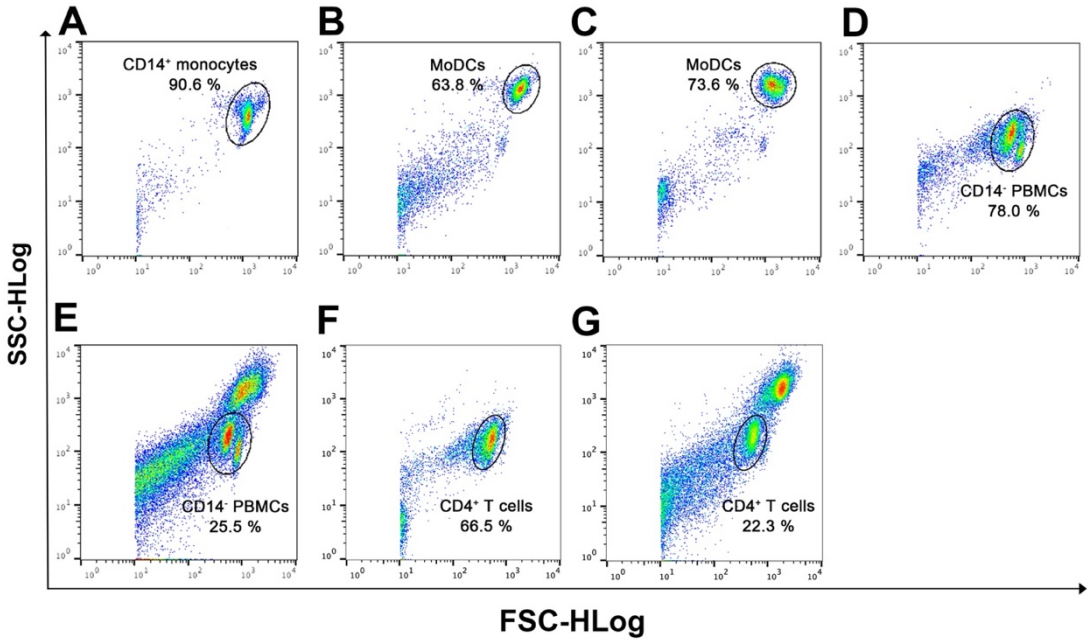

Supplementary Figure 1. Representative gating strategy for flow cytometry analyses. All analyzed cells were gated according to their size and granularity (forward scatter, FSC, cell size vs. side scatter, SSC, granularity) within the marked gate. (A) Dotplot of FSC vs. SSC-HLog for cell surface marker detection of $CD14^+$ monocytes. (B) Dotplot of FSC vs. SSC-HLog for cell surface markers detection of dendritic cells (DCs). (C) Dotplot of FSC vs. SSC-HLog for analysis of the phagocytic activity of DCs. (D-G) Dotplot of FSC vs. SSC-HLog for mixed lymphocyte reactions. (D) Gating of monocultured $CD14^-$ PBMCs. (E) Gating of $CD14^-$ PBMCs cocultured with DCs. (F) Gating of monocultured $CD4^+$ T cells. (G) Gating of $CD4^+$ T cells cocultured with DCs.

All percentages, mean fluorescent intensities and statistical analysis were performed inside the gate, excluding cell debris.

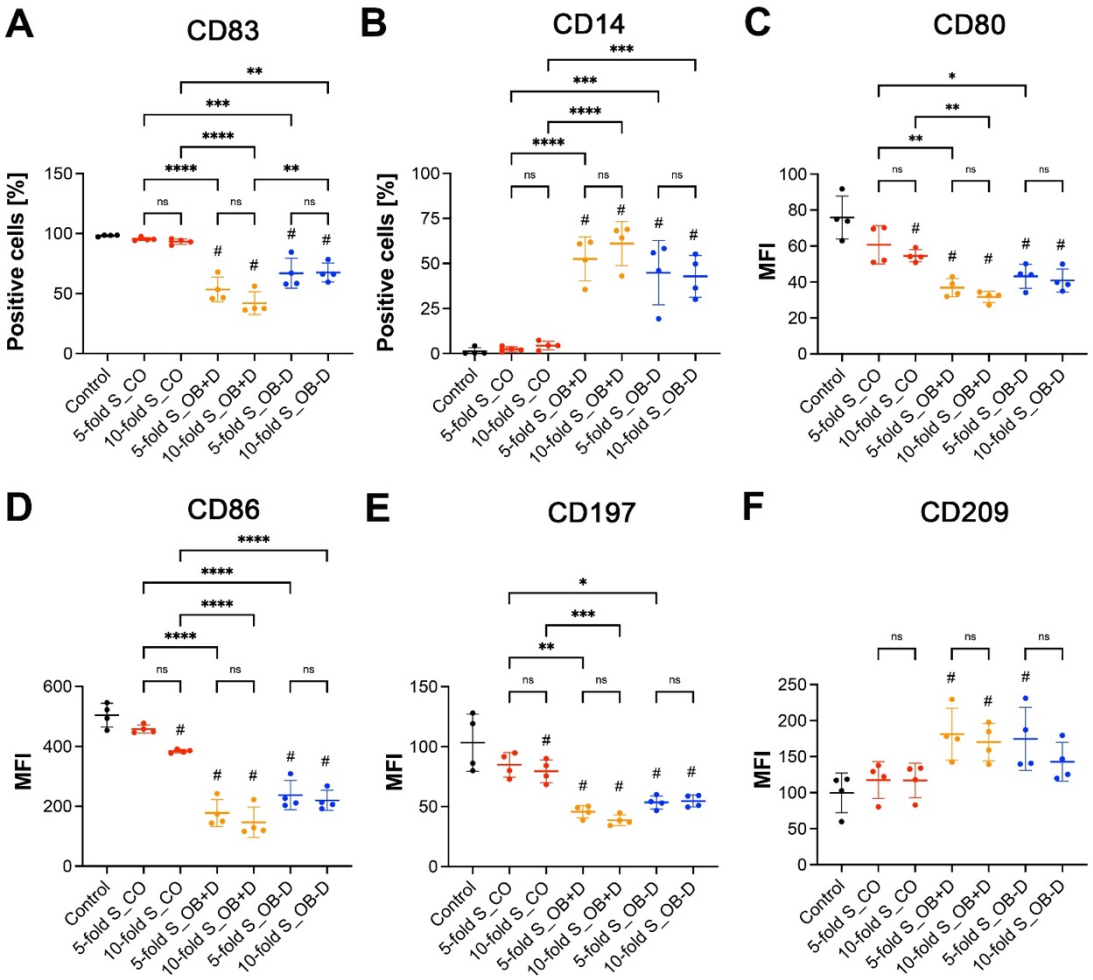

Supplementary Figure 2. Flow cytometry analysis (FACS) of cell surface markers on DCs generated without (control) or in the presence of 5 and 10-fold concentrated secretomes derived from JPCs treated with control medium (S_CO), osteogenic medium with or without dexamethasone (S_OB+D/S_OB-D). (A, B) Percentages of CD83 and CD14 positive cells. (C-F) Mean fluorescence intensity (MFI) of CD80, CD86, CD197 and CD209 surface expression. Data of four independent experiments are given as means ± SD and compared using one-way ANOVA followed by Tukey's multiple comparisons tests (n=4, $^{ns}p>0.05$, *p<0.05, **p<0.01, ***p<0.001, ****p<0.001; $^{\#}$ p< 0.5 compared to the group Control).

3. Discussion

The first goal of this cumulative thesis was to optimize the culture condition for JPCs seeded onto β-TCP scaffolds. In this context, cell functions such as the osteogenic differentiation potential and the penetration depth into the used material should be improved by changing static to dynamic culture conditions. The second part of this thesis aimed to provide evidence for the immunomodulatory capacities of JPCs by investigating their impact on dendritic and helper T cells. To sum up, the present thesis has contributed to an improvement of the application of JPCs in the field of bone tissue engineering and to the elucidation of their immunosuppressive functions. The entire results are discussed subdivided in single points as follows.

3.1 First study: Impact of flow rates and flow configurations on JPCs proliferation within β-TCP scaffolds

The commercial bioreactor applied for study I is a perfusion bioreactor, primarily for bone and cartilage tissues, that work by providing a medium flow to a cell culture, providing oxygen and nutrients through the cell-seeded constructs. However, the medium flow must be optimized for different types of bioreactors and different used cell types in order to achieve sufficient nutrition avoiding cell culture damage. Used flow rates for some of commercially available bioreactors are shown in Table 3.1. There is a widely variation of applied flow rates and only few studies compared a specific range of flow rates. However, in some cases, trends could be detected (Gaspar et al., 2012).

In study I of this cumulative thesis, cell viability and cell densities were remarkably improved under perfusion conditions with both used flow rates (100 and 200 µL/min) after a 5-day culture compared to the static condition (Figure 2.1.1C and Figure 2.1.2B). A study of Cartmell et al. (Cartmell et al., 2003) demonstrated that a high flow rate of 1.0 mL/min significantly increased the number of dead cells and vice-versa lowering the flow rate led to increased amount of viable murine pre-osteoblasts, and a flow rate of 100 µL/min led to the best effect in promoting cell growth. The flow rates applied in study I of this thesis were considered to be

in the range of reported values that induced expansion of bone forming cells (Cartmell et al., 2003, Leclerc et al., 2006).

Table 3.1 Selected perfusion bioreactors, used type of scaffolds, cell type, pore sizes and applied flow rate

Scaffold type	Cell type	Pore size	Flow rate
PLA nonwoven scaffolds	hMSCs	17 μm	0.6 mL/min (Sikavitsas et al., 2005)
Titanium nonwoven fibbers	hMSCs	Not reported	1 mL/min (Holtorf et al., 2005)
	hOBs	250 mm	0.3, 1 and 3 mL/min (Bancroft et al., 2002)
	hOBs	250 mm	0.3 mL/min (Sikavitsas et al., 2003)
	hOBs	29.8 and 65.3 mm	1 mL/min (Datta et al., 2006)
Skelite™	hMSCs	200 to 500 mm	0.1 mL/min (Bjerre et al., 2008)
Coralline hydroxyapatite	hMSCs	200 to 500 mm	0.1 mL/min (Bjerre et al., 2011)
Trabecular bone	MC3T3-E1	645 mm	0.2, 0.1 and 0.01 mL/min (Cartmell et al., 2003)
	hMSCs	600 to 1,000 mm	0.85 mL/min (Grayson et al., 2008)
Biphasic calcium phosphate	hMSCs	> 100 mm	4 mL/min (Janssen et al., 2006)
Polyurethane	MC3T3-E1	200 mm	1 mL/min (Sailon et al., 2009)

However, in the first study of this thesis, quite similar cell viabilities were detected under perfusion conditions with the used flow rates. In addition, the flow configuration types (tangential and sigmoidal setting) did not influence cell metabolic activities and cell numbers of 3D-cultured JPCs. These results could be based on the fact that the size of the used perfusion chambers in study I were much bigger than the size of used JPC-seeded scaffolds, leading to medium flowing around the surface of scaffolds rather than permeating through the whole scaffolds under both flow configuration types. As a result, the medium flow exerted shear stress in a similar laminar manner to the scaffold surface under both configuration types (Figure 2.1.1A, B), leading to similar results under both used configuration types. The fluid-generated shear stress forces of the used flow rates seemed to be very similar or the changes were too little to direct cellular metabolic activities.

Overall, the flow rates of 100 and 200 µL/min applied in the used perfusion bioreactor in this thesis were effective to promote cell proliferation on JPC-seeded β-TCP scaffolds by providing better nutrient supply compared to static culture and generating fluid flow as a stimulation on cell growth. The flow configuration types may not need to be taken into consideration when the goal of promoting cell proliferation of 3D-cultured must be reached in the present perfusion bioreactor.

3.2 Impact of flow rates and configurations on osteogenic differentiation of 3D-cultured JPCs

Bone forming cells control bone formation by responding to the changes of interstitial fluid-generated shear stress through the lacunar-canalicular network (Wittkowske et al., 2016), while the differentiation of their progenitors can be influenced by changes in the fluid static pressure and fluid-generated shear stress within the bone marrow (Gurkan and Akkus, 2008). Therefore, it is one of the essential functions for perfusion bioreactors to mimic such mechanical stimulations for osteogenic progenitors to promote their intercellular matrix production and osteogenic potential. The effect of perfusion flow on the osteogenic potential of bone-forming cells or their precursors observed in some previously published studies are summarized in Table 3.2.

Table 3.2 Effects of fluid flow on the osteogenic potential of different progenitor cell types

Publication	Cell type	Flow rate	Result
(Hosseinkhani et al., 2005)	Rat MSCs	0.2 mL/min	ALP activity ↑, OCN content ↑
(Alvarez-Barreto et al., 2011)	hMSCs	0.1 and 1 mL/min	ALP activity ↑, Calcium deposition ↑
(Cartmell et al., 2003)	MC3T3-E1	0.2 mL/min	ALP, OCN and Runx2 mRNA ↑
(Leclerc et al., 2006)	MC3T3-E1	5 μL/min	ALP activity ↑
(Chen et al., 2015)	hOBs	1 mL/min	ALP, OCN, Col1a1 and Runx2 mRNA ↑
(Filipowska et al., 2016)	hBMSCs	2.5 mL/min	Mineral and collagen production ↑

As an indicator of early osteogenic differentiation (Hoemann et al., 2009, Farley et al., 1983), alkaline phosphatase (ALP) was reported to be up-regulated by shear stress generated by fluid flow of different flow rates on gene expression and protein expression level in murine pre-osteoblasts (Cartmell et al., 2003, Leclerc et al., 2006), human osteoblasts (Chen et al., 2015) and human MSCs (Filipowska et al., 2016, Mygind et al., 2007). Based on the above evidence and resulting data as listed in Table 3.2, there was no doubt that fluid flow in a certain range of flow rates promoted more or less the osteogenic differentiation. With the perfusion bioreactor used for this thesis, the comparison of perfusion conditions and static condition in terms of gene expression levels of osteogenic markers showed that the used settings of perfusion conditions obviously upregulated the levels of ALP, collagen 1α1 and osteocalcin, and the tangential setting was more

capable of osteoinduction than the sigmoidal setting. Among all analyzed markers, ALPL mRNA levels were most affected by the dynamic conditions, with significantly up-regulated level detected under all used dynamic conditions compared to those induced under static conditions, and remarkably higher expression levels were observed under tangential setting in comparison to the sigmoidal setting under osteogenic condition (Figure 2.1.5D). In addition, the tangential setting appeared to be more effective compared to the sigmoidal flow setting with regard to promoting gene expression levels of collagen 1α1 and osteocalcin (Figure 2.1.6D, E and Figure 2.1.8C, D). However, dynamic culture conditions showed only little effect on RUNX2 gene expression.

Overall, the fluid flow generated by the used dynamic settings was able to enhance the osteogenic potential of 3D-cultured JPCs. Compared to the sigmoidal configuration, the tangential configuration is a better setting to promote osteogenic differentiation of 3D-cultured JPCs. The flow rates of 100 and 200 µL/min could be applied both in the present perfusion system as they have very similar stimulatory effects on the osteogenic potential of 3D-cultured JPCs.

3.3 Influence of secretomes collected from osteogenically induce JPCs on the maturation of $CD14^+$ MoDCs and helper T cells

DCs show significant functional and phenotypic heterogeneity. MoDCs generated in vitro after stimulation with GM-CSF and/or IL-4 develop phenotypes or DC functions similar to those found during inflammatory states (Yin et al., 2021). Many DC-specific markers, such as CD83, B7 family of molecules (B7-1 (CD80) and B7-2 (CD86)), C-C chemokine receptor type 7 (CCR7, also known as CD197) and MHC class II molecules, can be used to identify MoDCs that are in the mature state, making possible to distinguish between mature and immature DCs (Li et al., 2019, Azuma et al., 1993, Wilson et al., 2004, Yanagihara et al., 1998). In the second study included in the present thesis, secretomes collected from osteogenically differentiated JPCs remarkably decreased the expression levels of CD80, CD86 and CD197 on MoDCs surface (Figure 2.2.2C, D). Additionally, secretomes derived from JPCs, osteogenically induced with dexamethasone, decreased the number of MoDCs expressing CD83, and increased the number

of cells expressing CD14, a useful marker molecule for immature monocytes (Ziegler-Heitbrock and Ulevitch, 1993). In the tendency, the addition of secretomes derived from JPCs, osteogenically induced without dexamethasone, showed similar but slighter effects compared to those observed after the addition of secretomes derived from osteogenically induced JPCs in the presence of dexamethasone (Figure 2.2.2B).

We also made the observation that secretomes collected from osteogenically differentiated JPCs remarkably reduced the formation of cell aggregates and the size of formed DC clusters (Figure 2.2.3A, B). It has been shown that CD154-induced DCs could form cell aggregates, and DCs isolated from these clumps showed the phenotype of DCs in mature state, expressing high levels of MHC class II and molecules of the B7 family on their surface (Termeer et al., 2001). LPS stimulation led to DC aggregate formation after 24 h of incubation, which could be suppressed by the addition of a JAK inhibitor, following in decreased expression levels on DCs surface of molecules of the B7 family (Kubo et al., 2014). Based on the phenotypic properties of clump-derived DCs, it is likely that the formation of DC clumps is closely associated to the mature state of DCs.

Overall, the described results provided evidence that secretomes of osteogenically differentiated JPCs were able to partially inhibit the maturation of DCs in terms of phenotypic properties.

3.4 Influence of secretomes collected from osteogenically induced JPCs on the maturation of $CD14^+$ MoDCs in terms of function

As showed in Figure 3.1, danger signals can drive differentiation of classical mature DCs. The mature DC subset expresses a large amount of costimulatory molecules (CD40, CD80 and 86) and MHC class II molecules on their surface, release pro-inflammatory cytokines, migrate to the peripheral lymph nodes, and activate naive or memory T cells, resulting in T cell expansion and division of helper T cells (Th1, Th2 or Th7) (Kou and Babensee, 2011). During the steady state, the tolerogenic DC subset is naturally actively induced in response to apoptotic cells and self-antigens. The tolerogenic DC subset releases anti-

inflammatory factors and induce T cell anergy, T cell apoptosis and/or regulatory T cells expansion (Morelli and Thomson, 2007).

In the second study of the present thesis, MoDCs generated in the presence of secretomes collected from osteogenically differentiated JPCs significantly decreased the number of both parental and proliferating $CD4^+$ helper T cells (Figure 2.2.5 I). CD80/CD86 costimulatory effects were reported to be involved and required for optimal T cell activation (Azuma et al., 1992, Azuma et al., 1993). Dilioglou and co-authors showed that blockage of CD80/CD86 on MoDCs surface resulted in 24 % and 71 % decrease in naive $CD4^+$ T cell activation respectively (Dilioglou et al., 2003). As mentioned previously, secretomes collected from osteogenically differentiated JPCs remarkably decreased the expression levels of CD80 and CD86 on MoDCs surface. This might be one of the mechanisms by which DCs cultured in the presence of JPCs secretomes remarkably suppressed the proliferation/activation of co-cultured $CD4^+$ T cells.

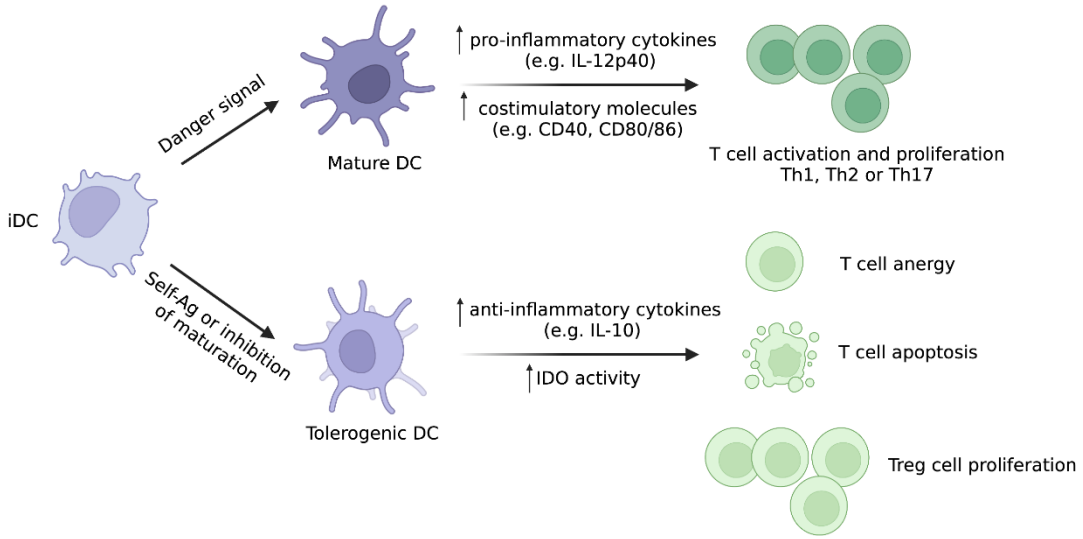

Figure 3.1 Schematic draft of DC subsets developed from immature DCs following different stimuli. The daft is created by BioRender.

In addition to direct cell-cell interaction through costimulatory molecules, mature DCs also stimulate T cells through secreting pro-inflammatory cytokines. Serving as a protein subunit of IL-12p70 and IL-23, IL-12p40 is an inducer of DC migration

and also a cytokine acting on T cells (Cooper and Khader, 2007). IFN-γ (Lighvani et al., 2001) and IL-12 (Macatonia et al., 1995, Zhu et al., 2012) have been reported to drive the Th1 transcriptional program, which promotes the up-regulation of the transcription factor T-bet and IL-12Rβ in CD4 T cells. IL-12p40 derived from DCs has been reported to play an essential role on the induction and maintaining of IFN-γ-secreting Th1 cells (Macatonia et al., 1995, Stobie et al., 2000). In the second study of the present thesis, secretomes collected from osteogenically differentiated JPCs significantly down-regulated IL-12p40 mRNA and protein expression in MoDCs (Figure 2.2.6 and 2.2.7). The IFN-γ mRNA level in MoDCs was detected to be extremely low or even absent in the presence of secretomes collected from osteogenically differentiated JPCs. Based on the obtained results, we postulate that secretomes collected from osteogenically differentiated JPCs potentially suppressed T cell stimulatory effects of MoDCs by decreasing their IFN-γ and IL-12p40 expression levels.

There is considerable evidence supporting the assumption that cells expressing IDO can inhibit T cell activation and induce T cell anergy (Mellor and Munn, 2004). In the second study of the present thesis, secretomes collected from osteogenically differentiated JPCs significantly up-regulated IDO protein levels in MoDCs, and among both used conditions for secretome collection, the one from osteogenically induced JPCs without dexamethasone seemed to be more efficient in promoting IDO release (Figure 2.2.7B). Additionally, secretomes collected from osteogenically differentiated JPCs led to a remarkable increase in IL-10 mRNA (Figure 2.2.6A) and protein levels (Figure 2.2.7). Tega and co-authors demonstrated that 30 years ago that human IL-10 inhibits mitogen-activated T cell proliferation (Taga and Tosato, 1992). DCs exposed to IL-10 can drive the proliferation of regulatory Treg cells, thereby restricting the proliferation of T helper cells (Th1, Th2) (Couper et al., 2008). This mechanism could be an explanation for the inhibitory function on T cell activation by the co-cultured DCs generated in the presence of secretomes collected from osteogenically differentiated JPCs. Furthermore, this finding might also be one of the mechanisms by which JPC secretomes collected from osteogenically induced

cells without dexamethasone significantly promoted $CD25^+$ Treg cell proliferation by co-cultured MoDCs (Figure 2.2.5K).

3.5 Influence of secretomes collected from osteogenically induced JPCs on the function of immature MoDCs

The antigen- (Ag) uptake ability of DCs is associated to the immature DC phenotype (Wilson et al., 2004). As an Ag-uptake receptor for some pathogens (Tassaneetrithep et al., 2003, Cambi et al., 2003, Colmenares et al., 2002, Ngaosuwankul et al., 2008), CD209 is widely present on the surface of DCs in the immature state (Tassaneetrithep et al., 2003, Bullwinkel et al., 2011) and a strong, robust increase in mRNA expression can be detected shortly after induction of DC differentiation (Bullwinkel et al., 2011). In the study described herein, we found a remarkable upregulation in CD209 mRNA expression in DCs cultured in the presence of secretomes collected from osteogenically differentiated JPCs (Figure 2.2.6). Furthermore, the used dextran-uptake demonstrated that JPC secretomes collected from osteogenically induced cells with dexamethasone remarkably expanded the DC subset that exert antigen uptake function, whereas JPC secretomes collected from osteogenically induced cells without dexamethasone enhanced only slightly the dextran-uptake capacity of MoDCs (Figure 2.2.4B, C).

3.6 Comparison of the effects starting from different JPC secretomes on MoDC maturation

It is worth noting that MSCs from different sources may have different immunomodulatory properties, and they may change their function depending on the used culture conditions (Mattar and Bieback, 2015). Throughout the second study of this thesis, the potential of JPC secretomes to inhibit the maturation of MoDCs appeared to be related to their osteogenic capacity. JPC secretomes collected from undifferentiated cells induced only little apparent effects on the maturation of MoDCs, whereas those from osteogenically induced JPCs had remarkably inhibitory effects on the maturating process and functions of MoDCs, which were most pronounced upon dexamethasone supplementation.

3.7 The application possibilities of JPCs in bone tissue engineering based on the results of the present thesis

After years of extensive research on JPCs, obtained results have shown evidence for the suitability of JPCs for BTE application. The present thesis reported for the first time the generation of a perfusion system for the 3D-culturing of JPCs, which was able to provide sufficient nutrition and mechanical stimulation of the used cells. The cell viability, cell expansion efficiency and osteogenic potential of 3D-cultured JPCs were significantly increased by using the optimized perfusion setting in this thesis, providing a novel alternative strategy or at least a feasible idea for the preparation of JPC-colonized constructs in vitro. The second study of the present thesis further demonstrated the immunosuppressive capacities of JPCs. Osteogenically differentiated JPCs suppressed the maturating process and function of dendritic cells in a secreted manner, indicating the reasonable use of this cell source in bone tissue engineering. The influence of dexamethasone on the immunomodulatory capacities of JPCs was also elucidated in the second study, expanding the knowledge of optimizing culture conditions and minimizing a too artificial microenvironment for JPCs. Apart from this, the second study suggested that secretomes collected from osteogenically differentiated JPCs, especially secretomes collected from osteogenically induced cells without dexamethasone may be beneficial for suppressing undesirable immune responses and building tolerance after transplantations.

Altogether, the results of the present thesis contribute to bring us closer to the clinical application of JPCs.

4. Summary

The present thesis addressed several issues that need to be addressed before JPC-seeded constructs can be used clinically. Study I aimed to set up an optimal dynamic condition so as to generate cell-enriched bone-like constructs. For this purpose, a perfusion bioreactor available in the market was used to culture JPCs seeded β-TCP scaffolds. Study II aimed to investigate the immunomodulatory function of JPCs secreted factors. For this purpose, we explored the influence of secretomes collected from undifferentiated and osteogenically induced JPCs on the phenotypic and functional maturation of $CD14^+$ monocyte-derived dendritic cells by supplementation of their culture medium with the relevant JPC secretomes. According to the obtained results, the main findings can be summarized as follows:

1) In terms of metabolic activity/proliferation and distribution within the β-TCP scaffolds, we observed remarkable differences compared to static culture, but we observed no correlation to hydrodynamic or to the scaffold position within the used perfusion bioreactor. The tangential setting appeared to promote osteogenic gene expressions by JPCs at a higher extent than the sigmoidal setting.

2) Secretomes collected from osteogenically induced JPCs seemed to suppress the maturation of MoDCs in terms of phenotypic properties by prevention of MoDC clump formation and downregulation of MoDCs' surface markers. In particular, JPC secretomes enhanced the antigen-uptake capacity of immature DCs, and suppressed the $CD4^+$ T cell stimulatory function of mature MoDCs by up-regulation of IL-10 and IDO release, down-regulation of CD80/86 on their surface and IL-12p40 release. The JPC secretomes collected from osteogenically differentiated cells without dexamethasone remarkably induced the proliferation of $CD25^+$ Treg cells. These obtained results suggested that sectetomes from osteogenically induced JPCs have the potential of immune response suppression promoting peripheral tolerance. The second study provides a further understanding of JPCs' secretory function involved in their immunoregulatory effects.

To sum up, application of perfusion bioreactors is a strategy to generate JPC-seeded constructs in vitro. A flow rate of 100-200 µL/min promotes proliferation and osteogenic differentiation of JPCs within β-TCP scaffolds. Further, JPCs possess immunosuppressive properties and can act as a promising stem cell source for bone tissue engineering.

5. German summary

Die vorliegende Dissertation befasste sich mit mehreren Problemen, die angegangen werden müssen, bevor JPC (jaw periosteal cell) -besiedelte Konstrukte klinisch angewendet werden können. Studie I zielte darauf ab, einen optimalen Perfusionszustand herzustellen, um zellreiche, knochenähnliche Konstrukte zu schaffen. Zu diesem Zweck verwendeten wir einen im Handel erhältlichen Perfusionsbioreaktor zur Kultur von JPCs, die auf β-TCP-Gerüsten ausgesät wurden. Studie II zielte darauf ab, die immunmodulatorische Funktion der sekretorischen Funktion von JPCs zu untersuchen. Zu diesem Zweck untersuchten wir die Wirkung von JPC-Sekretomen, die von undifferenzierten und osteogen differenzierten Zellen sezerniert wurden, auf die Reifung und Funktion von aus CD14+-Monozyten-abgeleiteten dendritischen Zellen (MoDCs), deren Medium mit JPC-Sekretomen supplementiert wurde. Basierend auf den experimentellen Ergebnissen können die wichtigsten Ergebnisse wie folgt zusammengefasst werden:

1) In Bezug auf die metabolische Zell-Aktivität/-Proliferation und Verteilung innerhalb der β-TCP-Gerüste, stellten wir signifikante Unterschiede im Vergleich zu statischen Bedingungen fest. Aber es konnte keine Korrelation zur Strömungsdynamik oder zur Gerüstposition innerhalb des verwendeten Bioreaktors festgestellt werden. Die tangentiale Flusskonfiguration schien die osteogene Genexpression durch JPCs in einem höheren Ausmaß zu aktivieren als die sigmoidale Flusskonfiguration.

2) JPC-Sektetome, die von osteogen induzierten Zellen gewonnen wurden, hemmten die phänotypische Reifung von MoDCs durch Verhinderung der MoDC-Clusterbildung und Herunterregulierung der MoDC-spezifischen Oberflächenmarkern. Darüber hinaus verbesserte die Sekretom-Supplementierung die Antigenaufnahmefähigkeit von unreifen dendritischen Zellen (iDCs). Weiterhin wurde die T-Zell-stimulatorische Funktion von reifen MoDCs durch die Hochregulierung von IL-10 und IDO und die Herunterregulierung von CD80/86 und IL-12p40 unterdrückt. Diese Ergebnisse zeigten, dass das JPC-Sekretom von osteogen differenzierten Periostzellen das

Potenzial zur Unterdrückung einer Immunantwort und zur Förderung der peripheren Toleranz hat. Die vorliegende Studie liefert ein weiteres Verständnis der Beteiligung der sekretorischen Fähigkeit von JPCs anihrer immunregulatorischen Funktion.

Zusammenfassend lässt sich sagen, dass die Anwendung von Perfusionsbioreaktoren eine geeignete Strategie darstellt, um JPC-gesäte Konstrukte in vitro zu erzeugen; Eine Flussrate von 100–200 μm/min fördert die Proliferation und osteogene Differenzierung von JPCs innerhalb von β-TCP-Gerüsten. Darüber hinaus weisen JPCs immunsuppressive Eigenschaften auf und können als vielversprechende Stammzellquelle für BTE angesehen werden.

6. Bibliography

AGGARWAL, S. & PITTENGER, M. F. 2005. Human mesenchymal stem cells modulate allogeneic immune cell responses. *Blood,* 105**,** 1815-22.

ALEXANDER, D., HOFFMANN, J., MUNZ, A., FRIEDRICH, B., GEIS-GERSTORFER, J. & REINERT, S. 2008. Analysis of OPLA scaffolds for bone engineering constructs using human jaw periosteal cells. *J Mater Sci Mater Med,* 19**,** 965-74.

ALEXANDER, D., RIEGER, M., KLEIN, C., ARDJOMANDI, N. & REINERT, S. 2013. Selection of osteoprogenitors from the jaw periosteum by a specific animal-free culture medium. *PLoS One,* 8**,** e81674.

ALEXANDER, D., SCHAFER, F., MUNZ, A., FRIEDRICH, B., KLEIN, C., HOFFMANN, J., BUHRING, H. J. & REINERT, S. 2009. LNGFR induction during osteogenesis of human jaw periosteum-derived cells. *Cell Physiol Biochem,* 24**,** 283-90.

ALEXANDER, D., SCHAFER, F., OLBRICH, M., FRIEDRICH, B., BUHRING, H. J., HOFFMANN, J. & REINERT, S. 2010. MSCA-1/TNAP selection of human jaw periosteal cells improves their mineralization capacity. *Cell Physiol Biochem,* 26**,** 1073-80.

ALLEN, M. R., HOCK, J. M. & BURR, D. B. 2004. Periosteum: biology, regulation, and response to osteoporosis therapies. *Bone,* 35**,** 1003-12.

ALVAREZ-BARRETO, J. F., LANDY, B., VANGORDON, S., PLACE, L., DEANGELIS, P. L. & SIKAVITSAS, V. I. 2011. Enhanced osteoblastic differentiation of mesenchymal stem cells seeded in RGD-functionalized PLLA scaffolds and cultured in a flow perfusion bioreactor. *J Tissue Eng Regen Med,* 5**,** 464-75.

ARDJOMANDI, N., HENRICH, A., HUTH, J., KLEIN, C., SCHWEIZER, E., SCHEIDELER, L., RUPP, F., REINERT, S. & ALEXANDER, D. 2015. Coating of ss-tricalcium phosphate scaffolds-a comparison between graphene oxide and poly-lactic-co-glycolic acid. *Biomed Mater,* 10**,** 045018.

ARDJOMANDI, N., HUTH, J., STAMOV, D. R., HENRICH, A., KLEIN, C., WENDEL, H. P., REINERT, S. & ALEXANDER, D. 2016. Surface biofunctionalization of beta-TCP blocks using aptamer 74 for bone tissue engineering. *Mater Sci Eng C Mater Biol Appl,* 67**,** 267-275.

ARDJOMANDI, N., KLEIN, C., KOHLER, K., MAURER, A., KALBACHER, H., NIEDERLANDER, J., REINERT, S. & ALEXANDER, D. 2012. Indirect coating of RGD peptides using a poly-L-lysine spacer enhances jaw periosteal cell adhesion, proliferation, and differentiation into osteogenic tissue. *J Biomed Mater Res A,* 100**,** 2034-44.

AZUMA, M., CAYABYAB, M., BUCK, D., PHILLIPS, J. H. & LANIER, L. L. 1992. CD28 interaction with B7 costimulates primary allogeneic proliferative responses and cytotoxicity mediated by small, resting T lymphocytes. *J Exp Med,* 175**,** 353-60.

AZUMA, M., ITO, D., YAGITA, H., OKUMURA, K., PHILLIPS, J. H., LANIER, L. L. & SOMOZA, C. 1993. B70 antigen is a second ligand for CTLA-4 and CD28. *Nature,* 366**,** 76-9.

BANCROFT, G. N., SIKAVITSAS, V. I., VAN DEN DOLDER, J., SHEFFIELD, T. L., AMBROSE, C. G., JANSEN, J. A. & MIKOS, A. G. 2002. Fluid flow increases mineralized matrix deposition in 3D perfusion culture of marrow stromal osteoblasts in a dose-dependent manner. *Proc Natl Acad Sci U S A,* 99**,** 12600-5.

BARTHES, J., OZCELIK, H., HINDIE, M., NDREU-HALILI, A., HASAN, A. & VRANA, N. E. 2014. Cell microenvironment engineering and monitoring for tissue engineering and regenerative medicine: the recent advances. *Biomed Res Int,* 2014**,** 921905.

BEYTH, S., BOROVSKY, Z., MEVORACH, D., LIEBERGALL, M., GAZIT, Z., ASLAN, H., GALUN, E. & RACHMILEWITZ, J. 2005. Human mesenchymal stem cells alter antigen-presenting cell maturation and induce T-cell unresponsiveness. *Blood,* 105**,** 2214-9.

BILKAY, U., TOKAT, C., HELVACI, E., OZEK, C., ZEKIOGLU, O., ONAT, T. & SONGUR, E. 2008. Osteogenic capacities of tibial and cranial periosteum: a biochemical and histologic study. *J Craniofac Surg,* 19**,** 453-8.

BJERRE, L., BUNGER, C., BAATRUP, A., KASSEM, M. & MYGIND, T. 2011. Flow perfusion culture of human mesenchymal stem cells on coralline hydroxyapatite scaffolds with various pore sizes. *J Biomed Mater Res A,* 97**,** 251-63.

BJERRE, L., BUNGER, C. E., KASSEM, M. & MYGIND, T. 2008. Flow perfusion culture of human mesenchymal stem cells on silicate-substituted tricalcium phosphate scaffolds. *Biomaterials,* 29**,** 2616-27.

BOHNER, M., SANTONI, B. L. G. & DOBELIN, N. 2020. beta-tricalcium phosphate for bone substitution: Synthesis and properties. *Acta Biomater,* 113**,** 23-41.

BRAUCHLE, E., CARVAJAL BERRIO, D., RIEGER, M., SCHENKE-LAYLAND, K., REINERT, S. & ALEXANDER, D. 2017. Raman Spectroscopic Analyses of Jaw Periosteal Cell Mineralization. *Stem Cells Int,* 2017**,** 1651376.

BRUDER, S. P., KURTH, A. A., SHEA, M., HAYES, W. C., JAISWAL, N. & KADIYALA, S. 1998. Bone regeneration by implantation of purified, culture-expanded human mesenchymal stem cells. *J Orthop Res,* 16**,** 155-62.

BULLWINKEL, J., LUDEMANN, A., DEBARRY, J. & SINGH, P. B. 2011. Epigenotype switching at the CD14 and CD209 genes during differentiation of human monocytes to dendritic cells. *Epigenetics,* 6**,** 45-51.

CAMBI, A., GIJZEN, K., DE VRIES L, J., TORENSMA, R., JOOSTEN, B., ADEMA, G. J., NETEA, M. G., KULLBERG, B. J., ROMANI, L. & FIGDOR, C. G. 2003. The C-type lectin DC-SIGN (CD209) is an antigen-uptake receptor for Candida albicans on dendritic cells. *Eur J Immunol,* 33**,** 532-8.

CAO, W., YANG, Y., WANG, Z., LIU, A., FANG, L., WU, F., HONG, J., SHI, Y., LEUNG, S., DONG, C. & ZHANG, J. Z. 2011. Leukemia inhibitory factor inhibits T helper 17 cell differentiation and confers treatment effects of neural progenitor cell therapy in autoimmune disease. *Immunity,* 35**,** 273-84.

CARTMELL, S. H., PORTER, B. D., GARCIA, A. J. & GULDBERG, R. E. 2003. Effects of medium perfusion rate on cell-seeded three-dimensional bone constructs in vitro. *Tissue Eng,* 9**,** 1197-203.

CASTRO, N., RIBEIRO, S., FERNANDES, M. M., RIBEIRO, C., CARDOSO, V., CORREIA, V., MINGUEZ, R. & LANCEROS-MENDEZ, S. 2020. Physically Active Bioreactors for Tissue Engineering Applications. *Adv Biosyst,* 4**,** e2000125.

CASTRO-MANRREZA, M. E. & MONTESINOS, J. J. 2015. Immunoregulation by mesenchymal stem cells: biological aspects and clinical applications. *J Immunol Res,* 2015**,** 394917.

CHEN, C. Y., KE, C. J., YEN, K. C., HSIEH, H. C., SUN, J. S. & LIN, F. H. 2015. 3D porous calcium-alginate scaffolds cell culture system improved human osteoblast cell clusters for cell therapy. *Theranostics,* 5**,** 643-55.

COLMENARES, M., PUIG-KROGER, A., PELLO, O. M., CORBI, A. L. & RIVAS, L. 2002. Dendritic cell (DC)-specific intercellular adhesion molecule 3 (ICAM-3)-grabbing nonintegrin (DC-SIGN, CD209), a C-type surface lectin in human DCs, is a receptor for Leishmania amastigotes. *J Biol Chem,* 277**,** 36766-9.

COOPER, A. M. & KHADER, S. A. 2007. IL-12p40: an inherently agonistic cytokine. *Trends Immunol,* 28**,** 33-8.

COUPER, K. N., BLOUNT, D. G. & RILEY, E. M. 2008. IL-10: the master regulator of immunity to infection. *J Immunol,* 180**,** 5771-7.

DAI, J., ROTTAU, D., KOHLER, F., REINERT, S. & ALEXANDER, D. 2018. Effects of Jaw Periosteal Cells on Dendritic Cell Maturation. *J Clin Med,* 7.

DAI, J., UMRATH, F., REINERT, S. & ALEXANDER, D. 2020. Jaw Periosteal Cells Seeded in Beta-Tricalcium Phosphate Inhibit Dendritic Cell Maturation. *Biomolecules,* 10.

DANALACHE, M., KLIESCH, S. M., MUNZ, M., NAROS, A., REINERT, S. & ALEXANDER, D. 2019. Quality Analysis of Minerals Formed by Jaw Periosteal Cells under Different Culture Conditions. *Int J Mol Sci,* 20.

DATTA, N., PHAM, Q. P., SHARMA, U., SIKAVITSAS, V. I., JANSEN, J. A. & MIKOS, A. G. 2006. In vitro generated extracellular matrix and fluid shear stress synergistically enhance 3D osteoblastic differentiation. *Proc Natl Acad Sci U S A,* 103**,** 2488-93.

DAVISSON, T., SAH, R. L. & RATCLIFFE, A. 2002. Perfusion increases cell content and matrix synthesis in chondrocyte three-dimensional cultures. *Tissue Eng,* 8**,** 807-16.

DELEMARRE, F. G., HOOGEVEEN, P. G., DE HAAN-MEULMAN, M., SIMONS, P. J. & DREXHAGE, H. A. 2001. Homotypic cluster formation of dendritic cells, a close correlate of their state of maturation. Defects in the biobreeding diabetes-prone rat. *J Leukoc Biol,* 69**,** 373-80.

DHODAPKAR, M. V. & STEINMAN, R. M. 2002. Antigen-bearing immature dendritic cells induce peptide-specific CD8(+) regulatory T cells in vivo in humans. *Blood,* 100**,** 174-7.

DHODAPKAR, M. V., STEINMAN, R. M., KRASOVSKY, J., MUNZ, C. & BHARDWAJ, N. 2001. Antigen-specific inhibition of effector T cell function in humans after injection of immature dendritic cells. *J Exp Med,* 193**,** 233-8.

DILIOGLOU, S., CRUSE, J. M. & LEWIS, R. E. 2003. Function of CD80 and CD86 on monocyte- and stem cell-derived dendritic cells. *Exp Mol Pathol,* 75**,** 217-27.

DWEK, J. R. 2010. The periosteum: what is it, where is it, and what mimics it in its absence? *Skeletal Radiol,* 39**,** 319-23.

EGGLI, P. S., MULLER, W. & SCHENK, R. K. 1988. Porous hydroxyapatite and tricalcium phosphate cylinders with two different pore size ranges implanted in the cancellous bone of rabbits. A comparative histomorphometric and histologic study of bony ingrowth and implant substitution. *Clin Orthop Relat Res***,** 127-38.

ENGLISH, K., RYAN, J. M., TOBIN, L., MURPHY, M. J., BARRY, F. P. & MAHON, B. P. 2009. Cell contact, prostaglandin E(2) and transforming growth factor beta 1 play non-redundant roles in human mesenchymal stem cell induction of CD4+CD25(High) forkhead box P3+ regulatory T cells. *Clin Exp Immunol,* 156**,** 149-60.

EVANS, S. F., CHANG, H. & KNOTHE TATE, M. L. 2013. Elucidating multiscale periosteal mechanobiology: a key to unlocking the smart properties and regenerative capacity of the periosteum? *Tissue Eng Part B Rev,* 19**,** 147-59.

FARLEY, J. R., WERGEDAL, J. E. & BAYLINK, D. J. 1983. Fluoride directly stimulates proliferation and alkaline phosphatase activity of bone-forming cells. *Science,* 222**,** 330-2.

FERRETTI, C. & MATTIOLI-BELMONTE, M. 2014. Periosteum derived stem cells for regenerative medicine proposals: Boosting current knowledge. *World J Stem Cells,* 6**,** 266-77.

FILIPOWSKA, J., REILLY, G. C. & OSYCZKA, A. M. 2016. A single short session of media perfusion induces osteogenesis in hBMSCs cultured in porous scaffolds, dependent on cell differentiation stage. *Biotechnol Bioeng,* 113**,** 1814-24.

GANDHI, J. K., KAO, S. W., ROUX, B. M., RODRIGUEZ, R. A., TANG, S. J., FISHER, J. P., CHENG, M. H. & BREY, E. M. 2019. Perfusion Bioreactor Culture of Bone Marrow Stromal Cells Enhances Cranial Defect Regeneration. *Plast Reconstr Surg,* 143**,** 993e-1002e.

GASPAR, D. A., GOMIDE, V. & MONTEIRO, F. J. 2012. The role of perfusion bioreactors in bone tissue engineering. *Biomatter,* 2**,** 167-75.

GEIJTENBEEK, T. B., KROOSHOOP, D. J., BLEIJS, D. A., VAN VLIET, S. J., VAN DUIJNHOVEN, G. C., GRABOVSKY, V., ALON, R., FIGDOR, C. G. & VAN KOOYK, Y. 2000a. DC-SIGN-ICAM-2 interaction mediates dendritic cell trafficking. *Nat Immunol,* 1**,** 353-7.

GEIJTENBEEK, T. B., TORENSMA, R., VAN VLIET, S. J., VAN DUIJNHOVEN, G. C., ADEMA, G. J., VAN KOOYK, Y. & FIGDOR, C. G. 2000b. Identification of DC-SIGN, a novel dendritic cell-specific ICAM-3 receptor that supports primary immune responses. *Cell,* 100**,** 575-85.

GRAYSON, W. L., BHUMIRATANA, S., CANNIZZARO, C., CHAO, P. H., LENNON, D. P., CAPLAN, A. I. & VUNJAK-NOVAKOVIC, G. 2008. Effects of initial seeding density and fluid perfusion rate on formation of tissue-engineered bone. *Tissue Eng Part A,* 14**,** 1809-20.

GROH, M. E., MAITRA, B., SZEKELY, E. & KOC, O. N. 2005. Human mesenchymal stem cells require monocyte-mediated activation to suppress alloreactive T cells. *Exp Hematol,* 33**,** 928-34.

GURKAN, U. A. & AKKUS, O. 2008. The mechanical environment of bone marrow: a review. *Ann Biomed Eng,* 36**,** 1978-91.

HE, F., UMRATH, F., REINERT, S. & ALEXANDER, D. 2021a. Jaw Periosteum-Derived Mesenchymal Stem Cells Regulate THP-1-Derived Macrophage Polarization. *Int J Mol Sci,* 22.

HE, F., UMRATH, F., VON OHLE, C., REINERT, S. & ALEXANDER, D. 2021b. Analysis of the Influence of Jaw Periosteal Cells on Macrophages Phenotype Using an Innovative Horizontal Coculture System. *Biomedicines,* 9.

HILLIGAN, K. L. & RONCHESE, F. 2020. Antigen presentation by dendritic cells and their instruction of CD4+ T helper cell responses. *Cell Mol Immunol,* 17**,** 587-599.

HOCK, J. M., KREAM, B. E. & RAISZ, L. G. 1982. Autoradiographic study of the effect of 1,25-dihydroxyvitamin D3 on bone matrix synthesis in vitamin D replete rats. *Calcif Tissue Int,* 34**,** 347-51.

HOEMANN, C. D., EL-GABALAWY, H. & MCKEE, M. D. 2009. In vitro osteogenesis assays: influence of the primary cell source on alkaline phosphatase activity and mineralization. *Pathol Biol (Paris),* 57**,** 318-23.

HOLTORF, H. L., DATTA, N., JANSEN, J. A. & MIKOS, A. G. 2005. Scaffold mesh size affects the osteoblastic differentiation of seeded marrow stromal cells cultured in a flow perfusion bioreactor. *J Biomed Mater Res A,* 74**,** 171-80.

HOSSEINKHANI, H., INATSUGU, Y., HIRAOKA, Y., INOUE, S. & TABATA, Y. 2005. Perfusion culture enhances osteogenic differentiation of rat mesenchymal stem cells in collagen sponge reinforced with poly(glycolic Acid) fiber. *Tissue Eng,* 11**,** 1476-88.

HSU, W. T., LIN, C. H., CHIANG, B. L., JUI, H. Y., WU, K. K. & LEE, C. M. 2013. Prostaglandin E2 potentiates mesenchymal stem cell-induced IL-10+IFN-gamma+CD4+ regulatory T cells to control transplant arteriosclerosis. *J Immunol,* 190**,** 2372-80.

HUEY, D. J., HU, J. C. & ATHANASIOU, K. A. 2012. Unlike bone, cartilage regeneration remains elusive. *Science,* 338**,** 917-21.

ISHIKAWA, K., MIYAMOTO, Y., TSUCHIYA, A., HAYASHI, K., TSURU, K. & OHE, G. 2018. Physical and Histological Comparison of Hydroxyapatite, Carbonate Apatite, and beta-Tricalcium Phosphate Bone Substitutes. *Materials (Basel),* 11.

JANSSEN, F. W., OOSTRA, J., OORSCHOT, A. & VAN BLITTERSWIJK, C. A. 2006. A perfusion bioreactor system capable of producing clinically relevant volumes of tissue-engineered bone: in vivo bone formation showing proof of concept. *Biomaterials,* 27**,** 315-23.

JIANG, X. X., ZHANG, Y., LIU, B., ZHANG, S. X., WU, Y., YU, X. D. & MAO, N. 2005. Human mesenchymal stem cells inhibit differentiation and function of monocyte-derived dendritic cells. *Blood,* 105**,** 4120-6.

JONES, D. B., NOLTE, H., SCHOLUBBERS, J. G., TURNER, E. & VELTEL, D. 1991. Biochemical signal transduction of mechanical strain in osteoblast-like cells. *Biomaterials,* 12**,** 101-10.

JUNG, Y. J., BAE, H. S., RYOO, H. M. & BAEK, S. H. 2018. A novel RUNX2 mutation in exon 8, G462X, in a patient with Cleidocranial Dysplasia. *J Cell Biochem,* 119**,** 1152-1162.

KAISHO, T. & AKIRA, S. 2001. Dendritic-cell function in Toll-like receptor- and MyD88-knockout mice. *Trends Immunol,* 22**,** 78-83.

KANCZLER, J. M. & OREFFO, R. O. 2008. Osteogenesis and angiogenesis: the potential for engineering bone. *Eur Cell Mater,* 15**,** 100-14.

KAPUR, R. A., AMIRFEYZ, R., WYLDE, V., BLOM, A. W., NELSON, I. W. & HUTCHINSON, J. 2010. Clinical outcomes and fusion success associated with the use of BoneSave in spinal surgery. *Arch Orthop Trauma Surg,* 130**,** 641-7.

KIM, D. H., YOO, K. H., CHOI, K. S., CHOI, J., CHOI, S. Y., YANG, S. E., YANG, Y. S., IM, H. J., KIM, K. H., JUNG, H. L., SUNG, K. W. & KOO, H. H. 2005. Gene expression profile of cytokine and growth factor during differentiation of bone marrow-derived mesenchymal stem cell. *Cytokine,* 31**,** 119-26.

KOU, P. M. & BABENSEE, J. E. 2011. Macrophage and dendritic cell phenotypic diversity in the context of biomaterials. *J Biomed Mater Res A,* 96**,** 239-60.

KUBO, S., YAMAOKA, K., KONDO, M., YAMAGATA, K., ZHAO, J., IWATA, S. & TANAKA, Y. 2014. The JAK inhibitor, tofacitinib, reduces the T cell stimulatory capacity of human monocyte-derived dendritic cells. *Ann Rheum Dis,* 73**,** 2192-8.

LECLERC, E., DAVID, B., GRISCOM, L., LEPIOUFLE, B., FUJII, T., LAYROLLE, P. & LEGALLAISA, C. 2006. Study of osteoblastic cells in a microfluidic environment. *Biomaterials,* 27**,** 586-95.

LEHNER, M., STOCKL, J., MAJDIC, O., KNAPP, W., HUTTNER, K., FELZMANN, T. & HOLTER, W. 2003. MHC class II antigen signaling induces homotypic and heterotypic cluster formation of human mature monocyte derived dendritic cells in the absence of cell death. *Hum Immunol,* 64**,** 762-70.

LI, Z., JU, X., SILVEIRA, P. A., ABADIR, E., HSU, W. H., HART, D. N. J. & CLARK, G. J. 2019. CD83: Activation Marker for Antigen Presenting Cells and Its Therapeutic Potential. *Front Immunol,* 10**,** 1312.

LIGHVANI, A. A., FRUCHT, D. M., JANKOVIC, D., YAMANE, H., ALIBERTI, J., HISSONG, B. D., NGUYEN, B. V., GADINA, M., SHER, A., PAUL, W. E. & O'SHEA, J. J. 2001. T-bet is rapidly induced by interferon-gamma in lymphoid and myeloid cells. *Proc Natl Acad Sci U S A,* 98**,** 15137-42.

LIU, Y., CHAN, J. K. & TEOH, S. H. 2015. Review of vascularised bone tissue-engineering strategies with a focus on co-culture systems. *J Tissue Eng Regen Med,* 9**,** 85-105.

MA, S., XIE, N., LI, W., YUAN, B., SHI, Y. & WANG, Y. 2014. Immunobiology of mesenchymal stem cells. *Cell Death Differ,* 21**,** 216-25.

MACATONIA, S. E., HOSKEN, N. A., LITTON, M., VIEIRA, P., HSIEH, C. S., CULPEPPER, J. A., WYSOCKA, M., TRINCHIERI, G., MURPHY, K. M. & O'GARRA, A. 1995. Dendritic cells produce IL-12 and direct the development of Th1 cells from naive CD4+ T cells. *J Immunol,* 154**,** 5071-9.

MACCARIO, R., PODESTA, M., MORETTA, A., COMETA, A., COMOLI, P., MONTAGNA, D., DAUDT, L., IBATICI, A., PIAGGIO, G., POZZI, S., FRASSONI, F. & LOCATELLI, F. 2005. Interaction of human mesenchymal stem cells with cells involved in alloantigen-specific immune response favors the differentiation of CD4+ T-cell subsets expressing a regulatory/suppressive phenotype. *Haematologica,* 90**,** 516-25.

MALDONADO, R. A. & VON ANDRIAN, U. H. 2010. How tolerogenic dendritic cells induce regulatory T cells. *Adv Immunol,* 108**,** 111-65.

MARTIN, I., WENDT, D. & HEBERER, M. 2004. The role of bioreactors in tissue engineering. *Trends Biotechnol,* 22**,** 80-6.

MATTA, B. M., CASTELLANETA, A. & THOMSON, A. W. 2010. Tolerogenic plasmacytoid DC. *Eur J Immunol,* 40**,** 2667-76.

MATTAR, P. & BIEBACK, K. 2015. Comparing the Immunomodulatory Properties of Bone Marrow, Adipose Tissue, and Birth-Associated Tissue Mesenchymal Stromal Cells. *Front Immunol,* 6**,** 560.

MCCOY, R. J. & O'BRIEN, F. J. 2010. Influence of shear stress in perfusion bioreactor cultures for the development of three-dimensional bone tissue constructs: a review. *Tissue Eng Part B Rev,* 16**,** 587-601.

MEISEL, R., ZIBERT, A., LARYEA, M., GOBEL, U., DAUBENER, W. & DILLOO, D. 2004. Human bone marrow stromal cells inhibit allogeneic T-cell responses by indoleamine 2,3-dioxygenase-mediated tryptophan degradation. *Blood,* 103**,** 4619-21.

MELLOR, A. L. & MUNN, D. H. 2004. IDO expression by dendritic cells: tolerance and tryptophan catabolism. *Nat Rev Immunol,* 4**,** 762-74.

MILLER, C. P., JEGEDE, K., ESSIG, D., GARG, H., BIBLE, J. E., BISWAS, D., WHANG, P. G. & GRAUER, J. N. 2012. The efficacies of 2 ceramic bone graft extenders for promoting spinal fusion in a rabbit bone paucity model. *Spine (Phila Pa 1976),* 37**,** 642-7.

MITTAL, M., TIRUPPATHI, C., NEPAL, S., ZHAO, Y. Y., GRZYCH, D., SONI, D., PROCKOP, D. J. & MALIK, A. B. 2016. TNFalpha-stimulated gene-6 (TSG6) activates macrophage phenotype transition to prevent inflammatory lung injury. *Proc Natl Acad Sci U S A,* 113**,** E8151-E8158.

MORELLI, A. E. & THOMSON, A. W. 2007. Tolerogenic dendritic cells and the quest for transplant tolerance. *Nat Rev Immunol,* 7**,** 610-21.

MYGIND, T., STIEHLER, M., BAATRUP, A., LI, H., ZOU, X., FLYVBJERG, A., KASSEM, M. & BUNGER, C. 2007. Mesenchymal stem cell ingrowth and differentiation on coralline hydroxyapatite scaffolds. *Biomaterials,* 28**,** 1036-47.

NAJAR, M., RAICEVIC, G., FAYYAD-KAZAN, H., DE BRUYN, C., BRON, D., TOUNGOUZ, M. & LAGNEAUX, L. 2015. Bone Marrow Mesenchymal Stromal Cells Induce Proliferative, Cytokinic and Molecular Changes During the T Cell Response: The Importance of the IL-10/CD210 Axis. *Stem Cell Rev Rep,* 11**,** 442-52.

NAM, J., PERERA, P., RATH, B. & AGARWAL, S. 2013. Dynamic regulation of bone morphogenetic proteins in engineered osteochondral constructs by biomechanical stimulation. *Tissue Eng Part A,* 19**,** 783-92.

NGAOSUWANKUL, P., PONGTANALERT, P., ENGERING, A. & CHAIYAROJ, S. C. 2008. Differential gene expression profiles of human monocyte-

derived antigen presenting cells in response to Penicillium marneffei: roles of DC-SIGN (CD209) in fungal cell uptake. *Asian Pac J Allergy Immunol,* 26**,** 151-63.

NGUYEN, B. N., KO, H., MORIARTY, R. A., ETHERIDGE, J. M. & FISHER, J. P. 2016. Dynamic Bioreactor Culture of High Volume Engineered Bone Tissue. *Tissue Eng Part A,* 22**,** 263-71.

OLBRICH, M., RIEGER, M., REINERT, S. & ALEXANDER, D. 2012. Isolation of osteoprogenitors from human jaw periosteal cells: a comparison of two magnetic separation methods. *PLoS One,* 7**,** e47176.

ORYAN, A., ALIDADI, S., MOSHIRI, A. & MAFFULLI, N. 2014. Bone regenerative medicine: classic options, novel strategies, and future directions. *J Orthop Surg Res,* 9**,** 18.

PIERRE, P., TURLEY, S. J., GATTI, E., HULL, M., MELTZER, J., MIRZA, A., INABA, K., STEINMAN, R. M. & MELLMAN, I. 1997. Developmental regulation of MHC class II transport in mouse dendritic cells. *Nature,* 388**,** 787-92.

RAFEI, M., CAMPEAU, P. M., AGUILAR-MAHECHA, A., BUCHANAN, M., WILLIAMS, P., BIRMAN, E., YUAN, S., YOUNG, Y. K., BOIVIN, M. N., FORNER, K., BASIK, M. & GALIPEAU, J. 2009. Mesenchymal stromal cells ameliorate experimental autoimmune encephalomyelitis by inhibiting CD4 Th17 T cells in a CC chemokine ligand 2-dependent manner. *J Immunol,* 182**,** 5994-6002.

RAMASAMY, R., FAZEKASOVA, H., LAM, E. W., SOEIRO, I., LOMBARDI, G. & DAZZI, F. 2007. Mesenchymal stem cells inhibit dendritic cell differentiation and function by preventing entry into the cell cycle. *Transplantation,* 83**,** 71-6.

RAUH, J., MILAN, F., GUNTHER, K. P. & STIEHLER, M. 2011. Bioreactor systems for bone tissue engineering. *Tissue Eng Part B Rev,* 17**,** 263-80.

RAVICHANDRAN, A., LIU, Y. & TEOH, S. H. 2018. Review: bioreactor design towards generation of relevant engineered tissues: focus on clinical translation. *J Tissue Eng Regen Med,* 12**,** e7-e22.

REN, G., ZHANG, L., ZHAO, X., XU, G., ZHANG, Y., ROBERTS, A. I., ZHAO, R. C. & SHI, Y. 2008. Mesenchymal stem cell-mediated immunosuppression occurs via concerted action of chemokines and nitric oxide. *Cell Stem Cell,* 2**,** 141-50.

RINCON, M., ANGUITA, J., NAKAMURA, T., FIKRIG, E. & FLAVELL, R. A. 1997. Interleukin (IL)-6 directs the differentiation of IL-4-producing CD4+ T cells. *J Exp Med,* 185**,** 461-9.

ROUWKEMA, J., RIVRON, N. C. & VAN BLITTERSWIJK, C. A. 2008. Vascularization in tissue engineering. *Trends Biotechnol,* 26**,** 434-41.

RYAN, J. M., BARRY, F., MURPHY, J. M. & MAHON, B. P. 2007. Interferon-gamma does not break, but promotes the immunosuppressive capacity of adult human mesenchymal stem cells. *Clin Exp Immunol,* 149**,** 353-63.

SAILON, A. M., ALLORI, A. C., DAVIDSON, E. H., REFORMAT, D. D., ALLEN, R. J. & WARREN, S. M. 2009. A novel flow-perfusion bioreactor supports 3D dynamic cell culture. *J Biomed Biotechnol,* 2009**,** 873816.

SALLUSTO, F. & LANZAVECCHIA, A. 1994. Efficient presentation of soluble antigen by cultured human dendritic cells is maintained by

granulocyte/macrophage colony-stimulating factor plus interleukin 4 and downregulated by tumor necrosis factor alpha. *J Exp Med,* 179**,** 1109-18.

SANTORO, R., OLIVARES, A. L., BRANS, G., WIRZ, D., LONGINOTTI, C., LACROIX, D., MARTIN, I. & WENDT, D. 2010. Bioreactor based engineering of large-scale human cartilage grafts for joint resurfacing. *Biomaterials,* 31**,** 8946-52.

SCHIMMING, R. & SCHMELZEISEN, R. 2004. Tissue-engineered bone for maxillary sinus augmentation. *J Oral Maxillofac Surg,* 62**,** 724-9.

SELLERI, S., BIFSHA, P., CIVINI, S., PACELLI, C., DIENG, M. M., LEMIEUX, W., JIN, P., BAZIN, R., PATEY, N., MARINCOLA, F. M., MOLDOVAN, F., ZAOUTER, C., TRUDEAU, L. E., BENABDHALLA, B., LOUIS, I., BEAUSEJOUR, C., STRONCEK, D., LE DEIST, F. & HADDAD, E. 2016. Human mesenchymal stromal cell-secreted lactate induces M2-macrophage differentiation by metabolic reprogramming. *Oncotarget,* 7**,** 30193-210.

SHAHIN, K. & DORAN, P. M. 2011. Strategies for enhancing the accumulation and retention of extracellular matrix in tissue-engineered cartilage cultured in bioreactors. *PLoS One,* 6**,** e23119.

SHI, Y., WANG, Y., LI, Q., LIU, K., HOU, J., SHAO, C. & WANG, Y. 2018. Immunoregulatory mechanisms of mesenchymal stem and stromal cells in inflammatory diseases. *Nat Rev Nephrol,* 14**,** 493-507.

SHORTMAN, K. & NAIK, S. H. 2007. Steady-state and inflammatory dendritic-cell development. *Nat Rev Immunol,* 7**,** 19-30.

SIKAVITSAS, V. I., BANCROFT, G. N., HOLTORF, H. L., JANSEN, J. A. & MIKOS, A. G. 2003. Mineralized matrix deposition by marrow stromal osteoblasts in 3D perfusion culture increases with increasing fluid shear forces. *Proc Natl Acad Sci U S A,* 100**,** 14683-8.

SIKAVITSAS, V. I., BANCROFT, G. N., LEMOINE, J. J., LIEBSCHNER, M. A., DAUNER, M. & MIKOS, A. G. 2005. Flow perfusion enhances the calcified matrix deposition of marrow stromal cells in biodegradable nonwoven fiber mesh scaffolds. *Ann Biomed Eng,* 33**,** 63-70.

SMITH, B. D. & GRANDE, D. A. 2015. The current state of scaffolds for musculoskeletal regenerative applications. *Nat Rev Rheumatol,* 11**,** 213-22.

SMUCKER, J. D., PETERSEN, E. B. & FREDERICKS, D. C. 2012. Assessment of MASTERGRAFT PUTTY as a graft extender in a rabbit posterolateral fusion model. *Spine (Phila Pa 1976),* 37**,** 1017-21.

SQUIER, C. A., GHONEIM, S. & KREMENAK, C. R. 1990. Ultrastructure of the periosteum from membrane bone. *J Anat,* 171**,** 233-9.

STEINMAN, R. M. & COHN, Z. A. 1973. Identification of a novel cell type in peripheral lymphoid organs of mice. I. Morphology, quantitation, tissue distribution. *J Exp Med,* 137**,** 1142-62.

STEINMAN, R. M., HAWIGER, D., LIU, K., BONIFAZ, L., BONNYAY, D., MAHNKE, K., IYODA, T., RAVETCH, J., DHODAPKAR, M., INABA, K. & NUSSENZWEIG, M. 2003a. Dendritic cell function in vivo during the steady state: a role in peripheral tolerance. *Ann N Y Acad Sci,* 987**,** 15-25.

STEINMAN, R. M., HAWIGER, D. & NUSSENZWEIG, M. C. 2003b. Tolerogenic dendritic cells. *Annu Rev Immunol,* 21**,** 685-711.

STEINMAN, R. M. & NUSSENZWEIG, M. C. 2002. Avoiding horror autotoxicus: the importance of dendritic cells in peripheral T cell tolerance. *Proc Natl Acad Sci U S A,* 99**,** 351-8.

STOBIE, L., GURUNATHAN, S., PRUSSIN, C., SACKS, D. L., GLAICHENHAUS, N., WU, C. Y. & SEDER, R. A. 2000. The role of antigen and IL-12 in sustaining Th1 memory cells in vivo: IL-12 is required to maintain memory/effector Th1 cells sufficient to mediate protection to an infectious parasite challenge. *Proc Natl Acad Sci U S A,* 97**,** 8427-32.

SUN, J. S., CHEN, P. Y., TSUANG, Y. H., CHEN, M. H. & CHEN, P. Q. 2009. Vitamin-D binding protein does not enhance healing in rat bone defects: a pilot study. *Clin Orthop Relat Res,* 467**,** 3156-64.

SVAJGER, U. & ROZMAN, P. 2014. Tolerogenic dendritic cells: molecular and cellular mechanisms in transplantation. *J Leukoc Biol,* 95**,** 53-69.

TAGA, K. & TOSATO, G. 1992. IL-10 inhibits human T cell proliferation and IL-2 production. *J Immunol,* 148**,** 1143-8.

TAN, J. T., DUDL, E., LEROY, E., MURRAY, R., SPRENT, J., WEINBERG, K. I. & SURH, C. D. 2001. IL-7 is critical for homeostatic proliferation and survival of naive T cells. *Proc Natl Acad Sci U S A,* 98**,** 8732-7.

TASSANEETRITHEP, B., BURGESS, T. H., GRANELLI-PIPERNO, A., TRUMPFHELLER, C., FINKE, J., SUN, W., ELLER, M. A., PATTANAPANYASAT, K., SARASOMBATH, S., BIRX, D. L., STEINMAN, R. M., SCHLESINGER, S. & MAROVICH, M. A. 2003. DC-SIGN (CD209) mediates dengue virus infection of human dendritic cells. *J Exp Med,* 197**,** 823-9.

TERMEER, C., JOHANNSEN, H., BRAUN, T., RENKL, A., AHRENS, T., DENFELD, R. W., LAPPIN, M. B., WEISS, J. M. & SIMON, J. C. 2001. The role of CD44 during CD40 ligand-induced dendritic cell clustering and maturation. *J Leukoc Biol,* 70**,** 715-22.

UCCELLI, A., MORETTA, L. & PISTOIA, V. 2006. Immunoregulatory function of mesenchymal stem cells. *Eur J Immunol,* 36**,** 2566-73.

UDDSTROMER, L. 1978. The osteogenic capacity of tubular and membranous bone periosteum. A qualitative and quantitative experimental study in growing rabbits. *Scand J Plast Reconstr Surg,* 12**,** 195-205.

UMRATH, F., STEINLE, H., WEBER, M., WENDEL, H. P., REINERT, S., ALEXANDER, D. & AVCI-ADALI, M. 2019. Generation of iPSCs from Jaw Periosteal Cells Using Self-Replicating RNA. *Int J Mol Sci,* 20.

UMRATH, F., THOMALLA, C., POSCHEL, S., SCHENKE-LAYLAND, K., REINERT, S. & ALEXANDER, D. 2018. Comparative Study of MSCA-1 and CD146 Isolated Periosteal Cell Subpopulations. *Cell Physiol Biochem,* 51**,** 1193-1206.

UMRATH, F., WEBER, M., REINERT, S., WENDEL, H. P., AVCI-ADALI, M. & ALEXANDER, D. 2020. iPSC-Derived MSCs Versus Originating Jaw Periosteal Cells: Comparison of Resulting Phenotype and Stem Cell Potential. *Int J Mol Sci,* 21.

VASANDAN, A. B., JAHNAVI, S., SHASHANK, C., PRASAD, P., KUMAR, A. & PRASANNA, S. J. 2016. Human Mesenchymal stem cells program macrophage plasticity by altering their metabolic status via a PGE2-dependent mechanism. *Sci Rep,* 6**,** 38308.

VASATURO, A., DI BLASIO, S., PEETERS, D. G., DE KONING, C. C., DE VRIES, J. M., FIGDOR, C. G. & HATO, S. V. 2013. Clinical Implications of Co-Inhibitory Molecule Expression in the Tumor Microenvironment for DC Vaccination: A Game of Stop and Go. *Front Immunol,* 4**,** 417.

VIZOSO, F. J., EIRO, N., CID, S., SCHNEIDER, J. & PEREZ-FERNANDEZ, R. 2017. Mesenchymal Stem Cell Secretome: Toward Cell-Free Therapeutic Strategies in Regenerative Medicine. *Int J Mol Sci,* 18.

WANG, G., CAO, K., LIU, K., XUE, Y., ROBERTS, A. I., LI, F., HAN, Y., RABSON, A. B., WANG, Y. & SHI, Y. 2018. Kynurenic acid, an IDO metabolite, controls TSG-6-mediated immunosuppression of human mesenchymal stem cells. *Cell Death Differ,* 25**,** 1209-1223.

WANNER, Y., UMRATH, F., WAIDMANN, M., REINERT, S. & ALEXANDER, D. 2017. Platelet Lysate: The Better Choice for Jaw Periosteal Cell Mineralization. *Stem Cells Int,* 2017**,** 8303959.

WATOWICH, S. S. & LIU, Y. J. 2010. Mechanisms regulating dendritic cell specification and development. *Immunol Rev,* 238**,** 76-92.

WEBER, M., UMRATH, F., STEINLE, H., SCHMITT, L. F., YU, L. T., SCHLENSAK, C., WENDEL, H. P., REINERT, S., ALEXANDER, D. & AVCI-ADALI, M. 2021. Influence of Human Jaw Periosteal Cells Seeded beta-Tricalcium Phosphate Scaffolds on Blood Coagulation. *Int J Mol Sci,* 22.

WILLIAMS, J. L., IANNOTTI, J. P., HAM, A., BLEUIT, J. & CHEN, J. H. 1994. Effects of fluid shear stress on bone cells. *Biorheology,* 31**,** 163-70.

WILSON, N. S., EL-SUKKARI, D. & VILLADANGOS, J. A. 2004. Dendritic cells constitutively present self antigens in their immature state in vivo and regulate antigen presentation by controlling the rates of MHC class II synthesis and endocytosis. *Blood,* 103**,** 2187-95.

WITTKOWSKE, C., REILLY, G. C., LACROIX, D. & PERRAULT, C. M. 2016. In Vitro Bone Cell Models: Impact of Fluid Shear Stress on Bone Formation. *Front Bioeng Biotechnol,* 4**,** 87.

WU, W., LE, A. V., MENDEZ, J. J., CHANG, J., NIKLASON, L. E. & STEINBACHER, D. M. 2015. Osteogenic performance of donor-matched human adipose and bone marrow mesenchymal cells under dynamic culture. *Tissue Eng Part A,* 21**,** 1621-32.

YANAGIHARA, S., KOMURA, E., NAGAFUNE, J., WATARAI, H. & YAMAGUCHI, Y. 1998. EBI1/CCR7 is a new member of dendritic cell chemokine receptor that is up-regulated upon maturation. *J Immunol,* 161**,** 3096-102.

YANG, L., MA, J., HE, Q. & LI, X. 2021. Immutol regulates CD4(+)Tregs, CD8(+)Tregs and pDCs via IDO signaling pathway to induce immune tolerance in rat heart allograft transplant. *Transpl Immunol,* 68**,** 101393.

YANG, Q., ZHENG, C., CAO, J., CAO, G., SHOU, P., LIN, L., VELLETRI, T., JIANG, M., CHEN, Q., HAN, Y., LI, F., WANG, Y., CAO, W. & SHI, Y. 2016. Spermidine alleviates experimental autoimmune encephalomyelitis through inducing inhibitory macrophages. *Cell Death Differ,* 23**,** 1850-1861.

YIN, X., CHEN, S. & EISENBARTH, S. C. 2021. Dendritic Cell Regulation of T Helper Cells. *Annu Rev Immunol,* 39**,** 759-790.

ZENG, L., WEI, J., HAN, D., LIU, H., LIU, Y., ZHAO, N., SUN, S., WANG, Y. & FENG, H. 2017. Functional analysis of novel RUNX2 mutations in cleidocranial dysplasia. *Mutagenesis,* 32**,** 437-443.

ZHANG, W., GE, W., LI, C., YOU, S., LIAO, L., HAN, Q., DENG, W. & ZHAO, R. C. 2004. Effects of mesenchymal stem cells on differentiation, maturation, and function of human monocyte-derived dendritic cells. *Stem Cells Dev,* 13**,** 263-71.

ZHANG, Z. Y., TEOH, S. H., CHONG, W. S., FOO, T. T., CHNG, Y. C., CHOOLANI, M. & CHAN, J. 2009. A biaxial rotating bioreactor for the culture of fetal mesenchymal stem cells for bone tissue engineering. *Biomaterials,* 30**,** 2694-704.

ZHU, J., JANKOVIC, D., OLER, A. J., WEI, G., SHARMA, S., HU, G., GUO, L., YAGI, R., YAMANE, H., PUNKOSDY, G., FEIGENBAUM, L., ZHAO, K. & PAUL, W. E. 2012. The transcription factor T-bet is induced by multiple pathways and prevents an endogenous Th2 cell program during Th1 cell responses. *Immunity,* 37**,** 660-73.

ZIEGLER-HEITBROCK, H. W. & ULEVITCH, R. J. 1993. CD14: cell surface receptor and differentiation marker. *Immunol Today,* 14**,** 121-5.

ZOU, X., ZHANG, G., CHENG, Z., YIN, D., DU, T., JU, G., MIAO, S., LIU, G., LU, M. & ZHU, Y. 2014. Microvesicles derived from human Wharton's Jelly mesenchymal stromal cells ameliorate renal ischemia-reperfusion injury in rats by suppressing CX3CL1. *Stem Cell Res Ther,* 5**,** 40.

7. Declaration of contribution

Contributions of my own

The dissertation work was carried out at the Department of Oral and Maxillofacial Surgery, University Hospital Tübingen under the supervision of Prof. Dr. Dorothea Alexander-Friedrich.

These two studies were designed in collaboration with Prof. Dr. Dorothea Alexander-Friedrich. All of the experiments and all of the statistical analysis were carried out independently by myself. I contributed in the main part of research concept, selection of methods, data acquisition, interpretation of results and preparation of manuscript in both studies.

I confirm that I wrote the manuscript of this dissertation myself (under the supervision of Prof. Dr. Dorothea Alexander-Friedrich) and that any additional sources of information have been duly cited.

Contributions of others

In study I, Suya Wang partially contributed in selection of methods, data acquisition and interpretation of results; Felix Umrath partially contributed in selection of methods and preparation of manuscript; Siegmar Reinert partially contributed in preparation of manuscript; Dorothea Alexander-Friedrich partially contributed in research concept, selection of methods, interpretation of results and preparation of manuscript.

In study II, Felix Umrath partially contributed in selection of methods, data acquisition and preparation of manuscript; Antonio Jose Salgado partially contributed in selection of methods; Siegmar Reinert partially contributed in preparation of manuscript; Dorothea Alexander-Friedrich partially contributed in research concept, selection of methods, interpretation of results and preparation of manuscript.

Signed_____on ___15.02.2023__in Tübingen